REPORT DOCUMENTATION PAGE

Form Approved
OMB No. 0704-0188

1. AGENCY USE ONLY *(Leave blank)*	2. REPORT DATE	3. REPORT TYPE AND DATES COVERED
	9 Jan 1998	Final 1 Aug 94 - 31 Dec 97

4. TITLE AND SUBTITLE
Modeling of Wide-Band-Gap Semiconductor Alloys

5. FUNDING NUMBERS
G#N00014-94-1-1000
PR# 97PR00895-00

6. AUTHOR(S)
W. R. L. Lambrecht

7. PERFORMING ORGANIZATION NAMES(S) AND ADDRESS(ES)
Case Western Reserve University
10900 Euclid Avenue
Cleveland, OH 44106

8. PERFORMING ORGANIZATION REPORT NUMBER

9. SPONSORING / MONITORING AGENCY NAMES(S) AND ADDRESS(ES)
ONR-312
800 N. Quincy Street
Arlington, VA 22317-5660

10. SPONSORING / MONITORING AGENCY REPORT NUMBER

11. SUPPLEMENTARY NOTES

19980120 196

a. DISTRIBUTION / AVAILABILITY STATEMENT
approved for public release, distribution unlimited

12. DISTRIBUTION CODE

13. ABSTRACT *(Maximum 200 words)*

Under this grant, a theoretical study was performed of the group-III nitride alloys. The energies of formation and band structures of various ordered compounds of InGaN, InAlN, AlGaN and InGaAlN were calculated using the full-potential linear muffin-tin orbital and density functional methods. These were used to study the miscibility and band-gap bowing in the alloy system. Bond length distributions and residual strain were found to have an important effect on these quantities. The band structure and the total energy properties of LiGaO2 were studied in relation to its possible role as a substrate for GaN growth and as a model system for cation ordering on wurtzite based lattices. The InN optical phonon modes were calculated and used to assist the interpretation of the Raman spectra obtained on bulk polycrystalline InN fabricated in the AASERT project associated with this grant. The project led to six publications among which one review book chapter and one invited conference proceedings paper.

14. SUBJECT TERMS	15. NUMBER OF PAGES
semiconductor alloys nitrides electronic structure	60
	16. PRICE CODE

17. SECURITY CLASSIFICATION OF REPORT	18. SECURITY CLASSIFICATION OF THIS PAGE	19. SECURITY CLASSIFICATION OF ABSTRACT	20. LIMITATION OF ABSTRACT
UNCLAS	UNCLAS	UNCLAS	

Final Technical Report
ONR Grant No. N00014-94-1-1000

Modeling of Wide Band Gap Semiconductor Alloys

PI: Walter R. L. Lambrecht
Department of Physics
Case Western reserve University
Cleveland, OH 44106-7079
email: wxl2@po.cwru.edu
phone: (216) 368-6120
fax: (216) 368-4671

1 Introduction

The goal of this grant was to study the properties of specific wide-band-gap semiconductor alloy systems of interest to the Electronics Division at ONR. More specifically this grant has focused on alloys related to the group-III nitrides. This class of materials is of great relevance to a variety of electronic and opto-electronic devices, notably blue LEDs (light emitting diodes) and LDs (laser diodes). The alloy properties play a crucial role in band structure engineering of the materials used in such devices.

The general questions of interest on semiconductor alloy systems which were investigated in this grant are:

- miscibility and phase diagrams
- band-gap bowing and direct vs. indirect transitions
- ordering effects
- crystal structure effects (e.g. wurtzite vs. zincblende)

Specific systems under study were $Al_xB_{1-x}N$, GaN_xP_{1-x}, $In_xGa_{1-x}N$, $In_xAl_{1-x}N$, and $Al_xGa_{1-x}N$. We also investigate a compound $LiGaO_2$ because we conjectured that it could be viewed as a model system for cation ordering in wurtzite III-N alloy systems. It is in addition of interest as a closely lattice

matched substrate for GaN growth. The references below refer to the list of publications in section 5.

2 Approach

The approach we followed was based on first-principles (i.e. local density functional) electronic structure calculations using the full-potential linear muffin-tin orbital method. This method provides the basic properties for well-defined crystal structures. To describe the disorder effects in the alloy systems, the methodology followed was to describe them in terms of a statistical average of the corresponding properties in particular crystal structures. Since these represent the various local environments, this technique is known as the cluster expansion method. Details are provided in our published papers.

A crucial question is how to deal with the bond length relaxations in those systems which contain atoms of different size. A good deal of our investigations was concerned with this question. Originally, we had hoped to be able to handle this with a semi-empirical approach such as the Keating model. This however proved to be insufficient and it was found that it could lead to inaccurate predictions such as deviations from Vegard's law [1], in particular in the way we had implemented it at first, in which the crystal was first relaxed vs. volume with ideal positions and only subsequently the atoms were allowed to relax at fixed volume. Subsequently, we spent a considerable effort to fully relax each of the structures under study to their minimum energy [2]. Finally, we realized that in a true random alloy, there is a certain amount of residual strain which has to be incorporated. We recently formulated a simple approach based on the actual bond length distribution as a function of concentration to handle this problem. This approach is similar to one that we previously had successfully applied to metalic alloy systems such as NiPt.[1]

[1] C. Amador, W. R. L. Lambrecht, B. Segall, and M. van Schilfgaarde, Strain effects on the phase diagram of Ni-Pt alloys, Phys. Rev. B **47**, 15276 (1993).

3 Technical Results

The most important results obtained during this grant are:

1. The electronic band structures and relaxed total energies were obtained for a set of zincblende based crystal structures for the In-Ga, In-Al and Al-Ga nitride alloy systems. These structures include the purely binary end compounds, the 50 % compounds in three different crystal structures: $L1_0$ (or (001)-ordering), $L1_1$ (or (111)-ordering) and chalcopyrite, and the 25 % structures in the $L1_2$ structure.

2. From these, the energies of formations as a function of concentration were determined for the disordered completely random alloys and compared to those of ordered structures. Generally, the disordered structures are found to have lower energy of formation than the so-called Connoly Williams structures of the same concentration. However, the $L1_1$ structure has higher energy and the chalcopyrite structure is a low energy structure. These findings agree with other alloy systems such as e.g. InGaAs.

3. From the band structures as a function of concentration, we can predict the direct-to-indirect transition in Al-containing alloys systems. In the Al-rich limit the gap switches from being direct at Γ to indirect at X. We also obtained the bowing coefficients. Finally, we obtained an interpolation formula for the band-gap bowing in the fully (cation) ternary system (or in more conventional terminology the fully quaternary system) $Al_xGa_yIn_zN$ with $x + y + z = 1$.

   These results were published in [2].

4. In the last stages of the proposal, we developed an "effective volume" approach to predict the miscibility phase diagrams. In this approach, we assume that the net effect of long-ranged elastic interactions leads to a distribution of bond lengths characterized by a certain amount of residual strain. We assume more precisely that the various nearest neighbor bond lengths vary linearly with concentration and can be determined by examining the dilute limits. For example, to determine the bond lenth of In-N in In-Ga alloys we examine the In-impurity in GaN and In-N bondlength in pure InN. The latter can simply be obtained

from a Keating model as described by Chen et al.[2] We use Keating model parameters obtained from our studies of the elastic constants.[3]

Next, we assume that in an alloy at concentration x, the nearest neighbor tetrahedron clusters of each type (4 In, 3 In and 1 Ga, etc.) have the corresponding bond lengths rather than the bond length which would minimize this structure when found in isolation in a pure crystal. This assumption reflects the frustration in finding the optimum relaxation in a disordered alloy. This leads effectively to a larger energy of formation than assuming perfect relaxation and thus quantifies the residual strain effect on the alloy energetics. From the complete set of results of the various crystal structures as a function of volume, we extract cluster energies $E_n(x)$ as function of bond length and hence for each concentration we can simply describe the energetics as a weigted average of $E_n(x)$ applicable at that particular concentration. Combined with the regular solution model we can then determine the spinodal and binodal curves of the miscibility gap. Our miscibility gap temperatures for InGaN are quite high, consistent with the observed tendency towards phase separation in this system. More quantitative details will be provided in a final paper, which is in preparation.

5. Some cation ordered wurtzite based structures were also calculated and their internal parameters relaxed. Their complete analysis in comparison with the zinblende results remains to be carried out. We find the energetics for wurtzite to be similar to those in corresponding zincblende alloys. In other words, the local chemistry (number of In or Ga neighbors to a N) is more important than the stacking (cubic or hexagonal). Some of these structures were inspired by the structure of $LiGaO_2$, discussed below.

[2]A.-B. Chen and A. Sher, Semiconductor pseudobinary alloys: bond-length relaxation and mixing enthalpies, Phys. Rev. B **32**, 3695 (1985).

[3]K. Kim, W. R. L. Lambrecht and B. Segall, "Elastic Constants and Related Properties of the Group-III Nitrides," in *Gallium Nitride and Related Materials*, p. 399 edited by R. D. Dupuis, F. A. Ponce, S. Nakamura, and J. A. Edmond, Mater. Res. Society Symp. Proceedings Vol. 395, (MRS, Pittsburgh 1996). and "Elastic constants and related properties of tetrahedrally bonded BN, AlN, GaN, and InN," Phys. Rev. B **53**, 16310-26, (1996); and Erratum Phys. Rev. B **56**, 7018 (1997).

6. We studied the band structure and total energy properties of $LiGaO_2$ in various structures.[3] We find the chalcopyrite structure based on zincblende to be close in energy and properties to the actual crystal structure, while alternative orderings in the wurtztie based lattice have very different energy and band gaps. We also determined the band offset of this material to GaN using the dielectric midgap level approach.

4 Impact on other research

The grant was complemented by an experimental AASERT award which had as original goal to grow $Al_xB_{1-x}N$ alloys. In the later stages of this AASERT grant, a novel method was developed to grow GaN from liquid Ga and InN from liquid In with a plasma activated nitrogen source. As part of these activities, we studied the phonon spectra of InN in order to support the experimental characterization by Raman spectroscopy [4]. This work also formed the basis for our renewal proposal which will study of the present grant which was meanwhile awarded and will among others study the growth process of GaN from liquid Ga.

The support trough this grant also allowed the PI to devote time to writing of two review articles on the band structures of the nitrides [5,6]. He also collaborated with a group of North Carolina State University, on a paper on SiC/AlN band offsets which was supported in part by ONR [7].

5 Publications and Presentations

5.1 Published papers and conference proceedings

1. W. R. L. Lambrecht, Band-gap bowing in $Ga_{1-x}In_xN$ Alloys, *Solid State Electronics*, **41**, 195-199 (1997).

2. Kwiseon Kim, Sukit Limpijumnong, Walter R. L. Lambrecht and Benjamin Segall, Theoretical study of group-III nitride alloys, in *III-V Nitrides*, ed. T. Moustakas, I. Akasaki, B. Monemar, and F. Ponce, Mater. Res. Soc. Symp. Proc. Vol. 449, (1997), p. 925-930

3. Sukit Limpijumnong, Walter R. L. Lambrecht, Benjamin Segall, and Kwiseon Kim, Band structure and cation ordering in $LiGaO_2$, in *III-V*

Nitrides, ed. T. Moustakas, I. Akasaki, B. Monemar, and F. Ponce, Mater. Res. Soc. Symp. Proc. Vol. 449, (1997), p. 905-910

4. J. S. Dyck, K. Kash, K. Kim, W. R. L. Lambrecht, C. C. Hayman, A. Argoitia, M. T. Grossner, W. L. Zhou, and J. C. Angus, Characterization of bulk, polycrystalline indium nitride grown at sub-atmospheric pressures, in *Nitride Semiconductors*, edited by S. DenBaars, S. Nakamura, B. Meyer, F. Ponce, and T. Strite, Mater. Res. Soc. Symp. Proc. Vol. 482, (1998), to be published.

5. W.R.L. Lambrecht, Band structure of the group-III nitrides, Chapter 12, pp. 369-407, in *III-Nitrides*, edited by J. I. Pankove and T. D. Moustakas, Semiconductors and Semimetals, Vol. 50, Series editors E. Weber and B. Willardson, (Academic Press, New York 1997)

6. W. R. L. Lambrecht, K. Kim, S. N. Rashkeev, and B. Segall, "Electronic and Optical Properties of the Group-III Nitrides, their Heterostructures and Alloys," in *Gallium Nitride and Related Materials*, edited by R. D. Dupuis, F. A. Ponce, S. Nakamura, and J. A. Edmond, Mater. Res. Society Symp. Proceedings Vol. 395, (MRS, Pittsburgh 1996), p.455

7. S. W. King, M. C. Benjamin, R. J. Nemanich R. F. Davis, and W. R. L. Lambrecht, "XPS Measurement of the SiC/AlN Band-offset at the (0001) Interface," in *Gallium Nitride and Related Materials*, p. 375. edited by R. D. Dupuis, F. A. Ponce, S. Nakamura, and J. A. Edmond, Mater. Res. Society Symp. Proceedings Vol. 395, (MRS, Pittsburgh 1996).

Copies of these papers are attached.

5.2 Presentations

1. Elastic Constants and deformation potentials of BN, AlN, GaN and InN, Kwiseon Kim, W. R. L. Lambrecht and B. Segall, Bull.Am. Phys. Soc. 40(1995)773(Q25.10) APS March Meeting 1995.

2. Electronic Properties of the Group-III Nitrides and Their Alloys, W. R. L. Lambrecht, K. Kim, and B. Segall, Topical Workshop on III-V Nitrides, Nagoya, Sept. 1995

3. Electronic and optical properties of the Group-III Nitrides, their heterostructures and alloys, W. R. L. Lambrecht, K. Kim, and B. Segall, First International Symposium on Gallium Nitride and Related Materials, MRS Fall Meeting Symposium AAA, Boston , Nov. 1995 (invited)

4. Elastic constants and related properties of the Group-III Nitrides, K. Kim, W. R. L. Lambrecht, and B. Segall, First International Symposium on Gallium Nitride and Related Materials, MRS Fall Meeting Symposium AAA, Boston , Nov. 1995

5. XPS measurement of the SiC/AlN band-offset at the (0001) Interface, Sean King, M. C. Benjamin, R. J. Nemanich, R. F. Davis, and W. R. L. Lambrecht, First International Symposium on Gallium Nitride and Related Materials, MRS Fall Meeting Symposium AAA, Boston , Nov. 1995

6. 7th Chemnitzer-Physik-Symposium – International Workshop on *First-principles, tight-binding and empirical methods for materials simulation*, Cheminitz, June 1996, invited talk on "Electronic and related properties of nitrides and SiC".

7. American Physcial Society March Meeting 1996, Kwiseon Kim, W. R. L. Lambrecht and B. Segall, contributed paper on "Effective Masses and Kohn-Luttinger Parameters in Zincblende and Wurtzite Group-III Nitrides," *Bull. Am. Phys. Soc* **41**, No. 1 (1996), p. 262, abstract F26.9

8. Materials Research Society Spring Meeting 1996, San Francisco, Symposium on *III-Nitride, SiC and Diamond Materials for Electronic Devices*, W. R. L. Lambrecht, B. Segall, and K. Kim, contributed paper on "Band-gap bowing and energy of formation in III-N alloys."

9. 13th North Coast Symposium AVS, Ohio Chapter, Cleveland, June 6, 1996, K. Kim, S. Limpijumnong, W. R. L. Lambrecht and B. Segall, contributed paper on "Band-gap bowing and energy of formation in $In_xGa_{1-x}N$ alloys."

10. Materials Research Society Fall Meeting 1996, Boston, Symposium on *III-V Nitrides*, Kwiseon Kim, Sukit Limpijumnong, Walter R. L. Lam-

brecht and Benjamin Segall, conrributed paper on "Theoretical study of group-III nitride alloys."

11. Materials Research Society Fall Meeting 1996, Boston, Symposium on *III-V Nitrides*, Sukit Limpijumnong, Walter R. L. Lambrecht, Benjamin Segall, and Kwiseon Kim, contributed paper on "Band structure and cation ordering in $LiGaO_2$."

12. Kwiseon Kim, Sukit Limpijumnong, W. R. L. Lambrecht, Benjamin Segall, Electronic structure and equilibrium properties of group III-Nitride alloys, Bull. Am. Phys. Soc. **42**, E22.09, p.210, (1997)

13. Sukit Limpijumnong, Kwiseon Kim, Walter R. L. Lambrecht, Benjamin Segall, Cation ordering in $LiGaO_2$ as a model structure for wurtzite alloys, Bull. Am. Phys. Soc. **42**, E22.10, p.210, (1997).

Pergamon

PII: S0038-1101(96)00165-7

Solid-State Electronics Vol. 41, No. 2, pp. 195–199, 1997

0038-1101/97 $17.00 + 0.00

BAND-GAP BOWING IN $Ga_{1-x}In_xN$ ALLOYS

WALTER R. L. LAMBRECHT

Department of Physics, Case Western Reserve University, Cleveland, OH 44106-7079, U.S.A.

Abstract—The band-gap bowing in $Ga_{1-x}In_xN$ is studied by means of linear muffin-tin orbital band structure calculations within the local density functional approach. A "virtual crystal"-like approximation is compared with the Connolly–Williams cluster expansion approach with and without volume and bond-length relaxations. A progressively stronger bowing is found as the physical model's complexity is increased. The final bowing parameter obtained is 2.6 eV, which is significantly larger than the value reported in the literature. © 1997 Elsevier Science Ltd

1. INTRODUCTION

The band-gap bowing in $Ga_{1-x}In_xN$ alloys is of significant interest for their use as active light-emitting layers in opto-electronic devices because the band-gap emission in this alloy system spans the violet to orange regions of visible light. Only limited experimental information[1] is available on the band-gap bowing because of the difficulties in obtaining homogeneous and high quality $Ga_{1-x}In_xN$ of high In content. From the theoretical point of view, the significant lattice mismatch between InN and GaN (about 10%) makes this system more challenging than the $Al_xGa_{1-x}N$ studied in earlier work[2].

In this paper, we present a study of the band-gap bowing with a progressively more complete physical model. We progress from a virtual-crystal type approximation to a cluster expansion statistical description within ideal structures, to a model in which volume relaxation and finally bond-length relaxations are taken into account. Ordering effects on the band gap are also briefly touched upon. We find a progressively stronger bowing as the complexity of the model is increased. After briefly describing the underlying computational method, we describe the results and end with a comparison of our results with literature data.

2. COMPUTATIONAL METHOD

The first principles band structure calculations reported here were carried out using the linear muffin-tin orbital (LMTO) method[3] in the atomic sphere approximation (ASA). The potential in this method is determined self-consistently within the local density approximation (LDA) to density functional theory[4]. As is well known, the LDA Kohn–Sham eigenvalues, which are not quasi-particle eigenvalues, underestimate the band gaps—by 1.0 eV for GaN and 1.7 eV in InN[5,6]. However, the required self-energy correction is expected to be fairly independent of structure[7,8] and can thus simply be linearly interpolated for the alloys. The calculations reported here are for the zincblende structure. We note that the valence-band maxima and conduction-band minima in both GaN and InN and in both zincblende and wurtzite occur at the Γ point. Since the corresponding states are very similar in nature in both structures, we expect the gap bowing in zincblende to be nearly the same as that in wurtzite. The only difference is that the absolute values of the gap are slightly smaller in the former—by 0.4 eV in both InN and GaN. The details of the methodology for alloy modelling are described below.

3. RESULTS

The first model we applied is a virtual crystal type approximation. Within the LMTO-ASA method, the Hamiltonian is described by a set of potential-independent structure constants $S_{RL,R'L'}$ where R denotes atomic sites and $L = (l,m)$ the spherical harmonic component, and a set of potential parameters—C_{al}, Δ_{al}, γ_{al} and p_{al}—describing the scattering at each type of atomic sphere a and for each angular momentum channel $l = (s,p,d)$. The C_{al} define essentially the center of the corresponding unhybridized bands which can be thought of as atomic energy levels, and the Δ_{al} define the corresponding widths ofthe bands and can be thought of as parametrizing the hopping integrals as $\sqrt{\Delta_{Rl}}S_{RL,R'L'}\sqrt{\Delta_{R'l'}}$. We now define virtual crystal averaged potential parameters by interpolating the corresponding parameters for InN and GaN, i.e.

$$C_{al}(x) = xC_{al}^{In} + (1-x)C_{al}^{Ga}, \tag{1}$$

and

$$\Delta_{al}(x) = (\Delta_{al}^{In})^x(\Delta_{al}^{Ga})^{1-x}. \tag{2}$$

The remaining parameters define further details in the dispersion of the bands which are less atom specific. To be unbiased, we average them linearly as in eqn (1). Within this approach, each cation is defined as an average cation with mixed In and Ga-like scattering properties and each nitrogen, N, is defined as an effective N with average scattering properties of those in InN and GaN. (We also average the parameters of the empty spheres that are introduced in the interstitial region as is necessary for open structures like zincblende.) This LMTO virtual crystal approximation (VCA) is in fact closer in spirit to the average t-matrix approximation because it is the scattering properties that are averaged rather than the potential. The results of this approach are shown as the squares interpolated by the full line in Fig. 1 and show a fairly small band-gap bowing. For convenience the linear interpolation between GaN and InN is indicated by the long dashed line.

Next, we incorporate the effect that in a real alloy, the atoms are actually either In or Ga rather than an average atom and thus different local neighborhoods exist around each N atom. This can be done by means of a cluster expansion approach[9]. Considering the tetrahedral nearest neighbor environment of each N atom, its surrounding cations can either be 4 Ga, or 3 Ga and 1 In, or 2 Ga and 2 In, or 1 Ga and 3 In, or 4 In. In the alloy of a given average In concentration x, each of these cluster configurations which can be specified by the number of In atoms $n = 0, \ldots, 4$ occur with certain probabilities $P_n(x,T)$ which generally depend on temperature T. In a general cluster expansion technique, not only tetrahedral nearest neighbor clusters but longer-range

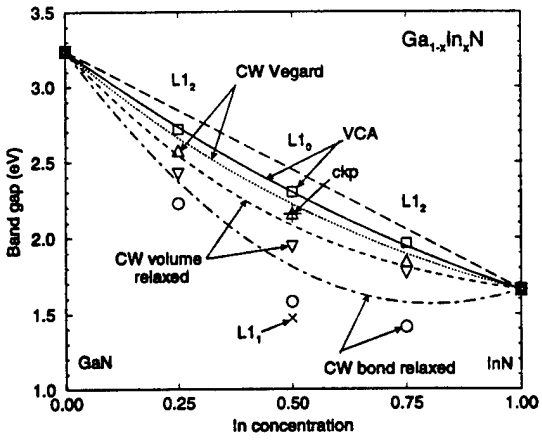

Fig. 1. Band gap of zincblende based $Ga_{1-x}In_xN$ alloys and ordered compounds in various models: VCA (□), quadratic interpolation through VCA (full line), CW structures with Vegard's law (△), random alloy deduced from it (dotted line), CW structures volume relaxed (▽), random alloy deduced from it (dashed line), CW with bond relaxation (○), random alloy deduced from it (dot-dashed line), ideal $L1_1$ ordering (×), ideal chalcopyrite (+). All LDA gaps are corrected by self-energy correction. Wurtzitic gaps are expected to be 0.4 eV higher.

pairs, triplet, quadruplet, etc., correlation functions are considered. Here we use only the tetrahedron approximation. For a system in thermal equilibrium the $P_n(x,T)$ can be determined by minimizing the total free energy. However, since non-equilibrium growth techniques are used to deposit III-nitride alloys from a gas phase, it is not very relevant here to solve this complex problem. Since a realistic modelling of the non-equilibrium growth process is far beyond the scope of this paper, we bypass the problem completely by simply assuming a random distribution of the clusters, which implies

$$P_n(x) = \binom{4}{n} x^n (1-x)^{4-n}. \tag{3}$$

In order to obtain the effective cluster parameters for the band-gap, we use the Connolly–Williams (CW) approach[10]. The desired quantity is calculated from first principles for a number of ordered configurations (i.e. crystal structures) and is expanded in a similar manner as the disordered configuration in the effective cluster interaction parameters. If the number of ordered configurations considered equals the number of cluster parameters to be determined, the resulting set of equations can be inverted. This is particularly simple for the tetrahedron approximation within the fcc sublattice of cations. Corresponding to each cluster one can find an ordered crystal configuration in which this cluster is the only one that occurs. The cluster parameter can thus be identified directly with the corresponding property for that particular ordered configuration. Specifically, the Ga_4 cluster corresponds to pure GaN; the Ga_3In cluster corresponds to the $L1_2$ ordered fcc based structure, in which the Ga atoms are placed in the face centers of the cube and the In atoms on the corners; and the Ga_2In_2 cluster corresponds to the $L1_0$ structure which consists of alternating (001) layers of Ga and In cations. The other ones are obviously obtained by replacing In by Ga. In addition to this "basis set" of CW structures from which we calculate the disordered random alloy properties, we have also considered a few other ordered structures to test how much the band gap depends on ordering. The other structures considered are the $L1_1$ structure which consists of alternating (111) layers of In and Ga, and the chalcopyrite (ckp) structure. The latter has been found to be more stable than the disordered alloy in alloys with large bond-length mismatch, in particular in $In_xGa_{1-x}As$[11]. Both correspond to 50% In.

We first assume ideal ordered compounds, in which all bond-lengths are equal and assume a lattice constant which follows Vegard's law, i.e. it is assumed to be linearly varying with the concentration. In Fig. 1, the calculated values for the band gap for the CW structures within this Vegard's law approximation are indicated by △. The band-gap behavior for the random alloy deduced from it in the

way explained above is indicated by the dotted line. The chalcopyrite structure and $L1_1$ gaps are indicated by + and × respectively.

We note first of all that the band-gap bowing within this model is slightly stronger than that in the VCA. Secondly, we note that the gaps of each of the ordered CW compounds are slightly lower than those of the random alloy of the same concentration. The gap of the (111) ordered compound ($L1_1$) is remarkably lower. This indicates that layer by layer growth of a (111) oriented 1 + 1 superlattice may result in even lower band gaps for $InGaN_2$ than the random alloy. This is relevant because a similar result is expected for a (0001) wurtzitic alternating In and Ga layered structure. Since this is the commonly used growth direction, this possibility is realistic. We also note that the chalcopyrite band gap is slightly closer to the random alloy line than the $L1_0$ structure. This is consistent with the fact that the ckp is one of the so-called special quasi-random structures (SQS)[12] which have correlation functions close to those of the random configuration. In other words, this special structure is a good representative of the random alloy.

Next, we consider relaxation effects. First, we keep the geometries ideal but allow the volume to relax. Figure 2 shows the variation of the calculated equilibrium lattice constant with concentration. A deviation from Vegard's law is clearly visible. The resulting gaps of the CW structures shown by ▽ in Fig. 1 and the random alloy gap deduced from it is shown by the dashed line. We note that this effect tends to increase the bandgap bowing substantially.

Finally, we allow the individual bond lengths to relax. Because the InN and GaN bond lengths can relax towards their ideal values (those in pure InN and pure GaN) by a simple displacement of the N sublattice, only weakly coupled to the overall lattice constant, such a displacement is expected to occur fully if only bond stretch force constants were

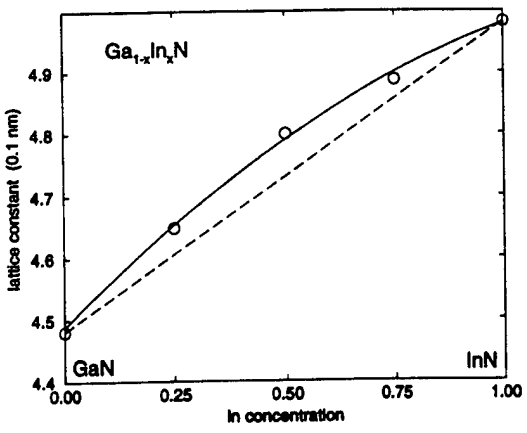

Fig. 2. Lattice constant in $Ga_{1-x}In_xN$ alloys. Vegard's law (dashed line), calculated equilibrium (○) with quadratic interpolation (full line).

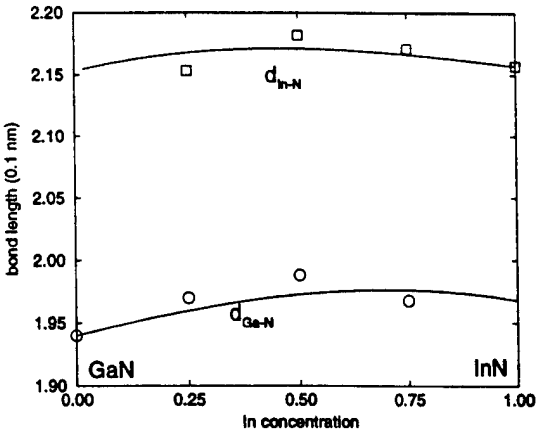

Fig. 3. Bond lengths in $Ga_{1-x}In_xN$ ordered CW compounds calculated using Keating's model: In–N (□) and Ga–N (○), and random alloy bond lengths (full lines) deduced from them.

present. The competition with bond angle deviations from perfect tetrahedral angles of 109° limits the bond-length relaxation. The well-known Keating model is adequate to deal with this optimization problem. The parameters for the Keating model of InN and GaN were derived from our calculated elastic constants and from experimental LO–TO phonon splittings[15]. From the individual bond lengths of the ordered compounds, the bond lengths in the random alloy are modelled by the cluster expansion

$$d^{AC}(x) = \frac{\Sigma_n P_n(x)\omega_n^{AC} d_n^{AC}}{\Sigma_n P_n(x)\omega_n^{AC}}, \tag{4}$$

where ω_n^{AC} is the number of AC-bonds in CW structure n. The resulting biomodal bond-length distribution is shown in Fig. 3. The band gaps obtained for the CW structures relaxed in that manner are indicated by circles in Fig. 1 and the random alloy gap deduced from it is shown by the dash–dotted line. We note that this has a substantial effect on the band-gap bowing.

Further work is necessary to investigate the combined effects of bond-length relaxation and volume relaxation. The bond-length relaxation could partially compensate for the deviation from Vegard's law and thus somewhat reduce the band-gap bowing. Also, in our present volume relaxed approach (with and without cation–anion bond-length relaxation) the average cation–cation distance is determined by the equilibrium lattice constant of the corresponding CW structure. This means that each cation tetrahedron cluster is implicitly assumed to be fully relaxed. Because each cluster is not independent of the other ones but embedded in a surrounding medium, this is not exactly the case in a truely random alloy[13,14]. We expect that neglecting this effect may lead to a slight overestimate of the band-gap bowing.

Table 1. Band-gap bowing coefficient b in $Ga_{1-x}In_xN$ alloys in various models

Model	b (eV)
VCA	0.60
CW volume interpolated	0.89
CW volume relaxed	1.45
CW bond relaxed	2.57
Expt[a]	1.00

[a]Osamura *et al.*[1].

The band-gap bowing is conveniently described by means of a bowing parameter defined as the coefficient of the quadratic term $bx(1-x)$ in the alloy gap as a function of concentration. Table 1 summarizes the band-gap bowing coefficients obtained in each of the treatments discussed above. We also include the experimental value for the bowing coefficient given by Osamura *et al.*[1].

Our calculated energies of formation E_f are quite large, of the order of 0.3 eV/atom for the (unrelaxed) 50% compound. The relaxation energy could not be calculated accurately with the Keating or ASA approach, but is expected to reduce E_f substantially. Even with E_f of the order of 0.1 eV/atom, though, the tendency towards phase separation is large in this system. This is consistent with experimental findings by Osamura *et al.*[1], who found phase separation behavior upon annealing above 600°C.

In order to properly discuss energies of formation E_f of different ordered and disordered structures, the chalcopyrite and $L1_1$ structure need to be relaxed. This should be done by means of full-potential LMTO calculations and is postponed to future work. At present, for the ideal structures, we obtain $E_f(L1_1) < E_f(\text{ckp}) < E_f(L1_0)$. This is the expected ordering for lattice-matched semiconductors[11]. However, relaxation effects are expected to change this ordering[11].

4. DISCUSSION

We find a substantially larger bowing coefficient than previously given in the literature[1]. However, in Osamura *et al.*[1] the concentration was obtained by measuring the change in lattice constant from X-ray diffraction data and by assuming Vegard's law to hold. Because of the upward bowing of the lattice constant seen in Fig. 2, this procedure overestimates the In concentration and hence underestimates the band-gap bowing. Using our calculated deviation from Vegard's law to correct the concentrations in the data of Osamura *et al.* we estimate that his measured band-gap bowing coefficient should be increased to ~ 1.8 eV. We conclude that it is important to do an independent measurement of the lattice constant and the In concentration. Inhomogeneities in the films, which are not unlikely given the tendency towards phase separation, may also contribute to uncertainties in the value of the band gap.

Other theoretical approaches, e.g. Jenkins and Dow[16] and Nakajima *et al.*[17], used a virtual crystal approximation combined with the tight-binding method and, as expected, obtain small bowing coefficients. As suggested above, some further refinements in the present calculations are desirable and may slightly overestimate our band-gap bowing. Nevertheless, we expect our main conclusion of a substantially larger bowing than previously accepted to hold.

We finally note that recent reports by Singh and Moustakas [18] and Scholz *et al.*[19] provide evidence of a larger bowing in $In_xGa_{1-x}N$ alloys than previously reported[1]. Unfortunately, these reports do not yet allow a quantitative determination of the bowing coefficient.

5. CONCLUSION

Using first-principles LMTO calculations, we have shown that local variations in bonding environment, deviations from Vegard's law, and bond-length relaxations each contribute substantially to the band-gap bowing parameter in $Ga_{1-x}In_xN$ alloys, which is found to be about 2.6 eV.

Acknowledgements—This work was supported by NSF (DMR92-22387) and ONR (N00014-94-1-100). I thank B. Segall for stimulating discussions.

REFERENCES

1. K. Osamura, S. Naka and Y. Murakami, *J. Appl. Phys.* **46**, 3432 (1975).
2. E. A. Albanesi, W. R. L. Lambrecht and B. Segall, *Phys. Rev. B* **48**, 17841 (1993).
3. O. K. Andersen, O. Jepsen and M. Šob, in *Electronic Band Structure and its Applications* (edited by M. Yusouff), p. 1. Springer, Heidelberg (1987).
4. W. Kohn and L. J. Sham, *Phys. Rev.* **140**, A1133 (1965).
5. W. R. L. Lambrecht and B. Segall, in *Properties of Group-III Nitrides* (edited by James H. Edgar), Chap. 4, pp. 125–156. Institution of Electrical Engineers, London (1994).
6. W. R. L. Lambrecht, B. Segall, J. Rife, W. R. Hunter and D. K. Wickenden, *Phys. Rev. B* **51**, 13516 (1995).
7. A Rubio, J. L. Corkhill, M. L. Cohen, E. Shirley and S. G. Louie, *Phys. Rev. B* **48**, 11810 (1993).
8. W. R. L. Lambrecht, B. Segall, M. Yoganathan, W. Suttrop, R. P. Devaty, W. J. Choyke, J. A. Edmond, J. A. Powell and M. Alouani, *Phys. Rev. B* **50**, 10722 (1994).
9. J. M. Sanchez, F. Ducastelle and D. Gratias, *Physica A* **128**, 334 (1984).
10. J. W. D. Connolly and W. R. Williams, *Phys. Rev. B* **27**, 5169 (1983).
11. S.-H. Wei, L. G. Ferreira and A. Zunger, *Phys. Rev. B* **41**, 8240 (1990).
12. A. Zunger, S.-H. Wei, L. G. Ferreira and J. E. Bernard, *Phys. Rev. Lett.* **65**, 353 (1990).
13. A.-B. Chen and A. Sher, *Phys. Rev. B* **32**, 3695 (1985); A. Sher, M. van Schilfgaarde, A.-B. Chen and W. Chen, *Phys. Rev. B* **36**, 4279 (1987).

14. C. Amador, W. R. L. Lambrecht, M. van Schilfgaarde and B. Seagall, *Phys. Rev. B* **47**, 15276 (1993).
15. K. Kim, W. R. L. Lambrecht and B. Segall, *Phys. Rev. B* **53**, 16310 (1996).
16. D. W. Jenkins and J. D. Dow, *Phys. Rev. B* **39**, 3317 (1989).
17. S. Nakajima, T. Yang and S. Sakai, *Silicon Carbide and Related Materials*, (Edited by S. Nakashima, H. Matsunami, S. Yoshida and H. Harima), p. 947. IDP, London (1996).
18. R. Singh and T. D. Moustakas, in *Gallium Nitride and Related Materials* (Edited by F. A. Ponce, R. D. Dupuis, S. Nakamura and J. A. Edmond), p. 163. MRS Pittsburgh, PA (1996).
19. F. Scholz, V. Härle, H. Bolay, F. Steuber, B. Kaufmann, G. Reyher and A. Dörnen, *Solid-St. Electron.* **41**, 141 (1997).

THEORETICAL STUDY OF GROUP-III NITRIDE ALLOYS

KWISEON KIM, SUKIT LIMPIJUMNONG, WALTER R. L. LAMBRECHT and B. SEGALL
Department of Physics, Case Western Reserve University, Cleveland, OH 44106-7079

ABSTRACT

Band gap bowing, structural relaxations, and energies of formation were calculated for the three pseudobinary nitride zincblende alloy systems Al-Ga, In-Ga and In-Al using the full-potential linearized muffin-tin orbital method. The cluster expansion and Connolly-Williams approaches were used to relate calculated band structures and energies of formation of ordered compounds to the behavior of disordered alloys. Effects of bond length and volume variation on those properties are discussed. An interpolation formula for the gap of the full pseudoternary $Al_xGa_yIn_zN$ system is proposed and tested by separate calculations. Extension of the results to the wurtzite alloys is discussed.

INTRODUCTION

Alloying among group-III nitrides in principle allows one to change the band gap from 1.9 eV in InN, to 6.3 eV in AlN. GaN intermediate in the series has a bandgap of 3.5 eV. Previous theoretical studies and most experimental work (see e.g. [1]) have focused on the pseudobinary[1] alloy combinations, AlGaN and InGaN [2, 3, 4]. However, for each concentration in those alloy systems, both the gap and the lattice constant are determined. Pseudoternary systems allow more freedom. For any desired band gap (except those for the extremes), there are several possible alloy combinations and hence lattice constants to choose from. Since it is desirable to have different layers in a heterostructure lattice-matched, it is useful to employ the full pseudoternary $Al_xGa_yIn_zN$ system ($x+y+z=1$). To guide such an alloy design, an accurate knowledge of the band gap and the lattice constant as functions of x, y and z is required.

A second important concern for the alloy design is the issue of phase separation. While it is widely believed that the nitrides are fully miscible, there is, in reality, a miscibility gap. In a closely lattice-matched $Al_xGa_{1-x}N$ alloy system, the miscibility gap temperature was shown [2] to be rather low and hence at a typical growth temperature one may expect to have a true solid solution. In $In_xGa_{1-x}N$, however, phase separation problems have been reported experimentally [5, 6].

In this paper, we present the first systematic study of the full psudoternary system using throughout the same first-principles computational scheme and including an accurate treatment of bond length relaxations.

METHOD OF CALCULATION

Our alloy model is based on the cluster expansion approach [7]. While the natural crystal structure for the nitrides is the wurtzite (wz), zincblende (zb) structures have also been stabilized. Since there is considerably more experience with alloy modeling in cubic

[1]We call and $A_xB_{1-x}N$ alloy pseudobinary and an $A_xB_yC_zN$ alloy pseudoternary to emphasize that the composition variation and disorder pertain only to the cation sublattice. The commonly used terminology is ternary for the former and quaternary for the latter.

Mat. Res. Soc. Symp. Proc. Vol. 449 © 1997 Materials Research Society

based materials than in hexagonal based materials, we have started our alloy investigation for the zincblende-based structures. Nevertheless, our results can easily be adapted to wz alloys because the electronic structure in both crystal structures are closely related and the relations between the two are well understood [8]. The wz/zb total energy differences are much smaller than the typical alloy energy differences. Direct calculations for wz alloys to verify these predictions are in progress.

As in previous work,[2, 4] we use the Connolly-Williams method [9] to obtain average properties of disordered alloys,

$$\overline{\Omega}(x) = \sum_n P_n(x,T)\Omega_n, \qquad (1)$$

where Ω is the property of interest, e.g. band gap or energy of formation, $\overline{\Omega}(x)$ is its ensemble averaged value for alloy concentration x, Ω_n the contribution from "cluster" n and $P_n(x,T)$ the frequency of occurrence of cluster n in a disordered alloy of concentration x and at temperature T. Specifically, we use the nearest neighbor tetrahedron approximation, in which case $n = 0 \ldots 4$ labels the number of B atoms in the $A_{4-n}B_n$ tetrahedron surrounding each anion C. Because thermodynamic equilibrium is not guaranteed under typical growth conditions for nitrides, we assume truly random probabilities $P_n(x,T) = \binom{4}{n} x^n (1-x)^{4-n}$ for simplicity. The values associated with each cluster n are obtained by using a similar expansion for known ordered compounds, for which we choose the usual fcc based structures, $L1_0$, $L1_2$ and pure fcc. Some additional ordered structures, such as chalcopyrite and $L1_1$, are calculated to investigate the sensitivity of the properties to particular ordering.

The main difference from our previous work is the way in which we treat bond-length relaxations. In a previous report on $In_xGa_{1-x}N$ by one of the authors [4], a rather high energy of formation was found and it was suggested that deviations from Vegard's law might be important in this system. However, as was cautioned in that work, the structural relaxation was not fully taken into account. In the ideal structure, the volume was relaxed first. The internal parameter, the relative position of nitrogen atom to cations, was then relaxed at the fixed volume. We will show here that a significantly smaller deviation from Vegard's law is found when the minimum energy is calculated with relaxed bond lengths at each volume. This also has important consequences for the band-gap bowings and the energies of formation which determine the miscibility gap. We find, in fact, that the band gap bowing is predominantly determined by the lattice constant since the various calculated results fall on a single curve when the band gap is plotted as a function of lattice constant (see Fig. 1(b)) instead of as a function of concentration. The present work assumes that full relaxation of the second nearest neighbor distance can take place. This may not be completely the case in a disordered alloy because of the residual strain [10] and may lead to a slight underestimate of the present energies of formation and bowing coefficients. Still, this residual strain would result from frustration due only to disorder in the cation lattice and not because of the unrealistic strain induced by keeping nearest neighbor cation-anion bond lengths unrelaxed, which in the previous work [4], yielded a significant overestimate of energies of formation and band-gap bowings.

We use the full-potential linearized muffin-tin orbital method [11] in conjunction with the local density functional theory (LDA) [12] with Hedin-Lundqvist parametrization [13] for all band structure and total energy calculations. Details of the method as applied to the nitrides are given elsewhere [14].

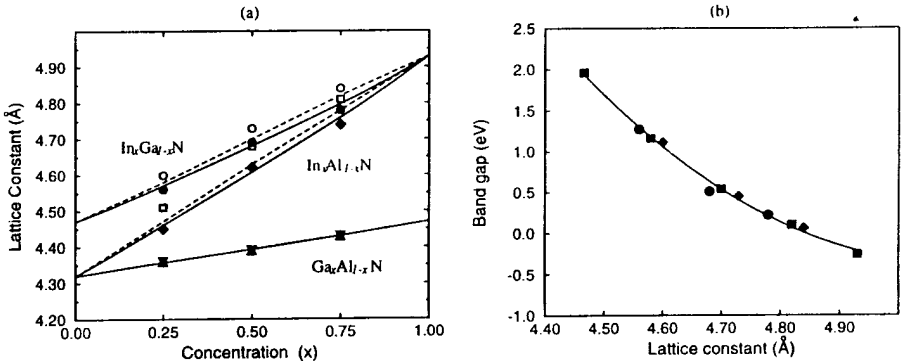

Figure 1: (a) Lattice constants of III-N alloy systems vs. concentration: dashed lines, Vegard's law; open symbols, volume relaxation only; filled symbols, full relaxation of bond lengths; solid lines, random alloy deduced from full relaxation. (b) Band gap (LDA) of $In_xGa_{1-x}N$ ordered compounds as a function of lattice constant: squares, Vegard's law; diamonds, volume relaxation only; circles, full relaxation; solid line, best fit parabola.

RESULTS AND DISCUSSION

Fig. 1(a) shows the lattice constants of the three pseudobinary nitride alloy systems as functions of concentration, once with only volume relaxation and ideal (i.e. equal bond length) structures, and once with full relaxation of the internal parameters before volume relaxation. It can be seen that the second set of results are much closer to Vegard's law, particularly for the $In_xAl_{1-x}N$ alloys where the lattice mismatch is the largest.

Fig. 1(b) shows the band gap as a function of lattice constant for $In_xGa_{1-x}N$ using the two relaxation approaches mentioned above. One can see that all results fall on the same curve, showing that the lattice constant is the primary factor in determining the band-gap bowing.

Fig. 2(a) shows the band gaps of $In_xGa_{1-x}N$ in our final fully relaxed calculation as a function of concentration for the various ordered compounds and the ensemble averaged value for the disordered compound deduced from it. One may note that the value of chalcopyrite lies on the disorder averaged line. This confirms the fact that the relaxations in chalcopyrite and the cation ordering are good representatives of average random behavior. This is the main idea behind the use of so-called special quasirandom structures [15]. We also see that particular ordered structures such as the $L1_1$ may have significantly lower gaps than the average. This can, in this case, be traced back to the occurrence of only A_3B and AB_3 tetrahedra as opposed to the A_2B_2 tetrahedra which predominate in the random alloy.

Since the wz and zb gaps are both direct at Γ in InN and GaN and differ only by a constant of about 0.3 eV in each case, we expect that the zb bowing coefficients should also apply to wz. The nearest neighbor ordering in a 1 + 1 (0001) superlattice of wz structure is the same as in the $L1_1$ structure. It is thus of interest to note that the calculated gaps for the superlattice, 3.14 eV, 1.26 eV, and 0.51 eV for $AlGaN_2$, $AlInN_2$, and $GaInN_2$ repectively, are indeed close to the values of $L1_1$, 3.04 eV, 1.13 eV, and 0.38 eV after including the constant shift between wz and zb gaps.

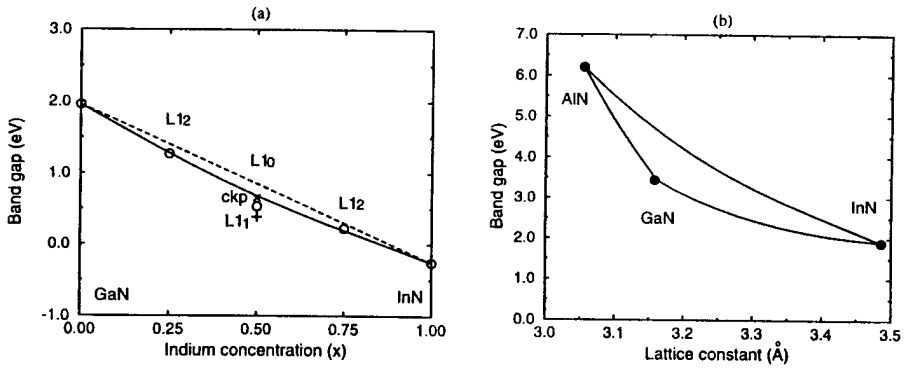

Figure 2: (a) Band gap (LDA) of $In_xGa_{1-x}N$ in ordered compounds and configurational average (solid line). Deviations from the linear variation (shown by the dashed line) correspond to the bowing. (b) Band gap (including estimated self-energy corrections, see text) of wurtzite III-nitride alloys as a function of wurtzite lattice constant.

We note that here we have shown the LDA gaps which are well known to be too small by a self-energy correction of about 1 eV in GaN, 2 eV in AlN and InN. Assuming that the correction varies linearly with concentration, it will not affect the bowing coefficients. In Fig. 2(b) we show the configurationally averaged band gaps of the three pseudobinary wurtzite alloy systems as a function of the wurtzite lattice constant. These were obtained by assuming that the wz gaps differ from the zb direct gaps by a constant shift. Self-energy corrections were linearly interpolated between those for the end point pure compounds, which in turn were chosen so as to yield the experimental gaps. We see that all of the curves can be well approximated by parabolas.

For the full pseudoternary system $Al_xGa_yIn_zN$, we propose the following interpolation scheme for the gap:

$$\begin{aligned} E_g(x,y,z) &= xE_g(\mathrm{AlN}) + yE_g(\mathrm{GaN}) + zE_g(\mathrm{InN}) \\ &\quad -b(\mathrm{AlGaN})xy - b(\mathrm{InGaN})yz - b(\mathrm{InAlN})xz, \end{aligned} \tag{2}$$

with b(AlGaN) the bowing coefficient of $Al_xGa_{1-x}N$, etc. Values for the bowing parameters are given in Table I. To test this equation we have directly calculated the gaps of several pseudoternary compounds. Full structural details on those calculations will be given elsewhere. They are obtained by a substitution in the $L1_2$ structures. The comparison between

Table I: Bowing parameters of of III-Nitrides in eV.

compound	b
AlGaN	0.27
AlInN	1.67
GaInN	0.69

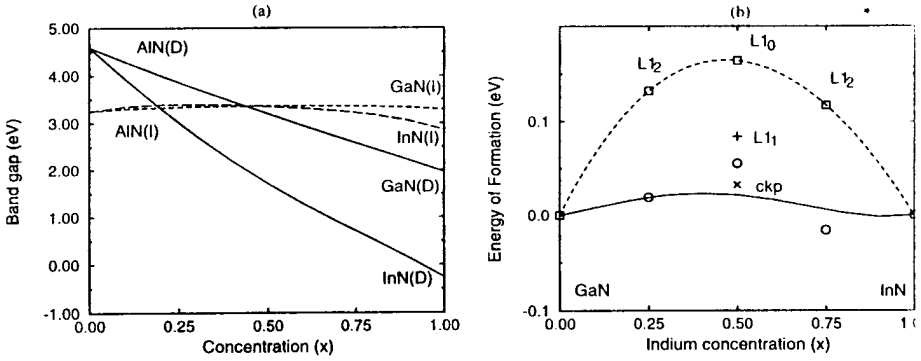

Figure 3: (a) Direct(solid line) and indirect(short dashed and long dashed lines) band gaps in $Ga_xAl_{1-x}N$ and $In_xAl_{1-x}N$ alloys. (b) Energy of formation of $In_xGa_{1-x}N$ alloys: squares, Vegard's law; dashed line, fit; circles, full bond length relaxation; solid line, random alloy deduced from it.

the results predicted by Eq. 2 and the directly calculated values is shown in Table II. The agreement is reasonably good.

Since AlN has an indirect gap at X in zb, it is also of interest to consider the X gaps as functions of concentration in InAlN and GaAlN. These are shown along with the direct gaps in Fig. 3(a). The indirect gaps are seen to vary much less with concentration than do the direct gaps. This is because the p-like states involved in the X-gap are less sensitive to the nuclear charge than are the s-like states involved in the minimum at Γ. The curves indicate that the crossover between the direct and the indirect gaps takes place at $x = 0.44$ and 0.19 for $Ga_xAl_{1-x}N$ and $In_xAl_{1-x}N$ respectively.

Fig. 3(b) shows the energy of formation of $In_xGa_{1-x}N$ as a function of concentration in various relaxation steps. It is evident that the relaxation of bond lengths has a strong and asymmetric effect on the energy of formation. The formation energies at 50 % give a rough indication of the tendency towards phase separation [2] because in a simple regular solution model it is proportional to the miscibility gap temperature T_{MG}. They are 20 meV/atom, 25 meV/atom and 12 meV/atom respectively for $In_xGa_{1-x}N$, $In_xAl_{1-x}N$ and $Ga_xAl_{1-x}N$. While a reliable calculation of T_{MG} would need a more advanced theory in view of the asymmetry of the energy of formation curve, the relative values indicate that T_{MG} for the In-containing systems would be about twice those of the $Al_xGa_{1-x}N$ system.

Table II: Band gaps (LDA) of pseudoternary III-Nitrides in eV.

compound	calculated value	interpolation
$Al_{0.25}Ga_{0.25}In_{0.5}N$	1.05	1.12
$Al_{0.25}Ga_{0.5}In_{0.25}N$	1.64	1.79
$Al_{0.5}Ga_{0.25}In_{0.25}N$	2.14	2.39

This is consistent with the experimental indications that higher growth temperatures are needed to incorporate In into the alloys. Kinetic effects may also play a role in this issue.

CONCLUSIONS

We have presented FP-LMTO results for the three pseudobinary alloy systems and the full pseudoternary $Al_xGa_yIn_zN$ system. Bond-length relaxation strongly affects the equilibrium lattice constant, the value of which is close to the Vegard's law prediction. Band gap bowing coefficients and energies of formation were obtained.

ACKNOWLEDGMENTS

This work was supported by ONR under grant No. N00014-94-1-100. K. Kim acknowledges the support from Korean Ministry of Education.

REFERENCES

1. Gallium Nitride and Related Materials, edited by F.A. Ponce, R.D. Dupuis, S. Nakamura, and J.A. Edmond (Mater. Res. Soc. Proc. **395**, Pittsburgh, PA, 1996)
2. E.A. Albanesi, W.R.L. Lambrecht, and B. Segall, Phys. Rev. B **48**, 17841 (1993).
3. A.F. Wright and J.S. Nelson, Appl. Phys. Lett. **66**, 3051 (1995); ibid., **66**, 3465 (1995).
4. W.R.L. Lambrecht, Solid State Electronics, Special Issue (Topical Workshop on Nitrides) (1996), in press.
5. K. Osamura, S. Naka, and Y. Murakami, J. Appl. Phys. **46**, 3432 (1975).
6. R. Singh and T.D. Moustakas, in [1], p. 163.
7. J.M. Sanchez, F. Ducastelle, and D. Gratias, Physica A **128**, 334 (1984).
8. W. R. L. Lambrecht in Diamond, SiC and Nitride Wide Bandgap Semiconductors, edited by C.H. Carter, Jr., G. Gildenblat, S. Nakamura, and R.J. Nemanich (Mater. Res. Soc. Proc. **339**, Pittsburgh, PA, 1994) p. 565.
9. J.W.D. Connolly and W. R. Williams, Phys. Rev. B **27**, 5169 (1983).
10. C. Amador, W.R.L. Lambrecht, M. van Schilfgaarde, and B. Segall, Phys. Rev. B **47**, 15276 (1993).
11. M. Methfessel, Phys. Rev. B **38**, 1537 (1988).
12. P. Hohenberg and W. Kohn, Phys. Rev. **136**, B864 (1964); W. Kohn and L.J. Sham, ibid. **140**, A1133 (1965).
13. L. Hedin and B.I. Lundqvist, J. Phys. C **4**, 2064 (1971).
14. K. Kim, W.R.L. Lambrecht, and B. Segall, Phys. Rev. B **53**, 16310 (1996).
15. A. Zunger, S.-H. Wei, L.G. Ferreira, and J.E. Bernard, Phys. Rev. Lett. **65**, 353 (1990).

BAND STRUCTURE AND CATION ORDERING IN $LiGaO_2$

Sukit Limpijumnong, Walter R. L. Lambrecht, Benjamin Segall, and Kwiseon Kim
Department of Physics, Case Western Reserve University, Cleveland, OH 44106-7079

ABSTRACT

Full-potential linear muffin-tin orbital calculations were performed for $LiGaO_2$ in different crystal structures in order to investigate the nature and origin of the cation ordering, structural relaxation and their effects on the band structure. It is found that the most important factor for the bonding is the exclusive occurrence of Li_2Ga_2 tetrahedra surrounding oxygen. Structures including $LiGa_3$ and Li_3Ga tetrahedra have significantly higher total energies and smaller bandgaps. The band-offset between GaN and $LiGaO_2$ is estimated using the dielectric midgap approach.

INTRODUCTION

One of the main difficulties in developing GaN as electronic materials is the lack of a closely lattice-matched substrate. While most efforts have concentrated on sapphire and SiC as substrates, several alternative substrates have been suggested recently and initial growth experiments on them have been carried out [1]. One of these materials is $LiGaO_2$ [2]. This material which has a wurtzite derived structure is closely lattice matched to GaN, having a mismatch of less than 1 % in the basal plane lattice constant a. Furthermore, large $LiGaO_2$ crystals can be grown by the Czochralsky method. Very little is presently known about the electronic properties of this material. This motivated us to perform an investigation of the electronic and related properties of this material. The present work is the first step towards an investigation of $LiGaO_2$/GaN interfaces. Our present results already allow us to make an estimate of the band-offset at this interface using the dielectric midgap approach [3].

One may think of this material as being derived from ZnO by replacing the two Zn (group-II) atoms by a pair of Li (group-I) and Ga (group-III) atoms, thus preserving the average valence of the cations. This kind of chemical substitution is well known in zincblende materials and leads in that case to the chalcopyrite structure. The latter constitutes a particular ordering of cations on the zincblende lattice which is accompanied by relaxation of the structure. The chalcopyrite structure is also of interest for III-V alloys. Among the various possible orderings of a 50 % ABC_2 alloy, the chalcopyrite structure appears to be particularly stable for large size mismatch between the constituent A and B atoms, for example in $InGaAs_2$ and Ga_2AsSb [4]. The structure is also a good representative of random alloy behavior, being one of the so-called special quasirandom structures (SQS) [5]. This suggests that the ordering of cations in $LiGaO_2$ in the naturally occurring structure may play a similar role in wurtzite alloys as chalcopyrite does for zincblende alloys. Thus, it is important to understand the nature and origin of the cation ordering in natural $LiGaO_2$. This information can subsequently be used to investigate cation ordering in III-N alloys. The latter are the subject of a separate investigation presented elsewhere in these proceedings [6].

In this paper, we present a first-principles electronic structure study of $LiGaO_2$ in various structures and discuss the above issues.

Mat. Res. Soc. Symp. Proc. Vol. 449 © 1997 Materials Research Society

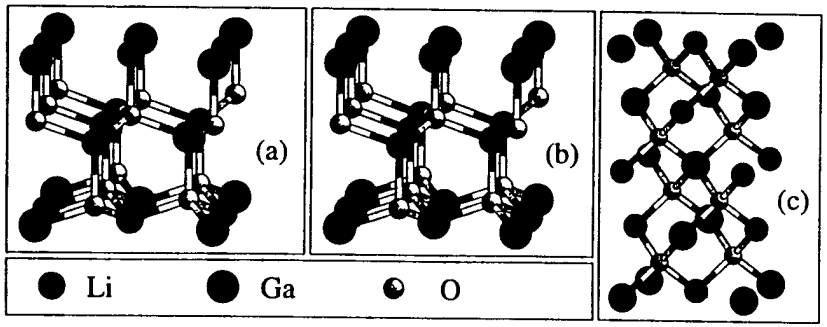

Figure 1: Crystal structures of $LiGaO_2$ investigated in the present work: (a) natural structure, (b) 1 + 1 (0001) superlattice, (c) chalcopyrite.

CRYSTAL STRUCTURE

The crystal structure of natural $LiGaO_2$ as determined by Marezio [7] is shown in Fig. 1. The structure is derived from wurtzite with a particular ordering of the Li and Ga cations accompanied by structural relaxation. A full description of the structural parameters is found in [7]. In particular, we note that all oxygens are surrounded by tetrahedra containing two Li and two Ga atoms and that different Li-O and Ga-O bond lengths occur in the structure. Each of the basal planes contains both Ga and Li atoms in a 2×2 supercell of the wurtzite unit cell.

In order to gain insight into the structural relaxation and its effects on electronic structure, we performed calculations for several other crystal structures. The first is an idealized $LiGaO_2$ structure in which bond lengths are all equal but the cation ordering is the same as the natural structure. Secondly, we considered a partially relaxed structure in which only the positions of the oxygens inside their Li_2Ga_2 tetrahedra are relaxed. This constitutes a nearest neighbor only relaxation model. Third, we considered an alternative ordering of cation in the wurtzite structure, consisting of alternating layers of LiO and GaO along the c-direction(1 + 1 (0001) superlattice). In this structure, there are alternatingly $LiGa_3$ and Li_3Ga tetrahedra surrounding oxygen. This structure was relaxed by adjusting both the Li-Ga interplanar spacings and the positions of oxygens inside the tetrahedra. We also considered the chalcopyrite structure. While we did not fully relax the latter (c/a of the tetragonal structure was kept ideal) we did relax the internal structural parameter determining the oxygen position inside its Li_2Ga_2 tetrahedra. As in the natural structure, this structure has only Li_2Ga_2 tetrahedra but the overall structure is derived from the cubic zincblende lattice instead of the hexagonal wurtzite lattice. Finally, we also performed calculations for the parent compound ZnO in the wurtzite structure. In all cases, the total energy was minimized with respect to volume or in-plane a lattice constant after internal parameter relaxation at each volume.

The above set of structures allows us to investigate the relative importance of local neighborhoods (chemical types of tetrahedra), the structural relaxation and the overall cubic vs. hexagonal stacking of layers.

METHOD OF CALCULATION

We use the full-potential linearized muffin-tin orbital method [8] in conjunction with the local density functional theory [9] with Hedin-Lundqvist parametrization [10]. Triple κ basis sets (*ddp* on Ga, *dpp* on O, *ddp* on Li) were employed. Some initial convergence test calculations used larger basis sets. The tails of the muffin-tin orbitals were expanded in empty sphere as well as atom centered muffin-tin augmentation spheres with an angular momentum cut-off of $l_{max} = 4$. The choice of empty spheres in wurtzite and zincblende derived structures is the same as in previous work on nitrides [11]. Brillouin zone summations were carried out using well-converged symmetry-reduced k-point sets on a regular $(4 \times 4 \times 4)$ mesh in the reciprocal unit cell, displaced to the center of the microzones. Structural relaxations were performed in the manner described above.

RESULTS

Table I gives our structural and binding energy results. Focusing first on the last column which gives the cohesive energy, we notice that the natural structure has a significantly higher binding energy (by 0.72 eV/formula unit) than the 1 + 1 (0001) superlattice (SL), but is very close in energy to the chalcopyrite structure. In view of the discussion of the structural elements given above these results indicate that the chemical arrangement of the local tetrahedral neighborhood is the dominant factor in the total energy. Both the natural and the chalcopyrite structure have only Li_2Ga_2 tetrahedra, while the SL has a mixture of $LiGa_3$ and Li_3Ga tetrahedra. This preference for a Li_2Ga_2 tetrahedron is, of course, closely related to maintaining local charge neutrality and average valence of the first neighbor coordination shell of each oxygen atom.

Considering the effect of relaxations, we can see in Table I that the relaxation energies are 0.13 eV for the natural structure and 0.29 eV for the (0001) SL, which are at least a factor 2 smaller than the energy difference between the SL and the natural structure itself. The above indicates that the relative stability of the natural structure is not primarily related to a particularly effective structural relaxation but is already present even in the ideal structure. In principle, of course, other cation ordering schemes need to be considered before claiming a rigorous conclusion.

We also note that the nearest neighbor relaxation only model appears to be quite satisfactory. The natural structure with only the oxygen position relaxed within each Li_2Ga_2 tetrahedron differs by only 0.01 eV/formula unit from that of the experimental structure. Furthermore, the Li-O and Ga-O bond lengths obtained from the nearest neighbor only relxation model are close to the average Li-O and Ga-O bond lengths of the experimental structure. The latter has four different Li-O and Ga-O bond lengths indicating that a secondary relaxation of the Li-Ga sublattice is taking place. The bond lengths in the chalcopyrite structure are also close to these averages.

It is notewhorthy that (in agreement with the experimental data on the crystal structure), the Li-O bond lengths are increased with respect to the idealized crystal structure while Ga-O bond lengths are decreased. This indicates a predominance of electrostatic over atomic size effects. In fact, it suggests rather weaker Li-O bonds and stronger Ga-O bonds than Zn-O bonds. The average bond length in ZnO is larger than that in $LiGaO_2$. This interpretation is confirmed by the analysis of the electronic structure given below, which indicates very little Li component in the occupied bands. That means that the LiO bond is very ionic and that Li essentially donates its electrons to oxygen.

Fig. 2 shows the band structure of $LiGaO_2$ in the natural crystal structure (i.e cation ordering) with experimental crystal structure parameters. The character of the bands

Table I: Structure, binding energy and LDA band gap results for $LiGaO_2$ and ZnO.

structure	a (Å)	c/a	V/atom (Å^3)	bond lengths (Å) Li-O	Ga-O	E_g (eV)	E^a_{coh} (eV)
			$LiGaO_2$				
natural (expt. param.)	3.170	1.605	10.61	1.991	1.826	3.415	21.61
				1.939	1.851		
				1.987	1.843		
				1.986	1.835		
		average		1.976	1.839		
natural (ideal)	3.056	1.633	10.09	1.872	1.872	3.227	21.47
natural (relaxed)	3.098	1.633	10.51	1.954	1.844	3.399	21.60
chalcopyrite (ideal)	3.047[b]	1.633	10.00	1.865	1.865	3.234	21.60
chalcopyrite (relaxed)	3.086	1.633	10.40	1.939	1.844	3.377	21.60
1 + 1 (0001) (ideal)	3.066	1.633	10.19	1.877	1.877	-0.053	20.59
1 + 1 (0001) (relaxed)	3.103	1.559	10.09	1.874	1.754	0.680	20.88
				1.877	1.906		
		average		1.876	1.868		
			ZnO				
				Zn-O			
wurtzite (ideal)	3.187	1.633	11.45	1.952		0.804	17.79
wurtzite (relaxed)	3.206	1.580	11.27	1.943		0.845	17.98
				1.941			
		average		1.943			
experiment [16]	3.250	1.601	11.91	1.992		3.44	
				1.976			
		average		1.988			

[a] Normalized per formula unit, not including spin-polarization of free atoms or zero-point motion corrections.

[b] This is $a_{tetragonal}/\sqrt{2}$, so as to be consistent with lattice-parameter in wurtzite basal plane of other cases.

is O2s like for the lowest band centered at -17 eV, Ga3d for the band at -12 eV and primarily O2p like for the bands between -6 eV and the valence band maximum (chosen as energy reference). The conduction band minimum is predominantly of Ga4s character. The bandgap is direct at Γ. The gap obtained from our calculations is 3.415 eV. We expect that the LDA underestimates the band gap and that the correction should be intermediate between those in ZnO (about 2.4 eV) and GaN (about 1 eV) but closer to GaN for reasons explained below. Thus $LiGaO_2$ itself may be a very interesting wide band gap semiconductor with an estimated direct gap of 4.4–5.8 eV. Self-energy corrections are also expected to be important for the Ga3d bands [12]. We estimate that these would shift the Ga3d bands down by about 4 eV which would then make them overlap with the O2s bands.

In comparing the $LiGaO_2$ bands to those for the parent compound ZnO, we note that in ZnO the Zn3d bands are higher up and, in fact, in the LDA overlap and hybridize with the bottom of the O2p like bands. While self-energy effects would again shift these levels down by a few eV they will still remain significantly closer to the valence-band maximum than in $LiGaO_2$. This tends to push the valence band maximum up in ZnO and is partly responsible for the reason why the gap in ZnO is smaller than that in $LiGaO_2$. This effect

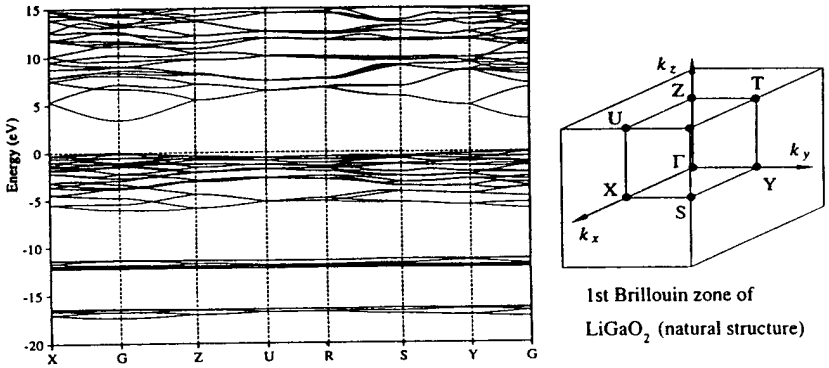

Figure 2: Band structures of $LiGaO_2$ in the experimental crystal structure.

of the Zn3d bands is also responsible for the larger self-energy correction of the gap in ZnO. Hence, in our above estimate of the gap correction of $LiGaO_2$ we expect the self-energy correction to be closer to that of GaN, i.e. the gap is expected to be ~4.4 eV. No experimental value for the gap of $LiGaO_2$ has been published to our knowledge.

The nearest neighbor cation ordering also has a marked influence on the gap. As can be seen in Table I, we find that the 1 + 1 (0001) SL has a much smaller gap than the natural structure while the chalcopyrite structure has a gap which is much closer. The structural relaxation effects on the gap are also significant but are smaller than those due to the chemical arrangement.

The band-offset between GaN and $LiGaO_2$ is an important parameter because the primary interest in $LiGaO_2$ is as a substrate for GaN growth. A simple estimate can be made using the dielectric midgap approach [3]. In this method, one assumes that the line-up of bands is in such a way as to preserve local charge neutrality [13]. Secondly, one assumes that there is a charge neutrality point (CNP) intrinsic to each semiconductor. This is a point in the gap such that the states above it must remain empty and below it must be filled when such states arise at the interface. This concept can be justified in various ways [3, 14, 15]. In practice, one identifies the charge neutrality point with a Brillouin zone (BZ) averaged midpoint of the gap. We used here the same averaging scheme as we did for our BZ summations of the charge density in the self-consistent calculations. We obtain the dielectric midgap points measured from the valence band maximum in $LiGaO_2$, GaN and ZnO to be 2.44 eV, 1.81 eV, and 1.99 eV, respectively, leading to valence-band offset estimates of 0.63 eV for GaN/$LiGaO_2$ and 0.18 eV for GaN/ZnO, respectively. For ZnO, this is in good agreement with our previous estimate using zincblende calculations [1].

Since the total gap difference between $LiGaO_2$ and GaN is $4.4 - 3.5 = 0.9$ eV, the offset is predicted to be about 2/3 in the valence bands and 1/3 in the conduction bands. To our knowledge no experimental results on this offset are available.

CONCLUSIONS

The most important conclusions of the present first-principles electronic structure investigation of $LiGaO_2$ are: (1) the bandgap and structural stability in $LiGaO_2$ are primarily

affected by the cation ordering while bond length relaxations play a secondary role; (2) the main reason for the structural stability of the naturally found crystal structure is the occurrence of only Li_2Ga_2 nearest neighbor tetrahedra surrounding oxygen because the latter preserve local charge neutrality and average valence; (3) natural $LiGaO_2$ has a direct gap estimated to be of order 4.4 eV; (4) the band-offsets of GaN with respect to $LiGaO_2$ are predicted to be about 0.6 eV in the valence and 0.3 eV in the conduction band.

Conclusion (2) above is based on a comparison of results for the natural cation ordering with those in the 1 + 1 (0001) superlattice and in the chalcopyrite structure. The former crystal structure is found to have about a 2.5 eV lower gap and a 0.7 eV higher total energy per formula unit.

Acknowledgments: This work was supported by ONR under grant No. N00014-94-1-100.

REFERENCES

1. See e.g. *Gallium Nitride and Related Materials,* edited by F. A. Ponce, R. D. Dupuis, S. Nakamura and J. A. Edmond, (Mater. Res. Soc. Proc. **395**,Pittsburgh, PA, 1996), p. 27, p. 51, p. 55, p. 61, p.67, and p. 535.
2. J. F. H. Nicholls, H. Gallagher, B. Henderson, C. Trager-Cowan, P. G. Middleton, K. P. O'Donnell, T. S. Cheng, C. T. Foxon, and B. H. T. Chai, in Ref. [1], p. 535.
3. M. Cardona and N. E. Christensen, Phys. Rev. B **35**, 6182 (1987).
4. S.-H. Wei, L. G. Ferreira, and A. Zunger, Phys. Rev. B **41**, 8240 (1990).
5. A. Zunger, S.-H. Wei, L. G. Ferreira, and J. E. Bernard, Phys. Rev. Lett. **65**, 353 (1990).
6. K. Kim, S. Limpijumnong, W. R. L. Lambrecht and B. Segall, in this proceeding.
7. M. Marezio, Acta Cryst. **18**, 481-4 (1965).
8. M. Methfessel, Phys. Rev. B **38**, 1537 (1988).
9. P. Hohenberg and W. Kohn, Phys. Rev. **136**, B864 (1964); W. Kohn and L. J. Sham, ibid. **140**, A1133 (1965).
10. L. Hedin and B. I. Lundqvist, J. Phys. C **4**, 2064 (1971).
11. K. Kim, W. R. L. Lambrecht and B. Segall, Phys. Rev. B **53**, 16310 (1996).
12. W. R. L. Lambrecht, B. Segall, S. Strite, G. Martin, A. Agarwal, H. Morkoç, and A. Rockett, Phys. Rev. B **50**, 14155 (1994).
13. F. Flores and C. Tejedor, J. Phys. C **20**, 145 (1987).
14. J. Tersoff, Phys. Rev. Lett. **30**, 3874 (1984); W. A. Harrison and J. Tersoff, J. Vac. Sci. Technol. B **4**, 1068 (1986).
15. W. R. L. Lambrecht and B. Segall, Phys. Rev. Lett. **61**, 1764 (1988); Phys. Rev. B **41**, 2832 (1990).
16. O. Madelung, M. Schulz, H. Weiss, *Numerical Data and Functional Relationships in Science and Technology, Group III Vol 17(b),* (Springer-Verlag, Berlin, 1982), pp. 35-44.

CHARACTERIZATION OF BULK, POLYCRYSTALLINE INDIUM NITRIDE GROWN AT SUB-ATMOSPHERIC PRESSURES

Jeffrey S. Dyck[a], Kathleen Kash[a], Kwiseon Kim[a], Walter R. L Lambrecht[a], Cliff C. Hayman[b], Alberto Argoitia[b], Michael T. Grossner[b], Weilie L. Zhou[c] and John C. Angus[b]
[a]Physics Dept., [b] Chemical Engineering Dept., [c]Materials Science and Engineering Dept.
Case Western Reserve University, Cleveland, OH 44106.

ABSTRACT

Polycrystalline, wurtzitic indium nitride was synthesized by saturating indium metal with atomic nitrogen from a microwave plasma source. Plasma synthesis avoids the high equilibrium pressures required when molecular nitrogen is used as the nitrogen source. Two types of growth were observed: 1) small amounts of indium nitride crystallized from the melt during cooling and 2) hexagonal platelets formed adjacent to the In metal source on the crucible sides. The mechanism of this latter growth is not established, but may involve transport of indium as a liquid film. The crystals were characterized by electron diffraction, X-ray diffraction, elemental analysis, scanning electron microscopy, and Raman spectroscopy. Lattice parameter and Raman active phonon modes are reported and compared with calculations based on the full-potential linear muffin-tin orbital method (FP-LMTO).

INTRODUCTION

Of the III-V nitride wide band gap semiconductors, indium nitride has received the least attention. Indium nitride is also the most difficult to grow; the equilibrium vapor pressure of N_2 over InN is higher than that over GaN and AlN [1]. Additionally, the In-N bond is the weakest among the III-V nitrides [2]. High quality InN crystals are of inherent scientific interest. Also, for obtaining blue light emission from nitride based structures, a significant amount of In (20-40%) must be incorporated into GaN [3,4].

Efforts at bulk synthesis of InN have primarily been at high pressures because of the high equilibrium pressures of N_2. Successful synthesis of small crystallites (5-50 micron) has been achieved at an N_2 pressure of 18-20 kbar and a temperature range of 700-900°C [5]. We have recently shown that GaN and InN can be synthesized at low pressures by use of atomic nitrogen, N, rather than molecular nitrogen, N_2, to saturate gallium or indium with nitrogen [6,7,8]. Subsequently, similar results were obtained by Krukowski, et al., for InN [9].

In this paper we report on the growth of well-faceted bulk InN using nitrogen ECR and ball plasma configurations at sub-atmospheric pressures. Comparisons of measured lattice constants and optical phonon modes are made to theoretical calculations done using the full-potential linear muffin-tin orbital method (FP-LMTO) [10].

EXPERIMENT/SYNTHESIS

The pure indium shot was held in either an h-BN crucible for experiments without a bias voltage, or a machined, nitrided stainless steel crucible lined with nitrided molybdenum foil for experiments with bias. The reaction chamber was initially evacuated to a base pressure of 10^{-6} torr. In order to remove indium oxide or other impurities from the surface, the indium was independently heated from below while being exposed to a hydrogen plasma with 800 watts of

microwave power at 20 torr for 30 minutes. Although the temperature at the bottom of the susceptor during this step was approximately 450°C, the actual temperature at the crucible was unknown as there is much additional heating from the plasma. After cleaning, the hydrogen flow was replaced with nitrogen, maintaining a pressure of 20 torr. A voltage of 20 Volts was applied to the crucible for bias experiments. At this point, ECR magnets were turned on for an ECR plasma, or left off for a ball plasma. The nitrogen pressure for ECR plasma experiments was lowered to 0.5 mtorr. For the growth cycle, the In was held at a susceptor temperature of 200-450°C while being exposed to the nitrogen plasma.

In experiments where the molten indium metal was visible, the formation of a dull crust of InN on the surface of the In was observed and periodic eruptions of gas and molten metal occurred for higher temperatures. The gas was not identified, but was likely N_2. In ball plasma experiments, formation of InN adjacent to the indium melt on the edges of the crucible became apparent after about 30 minutes. Often, most of the In was converted to InN of this form, leaving almost none in the crucible. After approximately 1 hour, the crucible was cooled with the plasma on to maintain the high nitrogen chemical potential. Additional formation of InN material occurred during cooling in many cases.

CHARACTERIZATION AND CALCULATIONS

Scanning electron micrographs (SEM) of the polycrystalline product are shown in Figures 1 and 2. Figure 1 reveals growth patterns of hexagonal platelets formed on the edges of the crucible assembled together in "pine cone" structures. Within the clusters of platelets, the crystals are oriented. Typical dimensions of isolated platelets are 0.75 microns thick and 5-20 microns wide. Additionally, InN was crystallized from the atomic nitrogen saturated indium melt held within the crucible. Figure 2 shows a typical growth morphology on the surface of the cooled indium. The "herring-bone" dendritic structure suggests uncontrolled freezing from a melt.

Transmission electron microscopy (TEM) was performed on a Philips CM 20 equipped with Tracor Northern 5500 detector system for Energy Dispersive X-ray (EDX) analysis. A small fragment of material was removed from the crust formed from InN crystallization from the melt and glued on a Ni grid for ion milling until it became transparent for TEM observation. Figure 3 shows an InN crystallite. EDX analysis of the small grain with black contrast embedded in the InN shows a high concentration of In. We believe that it is an inclusion of In. Planar defects were also found in the InN grains. An electron selected area diffraction pattern was taken along the $[11\bar{2}0]$ zone axis as shown in the inset to Figure 3.

The indium nitride crystals were confirmed to be wurtzitic by electron and x-ray diffraction, and by elemental analysis. EDX analysis indicated that the only constituents were indium and nitrogen. In Figure 4 we show a typical powder x-ray diffraction pattern of the unetched material. All the major wurtzite InN lines are observed with the correct relative intensities. A few weak peaks due to In inclusions in the material are also seen. From the diffraction pattern, the lattice constants were obtained and are shown in Table I. The peak positions of the indium inclusions were used to correct for instrumental shift of observed InN peaks in calculating the lattice constants. It should be noted that our material has atomic spacings that are less than previously reported values. Theoretical calculation of the lattice parameters was done by relaxing the wurtzite InN structure by minimizing the total energy. The equilibrium lattice constants and elastic constants were obtained in earlier work [11].

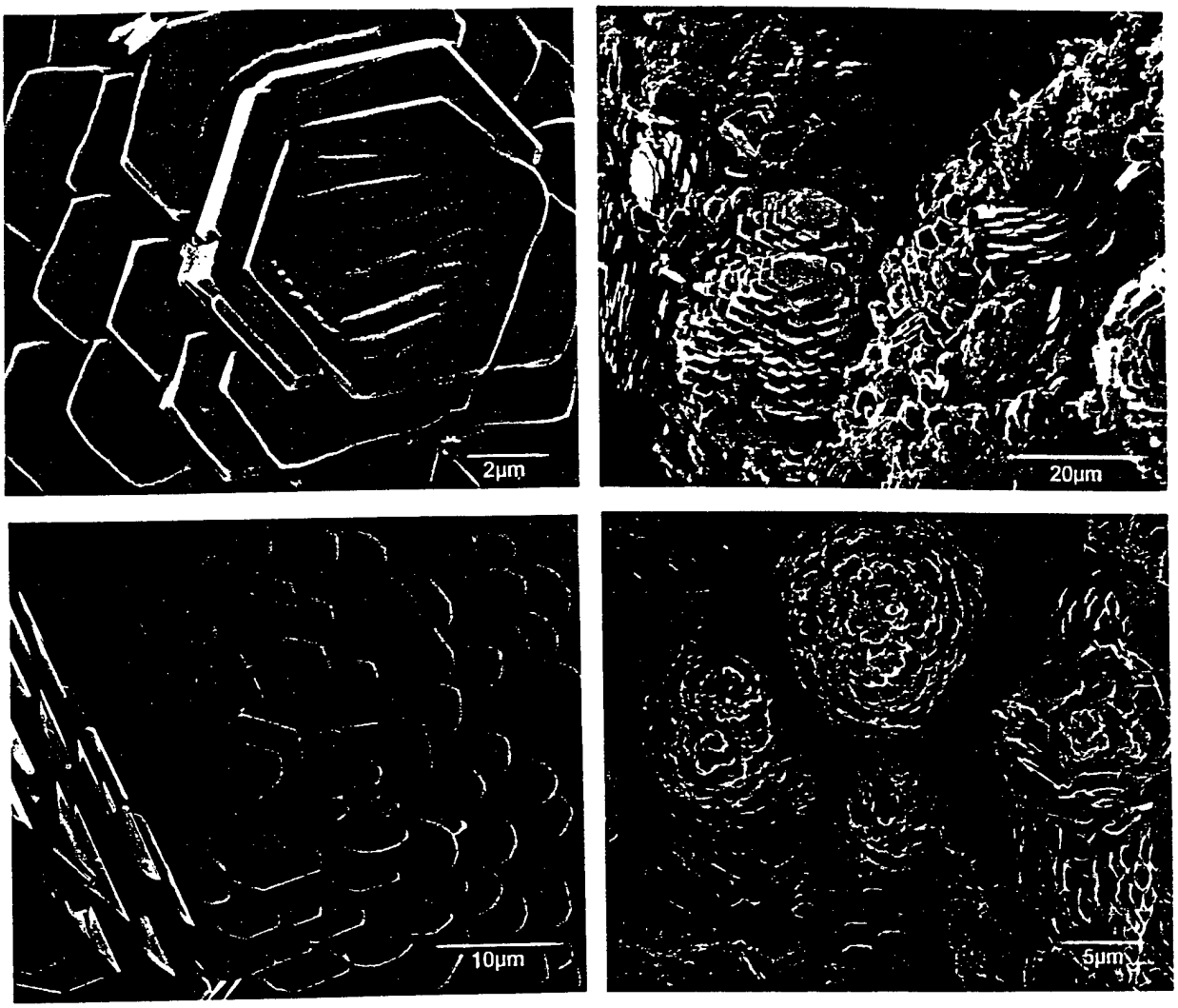

Figure 1. Scanning electron microscope images of InN from growth adjacent to the indium metal source on the crucible sides.

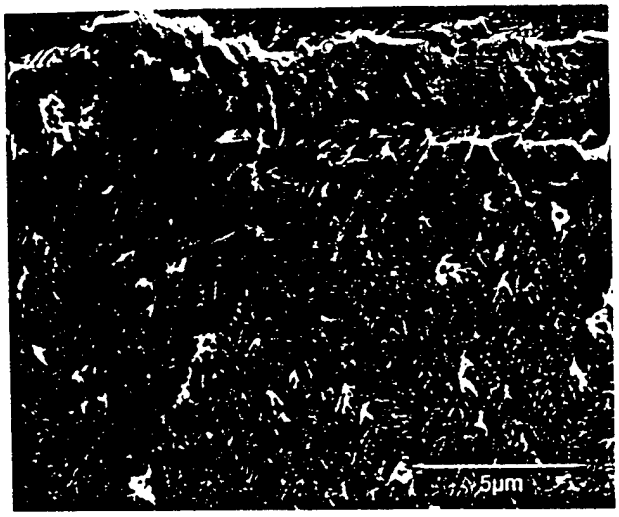

Figure 2. Scanning electron microscope image of InN grown by crystallization from a nitrogen saturated indium melt.

Figure 3. Transmission electron microscope image of InN grain. Dark region is believed to be an In inclusion. Inset is an electron diffraction pattern taken along the [11$\bar{2}$0] zone axis.

TABLE I. Measured and calculated Lattice parameters of InN. Values are given in angstroms.

	Literature	*Current Work*	
	[12]	*Theory[11]*	*Experiment*
a	3.53...3.6	3.525 +/- 0.005	3.526 +/- 0.026
c	5.705...5.963	5.679 +/- 0.005	5.686 +/- 0.041
c/a	1.59...1.69	1.611 +/- 0.005	1.613

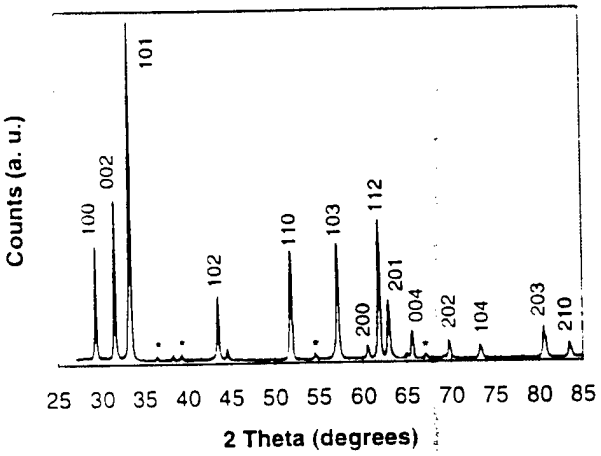

Figure 4. Powder x-ray diffraction pattern of un-etched InN. Peaks are labelled with the corresponding InN reflection plane. Asterisks mark peaks from In metal reflections.

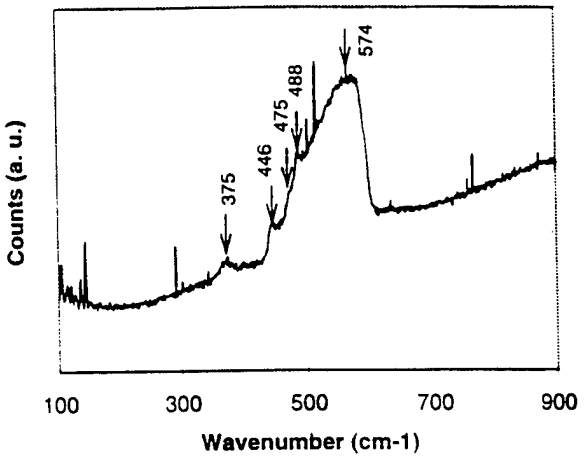

Figure 5. Depolarized Raman spectrum of InN crystallized from a nitrogen saturated In melt. Narrow peaks that are not labelled arise from noise at random frequencies.

Depolarized Raman spectra were taken in backscattering geometry. Given that the InN material consists of randomly oriented arrays of crystallites, all six Raman active modes are allowed. The Raman spectrum is shown in Figure 5. The three weak peaks at 446, 475, and 488 cm^{-1} are likely the A_1 and E_1 splitting in the TO mode and the E_2 high mode. The broad peak at 574 cm^{-1} is interpreted as a mainly LO-type plasmon coupled mode, and the peak at 375 cm^{-1} as the corresponding lower (mainly plasmon-like) mode. With this interpretation, the carrier density can be approximated from

$$\omega_p^2 = 4\pi ne^2/m^* \qquad (1)$$

and using $m^* \approx 0.1$ to be of order 10^{17} cm^{-3}. The LO-like mode shifts considerably from sample to sample and because of the coupling to the plasmon, the number in Table II should be considered an upper limit for the pure LO mode. The resulting LO-TO splitting of about 100 cm^{-1} is smaller than in GaN, indicating a lower ionicity. The E_2^1 mode was not observed. The calculated phonons were obtained by calculating the total energy changes and forces resulting from small selected atomic displacements. Assuming the harmonic approximation, these provide the dynamical matrix which is then diagonalized. Results of the calculations and experimental data are presented in Table II. The calculated (silent) B_1^2 mode is essentially an LO-type mode at the zone boundary of zincblende (at L_{zb}), folded onto the Brillouin zone center in wurtzite and thus should be close to the values for the LO phonons at the Gamma point. We cannot directly

TABLE II. Phonon modes of InN. Results from the literature are also presented for reference. Reported values are given in cm^{-1}.

Mode	*Literature*			*Current Work*	
	[14][b]	*[15]*	*[16]*	*Theory*	*Experiment*
E_2^1		190		104	
E_2^2		590[c]	495	483	488
$A_1^{(TO)}$		400		440	446
$E_1^{(TO)}$	478[a]	490[d]		472	475
$A_1^{(LO)}$			596		574[a]
$E_1^{(LO)}$	694[a]				
B_1^1				270	
B_1^2				530	

[a] as no polarization dependence of these lines was measured, no distinction between A_1 and E_1 character could be discerned

[b] extrapolated from InGaN alloys

[c] this is more likely to be an LO mode

[d] this line coincides with a mode of sapphire which was used as a substrate in these experiments

calculate the latter from displacements in the unit cell because the presence of a long range electric field breaks the periodicity. The calculated value of B_1^2 is consistent with our assignment of the experimental 574 cm^{-1} line. It should be noted that the InN was readily converted to In_2O_3 from the heating of the focused laser beam, and care was taken to avoid this contamination in the spectra.

DISCUSSION AND CONCLUSION

Bulk, polycrystalline InN is grown at pressures less than or equal to 20 torr from In metal and nitrogen derived from a plasma source. The method has been used to grow AlN, GaN, and InN without the aid of a substrate and is an attractive alternative to the high pressure techniques normally associated with bulk growth of these materials.

The InN has been verified to be of the wurtzite structure through both electron and x-ray diffraction experiments. There has been much uncertainty in the physical and optical properties of InN due to a lack of good bulk material to date. Existing data for the lattice parameters varies by about 1% and is highly dependent on the preparation technique. Our results give lattice constants less than previously reported in the literature and match well with calculations. In this study, optical phonon modes are observed through Raman spectroscopy and the fine structure of the TO modes is resolved for the first time. These data represent the first measurement of optical phonons from InN synthesized without the aid of a substrate [13-15]. Furthermore, these are the first ab-initio phonon calculations of wurtzite InN to the best of our knowledge.

ACKNOWLEDGMENTS

We acknowledge the generous support of the Ohio Board of Regents, the National Science Foundation, and the Office of Naval Research.

REFERENCES

1. S.M. Bedair, in *Gallium Nitride (GaN) I*, edited by J.I. Pankove and T.D. Moustakas (Semiconductors and Semimetals Series Vol. 50, Academic Press, San Diego, 1998) p. 128 - and references therein.
2. W. A. Harrison, *Electronic Structure and the Properties of Solids*, (W.H. Freeman and Co., San Francisco, 1980), p. 176.
3. S. Nakamura, T. Mukai, and M. Senoh, J. Appl. Phys. **76**, 8189 (1994).
4. S. Nakamura, M. Senoh, N. Iwasa, and S Nagahama, Jpn. J. Appl. Phys. **34**, L797 (1995).
5. I. Grzegory, J. Jun, S. Krukowski, P. Perlin, and S. Porowski, Jpn. J. Appl. Phys. **32**, Suppl. 32-1, 343 (1993).
6. A. Argoitia, C.C. Hayman, J.C. Angus, L. Wang, J.S. Dyck, and K. Kash, Appl. Phys. Lett. **70**, 179 (1997).
7. A. Argoitia, C.C. Hayman, J.C. Angus, L. Wang, J.S. Dyck, and K. Kash in *III-V Nitrides*, edited by F.A. Ponce, T.D. Moustakas, I. Akasaki, and B.A. Monemar (Mater. Res. Soc. Proc. **449**, Pittsburgh, PA, 1996) pp. 47-52.
8. J.C. Angus, A. Argoitia, C.C. Hayman, L. Wang, J.S. Dyck, and K. Kash in *Gallium Nitride and Related Materials II*, edited by C.R. Abernathy, H. Amano, J.C. Zolper (Mater. Res. Soc. Proc. **468**, Pittsburgh, PA, 1997).
9. S. Krukowski, A. Witek, J. Adamczyk, J. Jun, M. Bockowski, I Grzegory, B. Lucznik, G. Nowak, M. Wroblewski, A. Presz, S. Gierlotka, S. Stelmach, B. Palosz, and S. Porowski, J. Phys. Chem. Solids, (to be published).
10. M. Methfessel, Phys. Rev. B **38**, 1537 (1988).
11. K. Kim, W.R.L. Lambrecht, and B. Segall, Phys. Rev. B **53**, 16310 (1996); Phys. Rev. B **56**, 7018 (1997).
12. T.L. Tansley, *Properties of III-V Nitrides*, edited by J.H. Edgar, EMIS Datareviews Series, No. 11, INSPEC, (Institution of Electrical Engineers, London, UK, 1994) p. 36.
13. K. Osamura, S. Naka, and Y. Murakami, J. Appl. Phys. **46**, 3432 (1975).
14. T. Inushima, T. Yaguchi, A. Nagase, A. Iso, and T. Shiraishi in *Silicon Carbide and Related Materials 1995* edited by S. Nakashima, H. Matsunami, S. Yoshida, and H. Harima (Inst. Phys. Conf. Ser. **142**, Bristol and Philadelphia, 1996), p. 971
15. H. Kwon, Y Lee, O. Miki, H. Yamano, and A. Yoshida, Appl. Phys. Lett. **69**, 937 (1996).

ELECTRONIC AND OPTICAL PROPERTIES OF THE GROUP-III NITRIDES, THEIR HETEROSTRUCTURES AND ALLOYS

Walter R. L. Lambrecht, Kwiseon Kim, Sergey N. Rashkeev and B. Segall
Department of Physics, Case Western Reserve University, Cleveland, Oh 44106-7079

ABSTRACT

Various aspects of the electronic structure of the group III nitrides are discussed. The relation between band structures and optical response in the vacuum ultraviolet is analyzed for zincblende and wurtzite GaN and for wurtzite AlN and compared with available experimental data obtained from reflectivity and spectroscopic ellipsometry. The spin-orbit and crystal field splittings of the valence band edges and their relations to exciton fine structure are discussed including substrate induced biaxial strain effects. The band-offsets between the III-nitrides and some relevant semiconductor substrates obtained within the dielectric midgap energy model are presented and strain effects which may alter these values are discussed. The importance of lattice mismatch in bandgap bowing is exemplified by comparing $Al_xGa_{1-x}N$ and $In_xGa_{1-x}N$.

INTRODUCTION

The interest in group-III nitrides for opto-electronic applications is currently experiencing an explosive growth. Still, many of their fundamental materials properties are only poorly known in comparison with other semiconductors. In this paper, we review the current state of understanding of their band structure and related optical properties and discuss some particular aspects in detail.

While many band structure calculations have appeared over the last few years, (See [1] for an overview), the majority of these calculations have focused on obtaining a few of the important total energy properties such as lattice constants, bulk moduli and a general picture of the band structure without providing much discussion of their relation to experimental probes of the band structure. The early band structure work of the 1960's [2] used the semi-empirical pseudopotential method in which UV reflectivity data are used to adjust pseudopotential parameters. While by construction that approach accounts reasonably well for the optical response functions as they were known at the time, it suffers from non-uniqueness in assigning particular interband transitions to observed features in reflectivity. It turns out that the band structures obtained in this manner differ greatly from several recently reported band structure results based on the local density approximation (LDA) [3]. It thus appears necessary to re-examine the relation between the UV optical response and the band structures. The LDA band structure has the disadvantage that strictly speaking it does not provide the quasiparticle excitation energies but merely intermediate results in obtaining the total energy of bonding between electrons and nuclei. Quasiparticle energies are the energies for extracting and electron from or adding an electron to the system as measured by photoemission and inverse photoemission. Fortunately, calculations of the self-energy corrections to the LDA band structure have been carried out for GaN and AlN using the GW [1] approach by a few groups [4, 5]. Furthermore, considerable insights in the magnitude, k-point, specific state and energy dependence of these corrections has accumulated from studies in other semiconductors. From these studies, we know that the main correction to the LDA band structure is an almost constant gap correction for the bands within at least about 5 eV from the gap. Before we can gauge the accuracy of these rather involved GW calculations, however, we need a better understanding of the experimental spectra which means that we need to re-examine the assignment of interband transitions. We [6] (and some other authors [7, 9]) have recently calculated the dielectric response function $\epsilon_2(\omega)$ within the random phase approximation (RPA) from LDA band structures. In addition, we have analyzed in detail how the latter is decomposed into its various interband transition contributions. Here, we briefly present these results for zincblende GaN and wurtzite AlN while for wurtzite GaN this analysis can be found in [6]. We compare our results with experimental reflectivity [6, 8] and spectroscopic ellipsometry data[9, 10, 11]. This is not trivial because optical response (which basically probes two-particle excitations) may involve further many-body corrections beyond the GW approach for

[1] *GW* stands for the first term in a perturbation theoretical expansion for the self-energy introduced by Lars Hedin and Stig Lundqvist in *Solid State Physics*, Vol. 23, p. 1 (1969), with G the one-electron Green's function and W the screened Coulomb interaction.

Mat. Res. Soc. Symp. Proc. Vol. 395 © 1996 Materials Research Society

single particle excitations. Our interpretation of the discrepancies between theory and experiment differs from that of other authors [9, 10, 11]. Further insights are gained by also comparing the occupied states to photoemission data.

While the band structure probes on this large energy (several eV) scale are clearly strongly perturbed by many-body effects, the band structure details near the band edges should not suffer so much from these effects. Of course, excitonic effects are prominent but should not vary greatly with energy. We thus expect that the LDA band structures will account rather well for the excitonic fine structure related to the valence-band splittings near the valence-band maximum. The main issue here is whether the current calculations are sufficiently accurate at meV scale to be useful in the understanding of the strain effects on these splittings. We will show that they are by discussing the spin-orbit splittings and crystal field splitting and their dependence on uniaxial strain in the second part of this paper.

Band offsets at heterostructures among the III-nitrides are expected to depend strongly on interface specific effects because of the polar nature of the interfaces. However, as we shall discuss, we expect these interface and biaxial strain effects to become pertinent only when very high quality interfaces are obtained. Hence, for the time being, a much simpler bulk-like alignment of energy levels seems appropriate. We discuss this issue and provide band offsets between the nitrides and some relevant semiconductor substrates based on the dielectric midgap energy approach [12] and explain how bulk strain corrections can be added to the latter.

Finally, we discuss the band gap bowing in $In_xGa_{1-x}N$ which has recently become of great interest in view of the important role of this alloy in fine tuning the light emission in the blue-green region in nitride LEDs. By comparing with the results for $Al_xGa_{1-x}N$ we indentify the important role of bond length mismatch. A brief summary of the results concludes this paper.

COMPUTATIONAL METHOD

As discussed in the introduction, the LDA [3] is the basic approximation in our band structure approach. Specifically, we use the Hedin-Lundqvist parametrization [13] of exchange and correlation. For the band structure calculations we use the linear muffin-tin orbital method [14]. The band dispersions of the Ga3d and In4d semi-core levels are included. For the optical calculations we use the standard RPA formulation on which details can be found in [6]. The only difference with the method used in that paper is that we have recently set up an optical properties program using the more efficient tight-binding linear muffin-tin orbital implementation. Also, we have optimized the Brillouin zone (BZ) integrations, which use the tetrahedron method, by including the symmetry rotation operations on the matrix elements while integrating over the entire BZ (instead of only the irreducible wedge) following the approach described by Blöchl et al. [15]. The optical calculations were based on the band structure calculated within the atomic sphere approximation (ASA) and at the experimental lattice constants. We have separately checked the latter with full-potential (FP) [16] calculations which make no shape approximations to the potential or charge density and found that for the eV scale no significant deviations occur. For the calculations of the valence band edge fine structure and its strain dependence, however, where the relevant precision is meV, we found it important to use the FP approach. For the spin-orbit coupling, which mainly derive from the inner part of the atomic spheres, the ASA is adequate and was used.

UV OPTICAL RESPONSE

GaN

Fig. 1 compares our calculated $\epsilon_2(\omega)$ with experimental data for wurtzite (w) and zincblende (z) GaN. The data for wurtzite were obtained from Kramers-Kronig analysis of UV-reflectivity for synchrotron radiation up to 40 eV.[6] The data for zinblende GaN were obtained from spectroscopic ellipsometry also using synchrotron radiation [11]. These provide the largest range of energies presently available. These data agree well with previous ellipsometry studies for both z-GaN and w-GaN by Logothedis et al. [9, 10] in the lower energy region. The calculated results were in both cases shifted rigidly upwards by ~1 eV, which provides a minimum (room temperature) gap of 3.4 eV for w-GaN and 3.1 eV for z-GaN. For w-GaN, the peak positions in theory and experiment agree well over the whole range of energies considered, although there are rather strong deviations in intensity. For z-GaN on the other hand, the upper peaks agree well but the first peak usually identified as the combination of the E_1 and E_2 transitions, is at lower

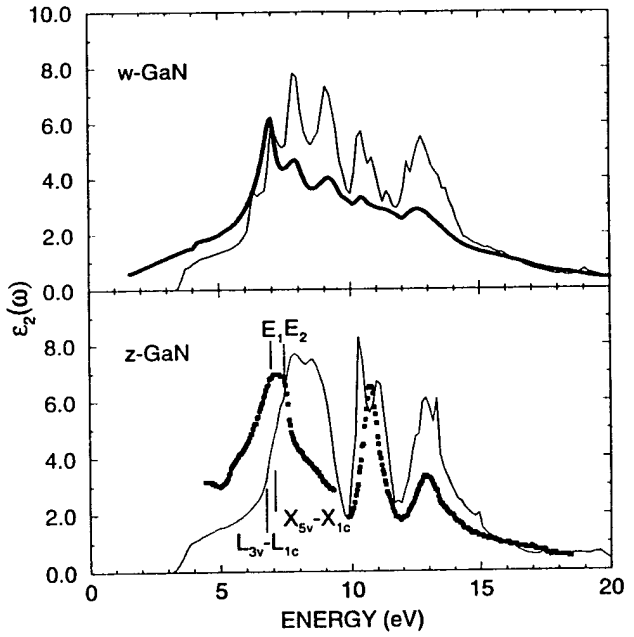

Figure 1: Calculated (thin lines) and experimental (thick lines) $\epsilon_2(\omega)$ for wurtzite [6] and zincblende [11] GaN.

energy than the calculated peak. We note that our theory/experiment alignment differs from that of Petalas et al. [9] and Janowitz et al. [11] who both compare directly with the LDA results without using any gap correction. In that case the lower peak agrees well but the upper peaks are too low and the minimum gap is too low. The latter authors ascribe the discrepancy for the upper peaks tentatively to problems of the calculations for higher energy transitions. However, it is rather difficult to explain why the peak in the 6–8 eV range would come out correctly from the uncorrected LDA calculation if the minimum gap is known to be underestimated by about 1 eV. The GW corrections[4] are found to be approximately constant, in fact slightly increasing, in this energy range rather than decreasing as would be needed to explain the theory-experiment alignment proposed by those authors.

In an attempt to understand the origin of this significant discrepancy, we first examine the nature of the transitions involved. A straightforward decomposition into individual band-to-band transitions (but still integrated over the whole BZ) reveals that the 7–9 eV (theoretical) peak derives mainly from transitions between the top valence band and the lowest conduction band. If the small influence of matrix elements is ignored (which we checked by comparing with a separate calculation with matrix elements assumed to be constant), the peaks should come mainly from the regions of large joint density of states, i.e., regions with nearly parallel bands. Fig. 2 shows the difference between the bands involved as a 2D function within the ΓLXK plane. Regions of constant energy difference in this plot correspond to parallel bands. As usual in most semiconductors, there is a region of nearly parallel bands along $\Lambda \equiv \Gamma - L$ near the L-point. The L-point itself is an M_1 saddle point, i.e., the curvature is upward in two directions and downward in one. This 2D singularity or critical line is usually associated with the E_1 transition, or the first peak above the minimum gap. We may note, however, that the $L_{3v} - L_{1c}$ transition itself occurs at 6.79 eV which is below the first main peak in this region. It rather corresponds to a minor change in slope barely detectable on the steeply rising slope. Similarly, there is a somewhat larger

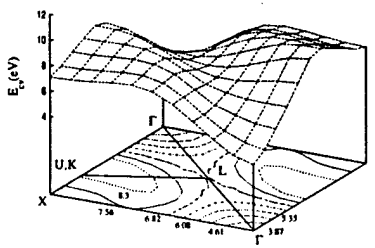

Figure 2: Interband transition energy $E_{c1}(\mathbf{k}) - E_{v1}(\mathbf{k})$ for z-GaN.

flat region along $\Delta \equiv \Gamma - X$ near X which is often associated with E_2. The $X_{5v} - X_{1c}$ critical point of type M_0 (a minimum) is at 7.09 eV and thus still below the main peak. It is noteworthy that these two critical points are unusually close in energy in GaN. Furthermore we see from Fig. 2 that they form part of a rather extended 2D region in k-space where the band difference is rather slowly varying. This flat region wraps itself around the maximum near the K point and extends from near the $X - K - \Gamma$ axis towards L and back to the $\Gamma - X$ axis. This extended region is responsible for the main first broad peak which has maxima at 7.8 and 8.5 eV in the calculated spectrum. The experimental peak positions labeled E_1 and E_2 are at 7.03 and 7.63 eV. This suggests that strong continuum excitonic effects of the type discussed by del Castillo-Mussot and Sham [17] for Si and Ge may be associated with these critical points. The net effect of these excitonic phenomena is to shift oscillator strength to lower energies. Since a particularly large region of truly parallel bands occurs along Δ near X we speculate that its excitonic strength could be quite pronounced. In fact, del Castillo-Mussot and Sham [17] found that the E_2 transition is reduced in intensity by these many-particle effects and gives rise to an exciton quasi bound state which for Si occurs 0.2 eV below the E_2 edge. Because the high-frequency dielectric constant is considerably lower in GaN, we may expect an even larger excitonic shift. Because the E_1 and E_2 edges in GaN are so close to each other, the E_2 related exciton might fall below the E_1 transition in a region of low spectral intensity and hence be less subject to Fano broadening by interaction with the continuum. These authors also find the E_1 edge to be slightly shifted and increased in intensity. As discussed by Hanke and Sham [18] for diamond and Si, local field effects are also important. From Hanke and Sham's work [18], however, the local-field effect alone without electron-hole attraction tends to shift oscillator strength to higher energies and would thus worsen the agreement with experiment.

What is puzzling is that these phenomena seem to affect z-GaN more strongly than w-GaN. We may note, however, that in w-GaN there is a strong reduction in peak intensity (in experiment compared to theory) with increasing energy. While we have previously argued [6] that this can at least partially be explained by diffuse scattering due to surface roughness and partial misalingment of grains, it could also be a manifestation of the same many-body effects which shift oscillator strength to lower energies. In w-GaN this effect would mainly appear to shift strength from one peak to another. In z-GaN, on the other hand, because of the close proximity of the E_1 and E_2 like transitions, which merge into a single broad band lying above a region of low intensity, the effect has more the appearance of a peak shift. We tentatively suggest that both in z-GaN and in w-GaN excitonic effects may be strong. Clearly, however, more work in this area is desirable.

AlN

Fig. 3 shows our calculated reflectivity for w-AlN compared to the data of Loughin et al. [8]. Again, we shifted the LDA results (by 1.7 eV) so as to adjust the minimum band gap (to 6.3 eV). This apparently provides good agreement for the entire lowest peak below 12 eV. There are some features in the experiment below the 6.3 eV gap which are probably related to defects. Oxygen

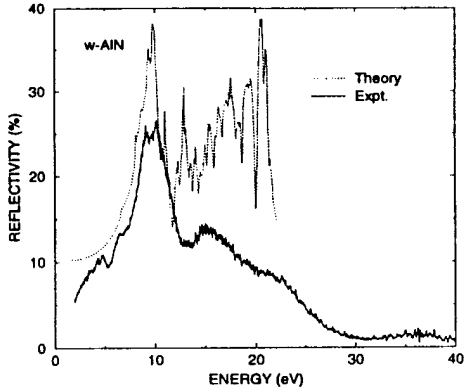

Figure 3: Calculated and measured (from Ref. [8]) UV-reflectivity of w-AlN.

is an important known contaminant in the samples measured by Loughin et al. [8] and may be responsible. Discrepancies in peak position and a strong attenuation of intensity, however, are apparent at higher energies. In particular the second peak in the experiment appears to occur at about 14-15 eV while in the theory it occurs at 12.5 eV. While in this case the shift is towards higher energies, which is a little more expected if self-energy corrections increase with increasing energy separation from the gap, a 1.5–2 eV eV shift is not expected from Rubio et al.'s [4] GW calculations. Our calculations of the decomposition into band-to-band transitions reveal that the 12.5 eV peak comes mostly from transitions to the 3rd and 4th conduction band in agreement with Christensen and Gorczyca's analysis [7]. The difference in GW corrections for these bands from those at the minimum gap is about 1.2 eV. Further work will be necessary to unravel these discrepancies.

Photoemission

X-ray photoelectron spectroscopy (XPS) of GaN was studied in [19]. There we showed that while the Ga3d states overlap and hybridize with the N2s band in the LDA band structure, the hole left behind when a Ga3d is extracted from the band has a binding energy well below that of the N2s band. This is just another example of the many-body effects which perturb a straightforward comparison of band structures with experimental spectroscopies. We also found that the N2s band undergoes a ~1.5 eV downward shift relative to the top of the valence band. This is in good agreement with the predictions of Rubio et al.'s [4] GW calculations.

In InN the same type of effects are expected. We calculated the expected shift of the In4d band from its LDA value to be about 3 eV. In AlN, it is easier to observe the N2s shift because it is not overshadowed by a closeby and strong Ga3d or In4d semicore peaks. Details on the AlN are provided elsewhere in these proceedings [20]. In summary, the comparison of our LDA calculated densities of states with recent photemission measurements confirms the need for self-energy shifts as predicted by Rubio et al. [4], which are slowly increasing with energy to about 0.5 eV as one goes down into the upper valence band and discontinuously increase to about 1.5 eV–2 eV in the lower N2s band. For the In4d and Ga3d semicore bands these effects are of order of 3–4 eV. Thus, as expected, the corrections become stronger with increasing localization of the orbitals involved.

BAND EDGE STRUCTURE

In this section, we consider the valence-band edge splittings which are revealed by the exciton fine structure. In z-GaN, the modulated reflectivity spectra of Ramirez-Flores et al. [21] reveal the usual E_0 and $E_0 + \Delta_0$ peaks typical of direct gap zincblende semiconductors. The spin-orbit splitting Δ_0 of the valence band Γ_{15} state into a fourfold Γ_8 and doubly degenerate Γ_7 was measured to be 17±1 meV.

For w-GaN, the reflectivity spectra of Dingle et al. [22], Shan et al. [23], Gil et al. [25],

photoluminescence excitation spectra by Monemar [26], and photoluminescence spectra as well as calorimetric absorption and reflection spectroscopy by Eckey et al. [24] show three well separated excitons labeled A, B and C. In the absence of spin-orbit coulping, the hexagonal crystal field splits the zincblende Γ_{15} state into a doublet Γ_6 and a singlet Γ_1 state (not counting spin degeneracy), whose splitting we shall denote by Δ_c. With the inclusion of the spin-orbit coupling, the Γ_6 states splits into a Γ_9 and Γ_7 state, while the Γ_1 becomes a Γ_7 state in the notation of the double group. The two Γ_7 states repel each other and lead to a simple quadratic eigenvalue problem with the result that the $\Gamma_9 - \Gamma_7$ splittings, which correspond to the A-B, A-C splittings, are given by

$$E_{\Gamma_9} - E_{\Gamma_7} = \frac{\Delta_c + \Delta_0}{2} \pm \frac{1}{2}\sqrt{(\Delta_c + \Delta_0)^2 - \frac{8}{3}\Delta_0\Delta_c}, \qquad (1)$$

within the quasi-cubic model of Hopfield[27].

We have separately calculated the spin-orbit splitting parameter Δ_0 of the cubic zincblende structure and the hexagonal crystal field splitting Δ_c and its uniaxial strain dependence, i.e. its dependence on c/a, and then combined them with Eq.(1) to obtain the A-B-C exciton splittings.

Spin-orbit splitting

Table I gives our calculated spin-orbit splitting parameters Δ_0 for zincblende BN, AlN, GaN and InN.

Table I: Spin-orbit splitting Δ_0 (in meV) in zincblende nitrides.

	theory	d as core	experiment
BN	22		
AlN	19		
GaN	19	21	17±1
InN	3	19	

We note that they are very similar in all nitrides except for InN. Within a tight-binding model for the Γ_{15}^v wave function $|\psi_v\rangle$ the spin-orbit splitting has as main contributions:

$$\Delta_0 = (3/2)(|\langle\phi_{N2p}|\psi_v\rangle|^2\zeta_{N2p} + |\langle\phi_{Xnp}|\psi_v\rangle|^2\zeta_{Xnp} - |\langle\phi_{X(n-1)d}|\psi_v\rangle|^2\zeta_{X(n-1)d}) \qquad (2)$$

where ζ_{Rnl} are atomic spin-orbit coupling parameters and $|\phi_{Rnl}\rangle$ are the atomic orbitals of quantum numbers nl on atomic site R, with X standing for the cation. Because of the strongly ionic character, the only major contribution for the nitrides (except InN) is from the atomic N2p coupling parameter ζ_p (which is 13.6 meV in the free atom and slightly renormalized by the ionic character in the solid). The contribution from the lower cation d-state (Ga3d and In4d) is negative for reasons explained by Shindo et al. [28] and as first noted empirically by Cardona [29] for the Cu-halides. It is much more significant for InN than for GaN because the In4d ζ_d (385 meV) is almost twice as large as that of Ga3d (206 meV) and because the d-mixing is stronger in InN. Additional evidence of this is that if we neglect the coupling to these d-states by treating them as core states, the GaN value is slightly larger and the InN value becomes similar to that of the other nitrides, as indicated in the second column in Table I. Our result for GaN is in good agreement with the experimental value.

Crystal field splitting and strain

The hexagonal crystal field splitting is similar to that induced by a [111] uniaxial rhombohedral strain in zincblende. Not unexpectedly, this splitting is strongly dependent on the c/a ratio which in turn is closely coupled to the internal structural parameter u, corresponding to a relative displacement of the anion versus the cation sublattice along the c-axis as in the A_1 transverse optical phonon mode[30]. We found that this optical mode deformation potential is quite strong.

Fig. 4 shows the calculated splitting of the Γ_6 and Γ_1 states relative to their weighted average in wurtzite GaN as a function of $\eta = c/a$ (with u relaxed at each point) and u (at the equilibrium c/a) at constant equilibrium volume. The crystal field splitting at the experimental c/a and u parameters is 19 meV, which combined with the 19 meV spin-orbit splitting leads to good agreement with the A-B-C excitonic splittings as can be seen in Table II. The variation

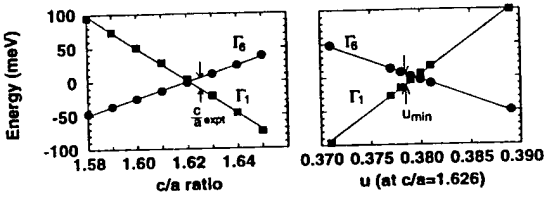

Figure 4: Crystal field splitting as a function of c/a and u in w-GaN.

between the experimental numbers is probably in part due to different strains in the samples. It is presently not entirely clear what the best experimental values are for strain-free material. The experimental determination is further complicated by the occurence of $n = 2$ excited states of the A exciton near the energy of the C exciton. Our present values were calculated at the experimental c/a and a lattice constants with u determined by energy minimization. We prefer this procedure over using entirely first-principles determined lattice constants because LDA is known to slightly underestimate the lattice constants. The experimental equilibrium value of u, however, is not known sufficiently well and is crucial because of the strong dependence of Δ_c on u.

Table II: Exciton splittings in GaN (in meV).

	A-B	A-C
present	8	30
Ref. [22]	6	27
Ref. [23]	8	32
Ref. [24]	6	22.5
Ref. [25]	7	29

The slopes of the lines in Fig. 4 are closely related to the deformation potentials. In fact, the strain along the c-axis $\epsilon_\parallel = (2/3)d\ln\eta$, and within the cubic approximation, we have

$$\begin{aligned} E_{\Gamma_6} &= -(1/2)D_3\epsilon_\parallel, \\ E_{\Gamma_1} &= -\Delta_c^0 + D_3\epsilon_\parallel, \end{aligned} \qquad (3)$$

in terms of the deformation potential D_3 (as defined by Bir and Pikus [31]). Within this cubic approximation, we have $D_3 = \sqrt{3}d$ where d is the deformation potential of zincblende under a rhombohedral distortion along [111]. The value we have calculated for d from z-GaN is -3.75 eV [33]. This predicts a value of -6.5 eV for D_3, whereas the direct calculation for w-GaN gives -5.7 eV.

Similarly, the slope as a function of u corresponds to the optical deformation potential for the A_1 transverse optical phonon, which we may define by $d(E_{\Gamma_6} - E_{\Gamma_1}) = D^{A_1}d\ln u$. Within the cubic approximation, the latter can be written in terms of the usual transverse optical mode deformation potential of zincblende (in Kane's notation d_{5o}), i.e. $D^{A_1} = (3/2)^{3/2}d_{5o}/4$. This gives 6.7 eV for D^{A_1} while the direct calculation for wurtzite gives 6.1 eV.

We note that under c/a expansion the A-B-C splittings are expected to increase while under compression they are expected to decrease. For GaN grown on sapphire and relaxed by misfit dislocations at high temperature one expects that upon cooling, the GaN film obtained will be under biaxial compression (because $\alpha(Al_2O_3) > \alpha(GaN)$ with α the thermal expansion coefficient). Using the Poisson ratio for the c-axis $\sigma = -2C_{13}/C_{33}$, one finds that c/a will be under tension or that the A-B-C splitting should be increased compared to the strain free situation. This has indeed been observed by Volm et al.[34] by comparing the exciton splittings in thick (supposedly strain free) films with those in thin films. On SiC, the opposite effect was obtained as expected because $\alpha(SiC) < \alpha(GaN)$. Similar results were also obtained by Monemar et al. [26]. However, if the film were pseudomorphic, i.e. below the critical thickness, and hence without misfit dislocations, one might expect that GaN on SiC would be under biaxial compression, and hence c/a tension, which would again result in an increased splitting of the excitons. This may be the explanation for the opposite data (an increase of the A-B splitting for GaN grown on SiC) reported by Edwards et al. [35] although further investigation of this is required.

Table III: Valence-band effective masses and Kohn-Luttinger parameters for GaN.

wurtzite				
$m_l^{hh} = m_t^{lh}$	m_l^{sh}	m_t^{hh}	m_t^{lh}	m_t^{sh}
2.04	0.18	1.81	0.19	1.88
A_1	A_2	A_3	A_4	A_5
-5.62	-0.53	5.13	-3.39	-2.31
zincblende				
A	B	C		
-5.05	-1.17	-5.85		

From calculations of the band structure in the immediate neighborhood of the valence-band maximum, we can also extract the effective mass parameters. In wurtzite, we must distinguish a longitudinal (along c) and transverse (indicated by subscripts l and t) heavy, light and split-off (indicated by superscript hh, lh, and sh) hole masses whose values are given in Table III. A more complete description of the valence-band manifold is obtained in terms of Kohn-Luttinger-like parameters (also indicated in Table III) as defined in Bir and Pikus for wurtzite [31] and by Luttinger for zincblende [32].

We have also obtained the conduction band masses given in Table IV. They appear to be in good agreement with the value obtained from recent Optically Detected Cyclotron Resonance (ODCR) data [36], the only direct measurement, and with the value obtained from free electron IR absorption [37]. They differ more from the value inferred rather indirectly from the g-value determined by conduction band Electron Spin Resonance (ESR) [38]. The value of Ref. [36] was interpreted as a polaronic mass and a value of 0.20 was deduced from it for the pure band structure mass.

Table IV: Conduction band effective masses in GaN

wurtzite	m_l ($\parallel c$)	0.19
	m_t ($\perp c$)	0.23
zincblende	m_c	0.19
Expt. [36]	ODCR	0.22
Expt. [38]	ESR	0.15
Expt. [37]	IR absorption	0.20

BAND OFFSETS

The band offset can be separated into two contributions

$$\Delta E_v = \Delta E_v^0 + D, \tag{4}$$

where the first ones gives the difference in bulk valence band edges as determined with respect to a common reference level such as the average electrostatic potential, and the second one is the interface dipole, which is the difference in the chosen local reference level across the interface. Each of these carry with them a certain degree of arbitrariness because the average electrostatic potential in a periodic bulk solid is not a uniquely defined quantity. Nevertheless, as long as we choose it consistently in the same way on the right and left of the interface, there is no problem. The band offsets between lattice-mismatched systems depend sensitively on the residual strain in the film. As mentioned above, one should distinguish the pseudomorphic situation below the critical thickness where the in-plane lattice constant matches that of the substrate and hence places the film under a biaxial strain, and the situation above the critical thickness where misfit disclocations relieve the strain. In the case of a density of dislocations $\kappa = 1/D$ with D the dislocation spacing and with Burgers vector component in the plane b, the residual in-plane strain is given by $\epsilon_\perp = a_f/a_s - 1 - b\kappa$. For a thick enough film, one may assume that the strain is completely relieved by the misfit dislocations ($\epsilon_\perp = 0$). In fact, in the case of large mismatch, it is likely that the critical thickness is less than a monolayer and that misfit dislocations are built in from the very start of the growth. The residual strain situation may also depend on experimental growth conditions and post-growth annealing procedures. For a given strain situation, the bulk changes in the band structure which affect ΔE_v^0 can be described by

deformation potentials. In general the strain can be decomposed into a hydrostatic component and a uniaxial strain component. The previous section describes the uniaxial strain effects on the valence band maximum in GaN for the basal plane or c-axis. Similar results for BN, AlN and InN will be published elsewhere [39]. Uniaxial deformation potentials for zincblende for all three symmetry irreducible strain components are given in Ref. [39] allowing one to calculate the strained band structure for any interface orientation. The hydrostatic pressure shift of the valence band maximum is somewhat more difficult to obtain because it itself requires an interface calculation. Below, we discuss a simple model which can provide some estimates of this effect.

For polar interfaces such as the wurtzite basal plane, it is possible that a uniform electric field exists over the thickness of the film, (or a zig-zag field in case of a periodic superlattice), produced by spontaneous polarization and the piezo-electric effect. These fields may complicate the analysis of the band-offsets. Since a uniform electric field over a substantial region of space is energetically costly, we expect that interface structural relaxation will tend to avoid such fields. This problem requires further study.

Table V: Energies (in eV) and absolute deformation potentials of the valence band maxima with respect to the dielectric midgap level in III-nitrides and some related semiconductors.

	AlN	GaN	InN	GaAs	SiC	ZnO
$E_D - E_v$	2.81	2.13	1.42	0.66	1.45	2.23
a_v	1.6	0.8	0.5	−0.5	0.5	0.6

Next, we consider the interface dipole. In principle, it is interface specific. While for the pseudomorphic case, it is feasible to calculate it from first principles using supercell models, it is rather difficult to include explicitily the effects of misfit dislocations. In practice, one usually finds that interface specific effects are washed out by a certain degree of disorder at the interfaces, for example by interdiffusion over a few atomic layers and by specific relaxations of the near interface planes, both of which tend to cancel out the induced dipoles [40, 41]. As discussed in Ref. [42], the screening of interface dipoles can be viewed as being equivalent to the minimization of the total energy of the system for a given long-range dipole potential. Somewhat heuristically, we can extend this concept even to situations where the atoms are displaced or interdiffusing. Because of the efficient screening of any interface specific effects on the dipole, band-offsets to a good approximation can be viewed as differences between bulk quantities. In the Charge Neutrality Point (CNP) model of Flores and Tejedor [43], one assumes that a certain energy level in the middle of the gap (called the CNP) should be aligned across the interface. The idea behind this is that states above this level will lead to an accumulation of negative charge when filled while states below it when empty will tend to produce a positive charge. In a variant of this model, called the Dielectric Midgap Model (DME),[12] this CNP is identified with the average of the highest valence and lowest conduction band over the Brillouin zone. In Table V, we

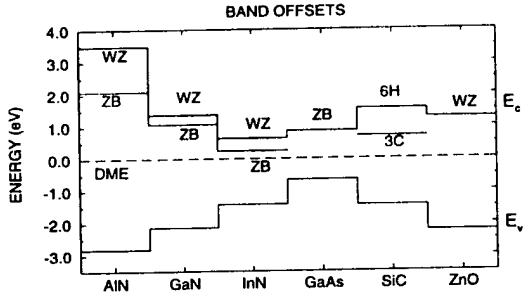

Figure 5: Band offsets within DME model.

provide the energy differences between between the valence band maximum and the DME level E_D, calculated for each semiconductor at its own equilibrium lattice constant. Thus, aligning the DME, one only needs to take differences between these values to obtain any desired band offset among the materials listed. This is illustrated in Fig. 5. The valence-band offset for GaN/AlN obtained in this manner (0.68 eV) is in fair agreement with the value obtained from explicit interface calculations for the (110) interface [44], which was 0.85 eV and with XPS results [45]. For the other nitrides, the values of the offsets obtained here deviate somewhat more from the previously given ones [44] because the latter referred to the situation where each solid was considered at the average lattice constant of the two.

The same DME model can be used to obtain the absolute hydrostatic deformation potentials. In fact, if we consider a semiconductor at two different lattice constants, their valence band line-up within this model is again obtained by aligning their E_D level. Thus we merely have to obtain the change in $E_D - E_v$ per fractional change in unit cell volume $d\ln V$, denoted by a_v and given in Table V.

ALLOYS

The band-gap bowing in $Ga_{1-x}In_xN$ was calculated using the LMTO method and various approximations to the alloy problem. Details of this work are given in Ref. [46]. Here we provide only a summary of the main results. The simplest approach we considered is to average the LMTO potential parameters of the constituents according to the composition. In such a model every cation is described as having average characteristics of the Ga and In cations. Local fluctuations in the potential depending on the various possible local environments of a N anion are totally ignored. We find that this seriously underestimates the band-gap bowing parameter b which, in this model is only 0.6 eV. Using instead a cluster expansion approach, we obtain $b = 0.89$ eV if we assume an average lattice constant and $b = 2.57$ eV if we include both volume and bond-length relaxations. The latter is much larger than the experimental value of $b = 1.0$ eV [47]. The discrepancy may be due in part to experimental difficulties such as the partial phase separation of InN and GaN in this system and to the assumption of Vegard's law used in the experimental work in converting lattice constants measured by X-ray diffraction to concentrations. The large value obtained here may explain why emission in the green region appears to have been obtained recently in $Ga_xIn_{1-x}N$ quantum wells with smaller In concentrations than previously expected. (See e.g. papers by Nakamura and Moustakas in these proceedings.) In view of the persisting problems in obtaining pure $Ga_{1-x}In_{-x}N$ alloys without inclusions of pure InN, further experimental work appears desirable. Our theoretical work may also require further refinements, e.g., to take into account the interplay between volume and bond-length relaxation and to allow for more elaborate descriptions of the disorder in the system. We can nevertheless safely conclude that the large bond-length mismatch in this alloy system is responsible for the large bowing coefficient. This is in sharp contrast to the $Al_xGa_{1-x}N$ system where we previously showed that the bandgap bowing is negligble [48].

CONCLUSION

In conclusion, in this paper we have presented new computational results on the UV optical properties of z-GaN from which it appears that continuum excitonic effects may be strong in this system. Our interpretation of the discrepancies with experimental data differs from that of other authors and was based in part on an analysis of the self-energy corrections on the band structure obtained by Rubio et al. [4]. These were found to be in good agreement with photoemission spectroscopy but fail to account for the discrepancies in the optical spectra from LDA calculations, indicating that additional two-particle many-body effects affect the optical transitions. Similar problems also appear to exist for w-AlN. Next, we have presented calculated results for the spin-orbit and crystal field splittings of the valence-band maximum, including strain effects. These results are in good agreement with measurements of the excitonic fine structure. The band-offsets problem was discussed and values based on the DME model were presented which should provide a reasonable starting point for strain relaxed heterojunctions. It was also outlined how specific strain effects could be taken into account if strain is found to be present in the particular film/substrate situation and experimental conditions. The band-gap bowing in $Ga_{1-x}In_xN$ was briefly discussed and found to be much larger than previously anticipated.

Acknowledgements

This work was supported by NSF (DMR-92-22387) and ONR (N00014-94-1-100). We wish to thank Dr. S. Loughin for sending his reflectivity results on AlN in numerical format and Dr. Janowitz for communicating his results prior to publication.

REFERENCES

1. W. R. L. Lambrecht and B. Segall, in *Properties of Group III Nitrides*, edited by J. H. Edgar, Electronic Materials Information Service (EMIS) Datareviews Series (Institution of Electrical Engineers, London 1994), Chapt. 5.
2. S. Bloom, G. Harbeke, E. Meier, and I. B. Ortenburger, *Phys. Stat. Solidi (b)* **66**, 161 (1974).
3. P. Hohenberg and W. Kohn, Phys. Rev. **136**, B864 (1964); W. Kohn and L. J. Sham, *ibid.* **140**, A1133 (1965).
4. A. Rubio, J. L. Corkill, M. L. Cohen, E. L. Shirley, and S. G. Louie, *Phys. Rev. B* **48**, 11810 (1993).
5. M. Palummo, L. Reining, R. W. Godby, C. M. Bertoni, and N. Börnsen, *Europhys. Lett.*, **26**, 607 (1994); and in *Proc. 21st Int. Conf. on the Physics of Semiconductors*, Eds. Ping Jiang, Hou-Zhi Zheng (World Scientific Press, Singapore 1993), p. 89.
6. W. R. L. Lambrecht, B. Segall, J. Rife, W. R. Hunter, and D. K. Wickenden, *Phys. Rev. B* **51**, 13516 (1995).
7. N. E. Christensen and I. Gorczyca, *Phys. Rev. B* **50**, 4397 (1994).
8. S. Loughin, R. H. French, W. Y. Ching, Y. N. Xu, and G. A. Slack, *Appl. Phys. Lett.* **63**, 1182 (1993).
9. J. Petalas, S. Logothetidis, S. Boutadakis, M. Alouani, and J. M. Wills, *Phys. Rev. B* **52**, 8082 (1995).
10. S. Logothetidis, J. Petalas, M. Cardona, and T. D. Moustakas, *Phys. Rev. B* **50**, 18017 (1994).
11. C. Janowitz, M. Cardona, R. L. Johnson, T. Cheng, T. Foxon, O. Günther, and G. Jungk, *BESSY Jahresbericht* (1994) p. 230
12. M. Cardona and N. E. Christensen, *Phys. Rev. B* **35**, 6182 (1987).
13. L. Hedin and B. I. Lundqvist, *J. Phys. C* **4**, 2064 (1971).
14. O. K. Andersen, O. Jepsen, and M. Šob, in *Electronic Band Structure and its Applications*, edited by M. Yussouff, (Springer, Heidelberg, 1987), p.1.
15. P. E. Blöchl, O. Jepsen, and O. K. Andersen, *Phys. Rev. B* **49**, 16223 (1994).
16. M. Methfessel, *Phys. Rev. B* **38**, 1537 (1988).
17. M. del Castillo-Mussot and L. J. Sham, *Phys. Rev. B* **31**, 2092 (1985)
18. W. Hanke and L. J. Sham, *Phys. Rev. B* **12**, 4501 (1975); *Phys. Rev. B* **21**, 4656 (1980).
19. W. R. L. Lambrecht, B. Segall, S. Strite, G. Martin, A. Agarwal, H. Morkoç, and A. Rockett, *Phys. Rev. B* **50**, 14155 (1994).
20. S. W. King, M. C. Benjamin, R. J. Nemanich, R. F. Davis, and W. R. L. Lambrecht, in these proceedings.
21. G. Ramírez-Flores, H. Navarro-Contreras, A. Lastras-Martínez, R. C. Powell, and J. E. Greene, *Phys. Rev. B* **50**, 8433 (1994).

22. R. Dingle, D. D. Sell, S. E. Stokowski, and M. Ilegems, *Phys. Rev. B* **4**, 1211 (1971).

23. W. Shan, T. J. Schmidt, X. H. Yang, S. J. Hwang, J. J. Song, and B. Goldenberg, *Appl. Phys. Lett.* **66**, 985 (1995).

24. L. Eckey, L. Podlowskii, A. Göldner, A. Hoffmann, I. Broser, B. K. Meyer, D. Volm, T. Streibl, T. Detchprohm, H. Amano, and I. Akasaki, in *Proc. 6th International Conference on Silicon Carbide and Related Materials, held in Kyoto, Sept. 1995*, to be published by (Institute of Physics, London 1995) .

25. B. Gil, O. Briot, and R.-L. Aulombard, *Phys. Rev. B* **52** 91995), to be published.

26. B. A. Monemar, *Phys. Rev. B* **10**, 676, and private communication.

27. J. J. Hopfield, *J. Phys. Chem. Solids* **15**, 97 (1960).

28. K. Shindo, A. Morita, and H. Kamimura, *J. Phys. Soc. Japan.* **20**, 2054 (1965)

29. M. Cardona, *Phys. Rev.* **129**, 69 (1963).

30. K. Kim, W. R. L. Lambrecht, and B. Segall, these proceddings.

31. G. L. Bir and G. E. Pikus, *Symmetry and Srain-Induced Effects in Semiconductors*, (John-Wiley & Sons, New York 1974).

32. J. M. Luttinger, *Phys. Rev.* **102**, 1030 (1956).

33. K. Kim, W. R. L. Lambrecht, and B. Segall, *Phys. Rev. B* **50**, 1502 (1994).

34. D. Volm, K. Oettinger, T. Streibl, D. Kovalev, N. Ben-Chorin, J. Diener, B. k. Meyer, J. Majewski, L. Eckey, A. Hoffmann, H. Amano, I. Akasaki, K. Hiramatsu, and T. Detchprom, to be published.

35. N. V. Edwards, M. D. Bremser, T. W. Weeks, Jr., H. Liu, A. E. Wickenden, K. Doverspike, R. A. Stall, D. K. Gaskill, J. A. Freitas, R. F. Davis, and D. E. Aspnes, these proceedings.

36. M Drechsler, B. K. Meyer, D. M. Hoffmann, D. Detchprohm, H. Amano, and I. Akasaki, *Jpn. J. Appl. Phys.* **34**, L1178 (1995).

37. A. S. Barker, Jr. and M. Ilegems, *Phys. Rev. B* **7**, 743 (1973).

38. M. Fanciulli, T. Lei, amd T. D. Moustakas, *Phys. Rev. B* **48**, 15144 (1993).

39. K. Kim, W. R. L. Lambrecht, and B. Segall, *Phys. Rev. B* (1995), submitted.

40. W. R. L. Lambrecht and B. Segall, *Phys. Rev. B* **41**, 2832 (1990).

41. M. S. Hybertsen, *J. Vac. Sci. Technol. B* **8**, 773 (1990).

42. W. R. L. Lambrecht, B. Segall, and O. K. Andersen, *Phys. Rev. B* **41**, 2814 (1990).

43. F. Flores and C. Tejedor, *J. Phys. C* **20**, 145 91987).

44. E. A. Albanesi, W. R. L. Lambrecht, and B. Segall in *Mater. Res. Soc. Symp. Proc.* Vol. **339**, p. 607 (1994); *J. Vac. Sci. Technol. B* **12**, 2470 (1994).

45. G. Martin, S. Strite, A. Botchkarev, A. Agarwal, A. Rockett, H. Morkoç, W. R. L. Lambrecht,a nd B. segall, *Appl. Phys. Lett.* **65**, 610 (1994).

46. W. R. L. Lambrecht, *Proc. Topical Workshop on Nitrides, Nagoya 95*, to be published in *Solid State Electron.* (1995).

47. K. Osamura, S. Naka, and Y. Murakami, *J. Appl. Phys.* **46**, 3432 (1975).

48. E. A. Albanesi, W. R. L. Lambrecht, and B. Segall, *Phys. Rev. B* **48**, 17841 (1993).

SEMICONDUCTORS AND SEMIMETALS, VOL. 50

CHAPTER 12

Band Structure of the Group III Nitrides

W. R. L. Lambrecht

DEPARTMENT OF PHYSICS
CASE WESTERN RESERVE UNIVERSITY
CLEVELAND, OHIO

I. Introduction

In this review, we present the current state of knowledge of the electronic band structure of group III nitrides as well as some historic perspective. The number of papers dealing with the electronic band structure of the nitrides and the variety of methods applied may seem bewildering to the nonexpert. It turns out that many of these are only "slight variations on a theme" and the good news is that most recent calculations agree pretty well with each other on the basic aspects. Thus, rather than attempting to be complete, we try here to highlight the key aspects and the most significant contributions.

In Section II, we give a brief historic overview of the most significant calculations, along with a short description of the various methods that have been employed.

ISBN 0-12-752158-5
0080-8784

In Section III, we turn to a discussion of the relation between the band structures in the two crystal structures of most practical interest, namely the zinc-blende and the wurtzite. As is well known, the III nitrides (except for BN which is more similar to diamond in many aspects, and is therefore mostly excluded from this review) naturally occur in the wurtzite structure, but the zinc-blende phase can be stabilized by epitaxial growth techniques. For GaN, this is done rather commonly and successfully, while for InN and AlN there have been only a few reports. We note that there is a third crystal structure of interest, namely the rocksalt structure, which occurs under high-pressure conditions. For electronic applications, however, the zinc-blende and wurtzite phases are far more important, and hence, we confine our discussion of the band structures to those two phases.

In Section IV, we discuss some of the trends in the band structures and related properties in terms of ionicity and cation.

In Section V, we discuss experimental probes of the band structures, such as X-ray and UV photoemission spectroscopy (XPS), UV reflectivity and spectroscopic ellipsometry (SE) and X-ray absorption near-edge spectroscopy (XANES).

Up to this point, we consider the band structures mostly at the scale of several eV. For most of the intended applications of the nitrides, the most important part of the band structure, however, is the region right next to the band edges, at a scale of meV. This pertains to questions on the effective masses, exciton splittings under strain, etc. Recently, several papers have appeared dealing with these aspects. A discussion of this work is given in Section VI.

Finally, in Section VII, we present an outlook for the future. What are still unresolved questions or where should we expect most progress in the coming years?

Overall, our presentation will focus on the qualitative aspects, and the issues that have been under discussion over the years, and will somewhat have the nature of a comment. While we include quantitative figures and tables where appropriate, the paper is not intended as a reference work for finding the most accurate, complete, or recent set of numerical values, and is hence not organized material by material. For that, we refer the reader to the original publications, and to the EMIS Datareview on Group III Nitrides (Lambrecht and Segall, 1994).

II. Overview of Calculations

1. Early Semi-Empirical Studies

The first studies of the band structure of the nitrides appeared in the late 1960's to early 1970's. The work of Bloom (1971), Bloom *et al.* (1974), and Jones and Lettington (1969) used the semi-empirical pseudopotential

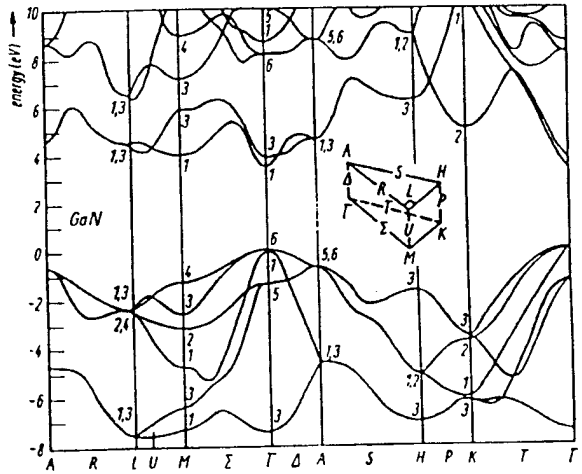

FIG. 1. Semiempirical pseudopotential band structure of wurtzite GaN by Bloom *et al.* (1974).

approach, in conjunction with optical reflectivity measurements. In this method, the Fourier components of the pseudopotential are adjusted in an iterative procedure, so as to adjust a few interband transitions to experimentally observed peak positions in reflectivity. The disadvantage of this approach, is that the assignment of experimental features to specific transitions is not always straightforward and not unique. Usually, similarity to other better known semiconductors is exploited to arrive at a consistent assignment.

The band structures obtained in this manner agree reasonably well with more recent calculations for the valence bands, but they differ significantly from the more recent calculations in the conduction bands. This is evident by comparing the bands of GaN in Fig. 1 with a recent calculation in Fig. 5 given below in Section III. Of particular importance, is that the energy difference between the lowest conduction band minimum at Γ and local minima at other k-points is much smaller in the older calculation. Also, the first Γ_6 band is much lower, and the second Γ_3 band below it is missing. Nevertheless, these band structures gave a fairly good account of the then available reflectivity spectra up to about 10 eV.

Other early calculations for GaN by Bourne and Jacobs (1972) using a muffin-tin potential differ substantially from the now accepted band struc-

ture. Even more recent semi-empirical pseudopotential calculations by Grinajew, Malachow, and Czaldyszew (1986) obtained an indirect gap incorrectly.

For AlN, there were even earlier Orthogonalized Plane Wave (OPW) calculations (Hejda and Hauptmanová, 1969), an approach which is a direct precursor of the pseudopotential methods.

For InN, the first experimental studies by Tyagai *et al.* (1977) suggested an indirect gap, while a later semi-empirical pseudopotential calculation by Foley and Tansley (1986) indicated a direct gap. These difficulties were in large part due to the problems in obtaining adequate samples.

In summary, the intrinsic ambiguities in the semi-empirical pseudopotential method left much uncertainty on even elementary questions on the band structures, such as direct or indirect nature of the gap. Results by different groups led to contradictory results, but nevertheless, provided important guidance to the optical studies of the time.

2. Local Density Functional Calculations

A boom in band structure calculations of the nitrides occurred in the late 1980's and early 1990's. During the intervening decade, the practice of band-structure theory had evolved considerably. The "standard" approach until this date is density functional theory (DFT) in the local density approximation (LDA) (Hohenberg and Kohn, 1965). Before discussing the application of this method to the nitrides, we briefly review some basics of the method.

a. Introduction to DFT, LDA, and GW Methods

In the present context, DFT can be thought of as a self-consistent field method for obtaining the crystal potential. The emphasis of band-structure theorists, however, has also mostly changed from electronic structure *per se* to using it as an intermediate step in calculating total binding energies of solids and from it, properties such as lattice constant, bulk modulus, elastic constants, phonon frequencies, etc. These are the properties, density functional theory is, strictly speaking, designed for. The electronc charge density is the basic quantity in this theory, and is determined by minimizing the total electronic energy of the solid. The expression for the total energy as functional of the density includes exchange and correlation effects in an average "electron-gas"-like way, which is referred to as the "local density approximation." In its most commonly used form, the charge density is

expressed in terms of occupied one-electron wave functions (the so-called Kohn-Sham states) whose corresponding eigenvalues constitute the band structure. The Kohn-Sham equation reads

$$\left\{-\frac{\hbar^2}{2m}\Delta + v_H[n(\mathbf{r})] + v_{xc}[n(\mathbf{r})]\right\}\psi_{nk}(\mathbf{r}) = \varepsilon_{nk}\psi_{nk}(\mathbf{r}), \tag{1}$$

with $v_H[n(\mathbf{r})]$ and $v_{xc}[n(\mathbf{r})] = \delta E_{xc}/\delta n$ the Hartree and exchange-correlation potentials, which are both known functionals of the density. More precisely,

$$v_H[n(\mathbf{r})] = \int\int \frac{n(\mathbf{r})n(\mathbf{r}')}{|\mathbf{r}-\mathbf{r}'|}\, d^3r d^3r' \tag{2}$$

is known exactly, and is the classic Coulomb interaction and $v_{xc}[n(\mathbf{r})]$ is approximated by its corresponding expression from the homogeneous electron gas, where n is a constant, but now applied at each point in space. Hence, the name, *local* density approximation. The density itself must be determined self-consistently from

$$n(\mathbf{r}) = \sum_{nk}^{occ} |\psi_{nk}(\mathbf{r})|^2 \tag{3}$$

In a purist point of view, the band structures ε_{nk}, appearing in this theory have nothing to do with the single-particle excitations (or quasiparticles) of the system. In other words, they do not correspond to the energies for adding or removing a single electron from the system. They correspond even less to the two-particle excitations involved in the optical spectra. Nevertheless, it is common practice to view the Kohn-Sham band structure as a first approximation to the true band structure. The reason why this is reasonable, is that the true quasiparticle band structure can be obtained from the closely related Dyson equation,

$$\left[-\frac{\hbar^2}{2m}\Delta + v_H(\mathbf{r})\right]\Psi_{nk}(\mathbf{r}) + \int \Sigma_{xc}(\mathbf{r}, \mathbf{r}', E_{nk})\Psi_{nk}(\mathbf{r}')d^3r' = E_{nk}\Psi_{nk}(\mathbf{r}), \tag{4}$$

the only difference being that the exchange-correlation potential is here replaced by a more complicated energy-dependent and non-local self-energy operator (Hedin and Lundqvist, 1969; Sham and Kohn, 1966). One can indeed view the exchange-correlation potential as a local approximation to

the self-energy operator

$$\Sigma_{xc}(\mathbf{r}, \mathbf{r}', E) \approx \delta(\mathbf{r} - \mathbf{r}')v_{xc}[n(\mathbf{r})]. \quad (5)$$

The current state-of-the-art for calculating self-energies is the so-called "GW" approach, in which the letters stand for the symbols used in Hedin's original paper (Hedin and Lundqvist, 1969) on this method for respectively the one-electron Green's function and the screened Coulomb interaction. The GW approximation is the first term in a perturbation expansion of the self-energy, or, alternatively, can be viewed as a "screened" Hartree-Fock theory. The method was computationally developed by Hybertsen and Louie (1986), Godby, Schlüter, and Sham (1988), and more recently, in an alternative basis set formulation by Aryasetiawan and Gunnarsson (1994).

In semiconductors, the "GW" band structures differ from the LDA band structures primarily by a shift of the conduction band relative to the valence band. In other words, LDA Kohn-Sham band structures underestimate band gaps in semiconductors, which is a well-known problem (Perdew and Levy, 1983; Sham and Schlüter, 1983). We emphasize that it is not a fundamental problem of LDFT, but rather a question of "using the wrong equation." We immediately clarify that the gap underestimate is not the only change, or that the shifts are strictly k-independent. In fact, thay are not. Nevertheless, the LDA band structures + constant shift form a convenient starting point to analyze the true band structure.

Most band structure calculations for the nitrides have been of the LDA type, and are discussed below. Recent calculations beyond LDA are discussed in Subsection 3.

b. Introduction to Band-Structure Methods

A variety of band structure methods have been used within this general framework. We distinguish here between pseudopotential and all-electron methods. In the first of these, the atomic potential is replaced by a smooth (norm-conserving non-local) pseudopotential (Hamann, Schlüter, and Chiang, 1979; Kerker, 1980) whose valence-eigenstates agree with those of the true system outside the core of the atom, but differ from them in the core region which is unimportant for chemical bonding. Usually, the wave functions are expanded in plane waves although localized atom-centered basis sets such as Gaussian orbitals or mixed basis sets have also been used. There is some flexibility in how to construct the potential: one refers to hard or soft pseudopotentials depending on the core radius applied. In principle, the softer one makes the potential, the less it becomes transferable from one situation to another, although new approaches to overcome these difficulties have been introduced (Vanderbilt, 1990; Blöchl, 1994). At the same time, the softer the potential, the easier it becomes to do the calculation because fewer plane waves are required to obtain convergence of the wave functions. Thus, a soft pseudopotential may be more accurate than a hard pseudopotential when used with the same plane wave energy cut-off. These variations and the computationally affordable cut-offs explain the differences between the results of the earlier calculations on the nitrides using this approach.

Most all-electron methods treat the inner part of the atoms in another way, known as augmentation. That is, the actual solutions of the spherical part of the potential within a sphere around the atom and their energy derivatives are used to expand the wave functions and matched to envelope functions outside the spheres. These methods include the linear muffin-tin orbital (LMTO) and linearized augmented plane-wave (LAPW) methods (Andersen, 1975). While nowadays, these methods can be applied without shape approximations and are designated as full-potential (FP) methods (Methfessel, 1988), the earlier applications of LMTO made the so-called atomic sphere approximation (ASA). In the ASA, the crystal potential is approximated by a superposition of slightly overlapping spherical potentials centered on atomic sites in such a way that the spheres are filling space. For open structures, one usually also includes spheres centered on interstitial sites. It turns out that this potential is rather close to the true full potential (Andersen, Postnivok, and Savrasov, 1992), and much better than the original muffin-tin potentials which are constant in the interstitial region and spherical within non-overlapping spheres. In practice, it is usually combined with a spherical approximation to the charge density in the same spheres. While this is quite satisfactory for most aspects of the band structure to a precision of ~ 0.1 eV or better, it is not entirely satisfactory when addressing very delicate aspects of the band structure, which crucially depend on local symmetry breaking, or for total energy variations such as those involved in frozen phonon calculations. In particular, the very small total energy differences between the zincblende and wurtzite are not accurately obtained within ASA-LMTO. Another quantity that is very subtle is the crystal field splitting of the valence-band maximum. Thus, the early calculations of this type have the order of the doublet and singlet of wurtzite inverted for GaN.

c. Calculations for the Nitrides

With these considerations in mind, we now examine some of the calculations that have been performed for the nitrides. Gorczyca *et al.* (1992) and Christensen and Gorczyca (1994) applied the ASA-LMTO to the III-

nitrides in a series of papers, that was mostly focused on the study of the high-pressure transition to rocksalt. A FP-LMTO study of AlN structural aspects under pressure was also performed by these authors (Christensen and Gorczyca, 1993) as well as a study of some of the important phonon modes (Gorczyca *et al.*, 1995). Lambrecht and Segall (1992) applied ASA-LMTO to study the relations between zinc-blende and wurtzite band structures, discussed direct versus indirectness of the gaps and trends in the materials (Lambrecht, 1994). They went on to study photoemission (Lambrecht *et al.*, 1994) and UV optical properties (Lambrecht *et al.*, 1995). Kim, Lambrecht, and Segall (1994, 1996) subsequently used FP-LMTO calculations to study elastic constants and strain effects on the band structures. Fiorentini, Methfessel, and Scheffler (1993) also applied FP-LMTO to zincblende GaN and focused on the effects of Ga3d electrons. The latter were also discussed by Lambrecht *et al.* (1994). Muñoz and Kunc (1993) presented a FP-LMTO study for InN. These various all-electron calculations all included Ga3d and In4d band dispersion and hybridization with the rest of the bands.

The early norm-conserving pseudopotential calculations by Van Camp, Van Doren, and Devreese (1991), Muñoz and Kunc (1991), and Palummo *et al.* (1993) did not include the effects of the d-electrons. Reaching convergence in plane wave expansions proved difficult, because of the deep N pseudopotential and was continuously found to require higher cut-offs from one calculation to the next. Min, Chan, and Ho (1992) used a mixed basis set to overcome this difficulty, but obtained the somewhat unexpected result that zinc-blende GaN would be lower in energy than wurtzite, which was not bourne out by later well-converged plane-wave calculations (Yeh *et al.*, 1992; Wright and Nelson, 1995a) and seems to contradict the experimental fact that natural bulk crystals of GaN have the wurtzite structure. Yeh *et al.* (1992) focused on precisely this question for a number of semiconductors including the nitrides. Their work is also the first to fully relax the structural parameters for wurtzite.

An issue that was discussed repeatedly between pseudopotential and all-electron practitioners is the role of the d-bands. The reason for this is that the semi-core Ga3d and In4d states overlap in energy with the deep N2s states. They thus play a non-insignificant role in the bonding. While this is also known to be the case in GaAs, it is more strongly pronounced here because of the close proximity of the Ga atoms, the lattice constants of these materials being rather small. The various ways in which d-electrons can be treated: as core orbitals with or without nonlinear core corrections (i.e., including or excluding core-valence exchange), or as pseudized valence states in pseudopotential methods; frozen core or relaxed core or valence with single or two-panel approaches in linear methods, lead

to some confusions, which were discussed rather extensively by Fiorentini, Methfessel, and Scheffler (1993) and Lambrecht *et al.* (1994). In the pseudopotential framework, accurate calculations treating the Ga3d and In4d explicitly as valence states were performed by Wright and Nelson (1995a). These authors also pushed the plane wave cut-offs to 240 Ry, to insure convergence. An interesting aspect is that while d-electron hybridization is important in bonding, they nevertheless appear as separate states, when considering quasiparticle excitations in photoemission (Lambrecht *et al.*, 1994).

Another aspect which influences the accuracy of the calculations is whether or not full structural relaxation is taken into account. One is faced with the dilemma of taking either the experimental crystal structure parameters or the theoretical equilibrium values obtained self-consistently from the density functional calculation. Typically, the local density functional calculations underestimate the lattice constants by a percent or so. Since the bandgap deformation potentials in these materials are substantial, that does affect the band structure considerably. For wurtzite, the structure is not entirely fixed by symmetry: the c/a ratio and the internal parameter u (defining the bond length along the c-axis by $d = cu$) need to be determined by total energy minimization. While c/a is well known from experiment, the internal parameter is more difficult to obtain accurately experimentally, and substantial variation exists among the reported experimental values. Hence, the most accurate calculations are those in which u is determined theoretically. Of course, accuracy should not be our only criterion. Understanding the trends is what will be emphasized in the later sections.

Other groups have presented pseudopotential calculations mainly as a test to go on to defect calculations and surface calculations (Neugebauer and Van de Walle, 1996; Boguslawski, Briggs, and Bernholc, 1995) dielectric constant and nonlinear susceptibility (Chen, Levine, and Wilkins, 1995), or phonon calculations (Miwa and Fukumoto, 1993; Karch *et al.*, 1996). Other calculations worth mentioning are those of Corkill, Rubio, and Cohen, (1994), who addressed the role of d-bands on the gaps and Yeh, Wei, and Zunger (1994) addressing the relation of bandgaps in wurtzite and zinc-blende. Some other methods were also applied: LCAO with gaussian type orbitals by Huang and Ching (1985), Ching and Harmon (1986), Xu and Ching (1993), and tight-binding by Kobayashi *et al.* (1983) and Jenkins and Dow (1989).

Although slight variations persist among the results of the different methods, the origin of which is hard to trace back, the well-converged LDA calculations agree well on basic predictions of the topology of the bands, bandwidths, size of the bandgaps (to within a few 0.1 eV), lattice constants, bulk moduli and other total energy properties.

3. BEYOND LDA

A few calculations for the nitrides have been performed in the Hartree-Fock approximation rather than the local density functional theory. These include a calculation for GaN by Pandey, Jaffe, and Harrison (1993) and for AlN by Ruiz, Alvarez, and Alemany (1994). In Hartree-Fock, exchange is treated exactly, but correlations are completely neglected. Contrary to LDA, Hartree-Fock calculations overestimate the gaps of semiconductors.

As mentioned in the introduction of the previous subsection, a considerable better approach is the GW approximation. GW calculations were performed for wurtzite and zinc-blende GaN and AlN by Rubio *et al.* (1993), for zinc-blende GaN by Palummo *et al.* (1994, 1995). These calculations agree fairly well among each other in their basic predictions.

One finds that the valence bands shift down with respect to the LDA results, and the conduction bands shift up. The downward shift of the valence bands increases with increasing energy below the valence band maximum, and in particular, with the more localized character of these

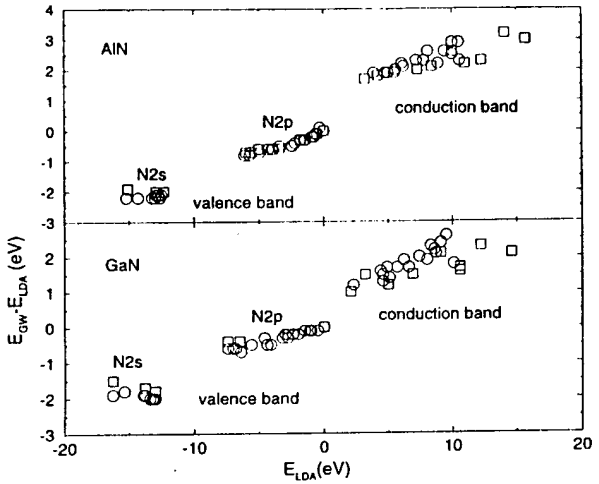

FIG. 2. Self energy corrections to the LDA band structures, that is, GW eigenvalues minus corresponding LDA eigenvalue as function of LDA eigenvalues for GaN and AlN from tabulations in Rubio *et al.* (1993). Circles correspond to wurtzite and squares to zinc-blende.

states. Thus, the N2s states shift by about 1.5–2 eV more than the valence band maximum. The bottom of the N2p valence band which is of mixed N2p cation-s character shift by about 0.5 eV more than the maximum. This can be seen clearly in Fig. 2, which is based on tabulated results by Rubio *et al.* (1993).

The absolute shift of the valence-band maximum is a somewhat more problematic quantity in current GW theories. Even for well studied materials such as Si (Godby, Schlüter, and Sham, 1988), the various calculations agree less upon this than for the gap corrections. In fact, it appears to depend sensitively on which parameterization is used for the LDA starting point of the calculation. The GW changes the gap by about 1 eV in GaN and about 2 eV in AlN, thus giving excellent agreement with experiment. The conduction band corrections are found to vary by a few 0.1 eV among different k-points and specific states, and appear to increase as one goes up in energy (see Fig. 2). However, strict tests of this cannot be done until these states have been determined more accurately experimentally, which is the subject of Section V.

III. Relations Between Brillouin Zones of Wurtzite and Zinc-blende

The relation between the band structures in zinc-blende (zb) and wurtzite (wz) can largely be understood in terms of band structure folding effects. While there are not exact relations, they are quite helpful in comparing the band structures. The relation is based on the fact that the wurtzite basal planes are essentially the same as the zinc-blende {111} planes, but with a different relative stacking, ABC in cubic and AB in wurtzite. Thus, the first step to obtain a common framework to compare the band structures is to use a set of cartesian coordinates for cubic materials which is more closely related to the one used for the wurtzite. We can do this by choosing a z' axis along [111] of cubic. In the (111) plane of zinc-blende and the (0001) plane of wurtzite, the crystal structure consists of buckled hexagonal rings of alternating nitrogen and cation. Thus, by aligning these hexagons, we specify completely the relation between the new set of coordinate axes in zinc-blende and those in wurtzite. Specifically, one has the rotation matrix:

$$\begin{pmatrix} x' \\ y' \\ z' \end{pmatrix} = \begin{pmatrix} 1/\sqrt{2} & -1/\sqrt{2} & 0 \\ 1/\sqrt{6} & 1/\sqrt{6} & -2/\sqrt{6} \\ 1/\sqrt{3} & 1/\sqrt{3} & 1/\sqrt{3} \end{pmatrix} \begin{pmatrix} x \\ y \\ z \end{pmatrix} \tag{6}$$

In other words, the following directions in zinc-blende and wurtzite corre-

TABLE I

EQUIVALENCE BETWEEN WURTZITE AND ZINC-BLENDE SYMMETRY k-POINTS, ASSUMING THE IDEAL c/a RATIO FOR WURTZITE

Zinc-blende	Wurtzite
L	Γ
L	U at 2/3 of $M - L$
X	U at 2/3 of $M - L$
W	T at 3/4 of $\Gamma - K$
U, K	Σ at 3/4 of $\Gamma - M$

spond to each other:

wurtzite [0001] ∥ zincblende [111]

wurtzite $[11\bar{2}0]$ ∥ zincblende $[10\bar{1}]$

wurtzite $[1\bar{1}00]$ ∥ zincblende $[1\bar{2}1]$

The above transformation can now be applied to any k-point of the reciprocal space to find equivalences between cubic BZ high-symmetry points and their location in the hexagonal Brillouin zone. These are summarized in Table I. The relations are further clarified in Fig. 3.

In Figs. 4 and 5, we compare the zinc-blende and wurtzite band structures of AlN and GaN both shown in the same wurtzite BZ. These were obtained in the LDA using the FP-LMTO method at the experimental lattice constants and with optimized u values. Although deformation potential results obtained from these band structures were given elsewhere (Kim, Lambrecht, and Segall, 1996), these full and accurate band structure figures were not published before. One may now appreciate the similarities and the true differences brought about by the different structure without being confused by the conventional way of plotting these bands in their own and different BZs. Figures of the zinc-blende band structures in the conventional zinc-blende BZ can be found in Lambrecht and Segall (1994).

It should be understood, that when we plot the zinc-blende bands in a wurtzite Brillouin zone, we plot the bands of a unit cell twice the size of the primitive unit cell of ZB, and consisting of two {111} layers. Even so, the reciprocal lattice of this supercell does not correspond to the wurtzite one. We merely show the bands along the high-symmetry lines of wurtzite in k-space, which we can always do, even if this is not a proper BZ. This implies among others that zinc-blende bands do not have the full symmetry

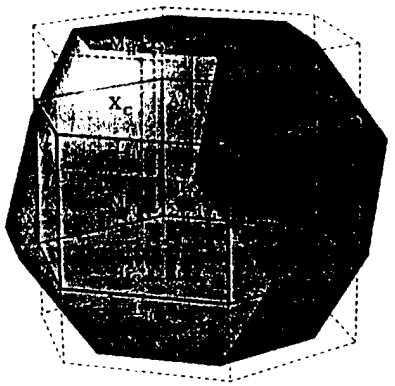

FIG. 3. Relation between zinc-blende and wurtzite Brillouin zone. Half of the adjacent wurtzite Brillouin zones along the c-axis are shown in addition to the central one. This way, one can see that both the X_C (center of the square face and L_C^1 point (center of one of the hexagonal sides) lie at 2/3 of the hexagonal ML_H line. The L_C point on the top and bottom hexagonal faces correspond to the center of the hexagonal BZ, for example, fold on Γ_H. One may also see that the cubic LW_C^1 line will be folded onto the hexagonal $\Gamma - K_H$ line.

required of a hexagonal Brillouin zone. Thus, some of the eigenvalues at Γ_H are true Γ_C eigenvalues of zb and some are folded L_C points. Specifically, the Γ_3 states are essentially folded L_C states. Similarly, the bands at the point 2/3 of ML_H correspond to both the X_C and L_C^1 points of zb. While in the true hexagonal crystal, some of the hidden cubic symmetries are broken, there are also new symmetries related to the presence of a hexagonal axis not present in cubic. The wurtzite structure has point group C_{6v}. This is not a subgroup of the tetrahedral group T_d of zinc-blende. However, both have a common subgroup C_{3v}. In spite of these differences resulting from the different symmetry, the corresponding states are closely related in physical character. We now discuss some of these in more detail.

We first focus on the states near the gap at the Γ-point. The gaps obtained from our FP-LMTO band-structure calculations are given in Table II. One finds that the direct gap at Γ is slightly larger in wurtzite than in zinc-blende in all cases. The splitting of the Γ_{15} valence band maximum into Γ_6^v and Γ_1^v leads to a slightly repulsive interaction of the Γ_1^v state with the conduction band Γ_1^c, and hence, an opening of the gap. Since the Γ_1^v however, is mostly p_z-like, and the Γ_1^c state is mostly s-like, this effect is rather small.

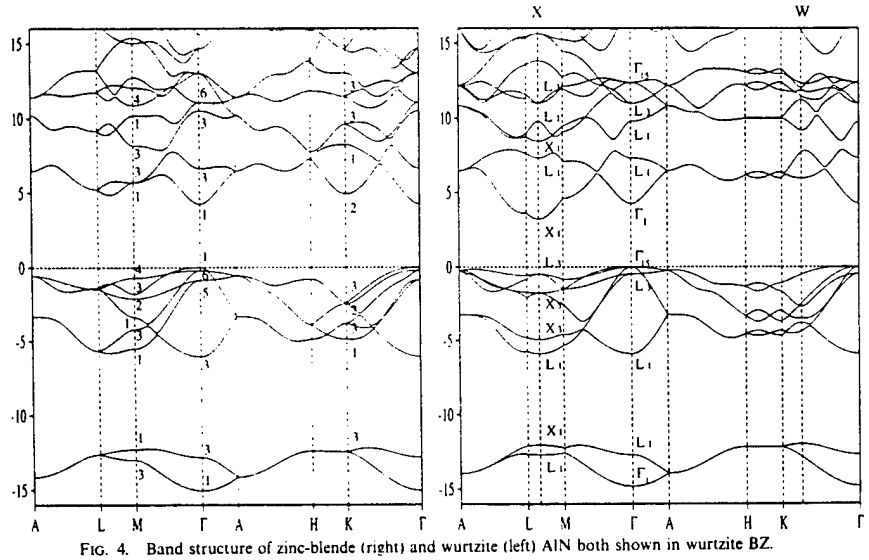

FIG. 4. Band structure of zinc-blende (right) and wurtzite (left) AlN both shown in wurtzite BZ.

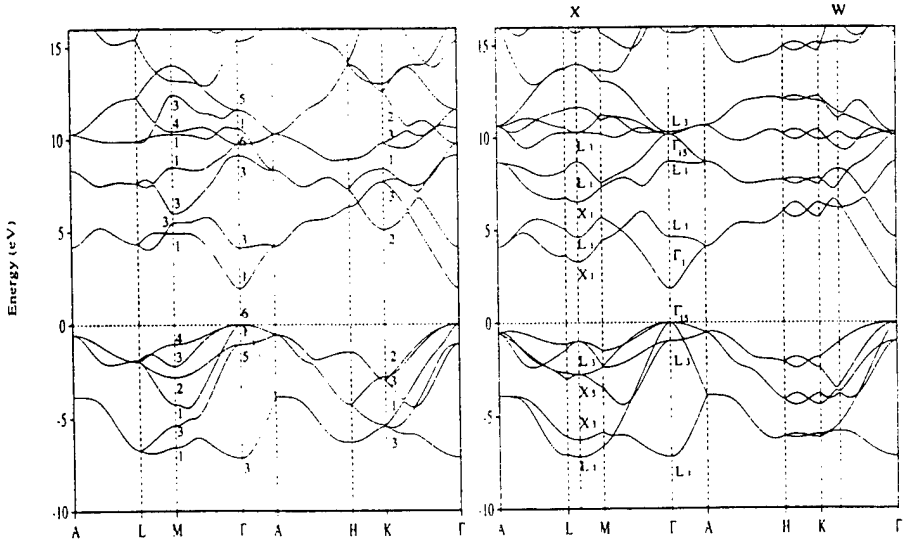

FIG. 5. Band structure of zinc-blende (right) and wurtzite (left) GaN both shown in wurtzite BZ. The lower N2s and Ga3d bands are not shown here.

TABLE II

LDA BANDGAPS IN WURTZITE AND ZINC-BLENDE (IN eV) FROM LDA FP-LMTO CALCULATIONS

	Zinc-blende	Wurtzite	Difference
AlN	4.236	4.255	0.019
GaN	1.763	1.935	0.172
InN	−0.399	0.064	0.463

Furthermore, it is partially cancelled by the fact that the minimum gap is actually the $\Gamma_6^c - \Gamma_1^c$ gap. Also, this ignores interactions with the higher lying Γ_{15}^c or rather its derived Γ_1^c conduction band. The latter lies farther away in the nitrides than the valence band maximum, and furthermore, has generally smaller interaction matrix elements with the state of interest. In earlier ASA-LMTO calculations, we obtained a value of about 0.3 eV for the gap difference in GaN (Lambrecht and Segall, 1994). Pseudopotential calculations (Palummo *et al.*, 1993; Wright and Nelson, 1995a; Rubio *et al.*, 1993) give values 0.1–0.2 eV. Experimentally, the most accurate values for the exciton gap in wurtzite GaN appears to be 3.48 eV (Eckey *et al.*, 1996) and for zinc-blende 3.27 eV (Okumura *et al.*, 1996), and 3.30 eV (Ramirez-Flores *et al.*, 1994), giving a difference of 0.2 eV. In AlN, the c/a ratio is significantly lower than the ideal value. This leads to an inversion of the Γ_1^c and Γ_6^c states. This upward shift of the Γ_1^c tends to lower the gap.

Other notable differences are the lowering of the bands (at 2/3 ML_w equivalent to X when going to the cubic structure) and the lowering of the K_2 state in wurtzite. These effects are purely structurally and symmetry-lowering related. The same kind of shifts occur in other materials (e.g., diamond, SiC).

For example, X_c is a high symmetry point in cubic but not in wurtzite. Because of the higher symmetry of this state in the cubic material, fewer states between conduction band and valence band can interact. In fact, the minimum has X_1 symmetry and only interacts with the N2s like states about 12 eV below in the zinc-blende structure. In the wurtzite structure, the band at this same k-point have symmetry U_3 and hence can interact with N2p-like states in the valence band much closer by, which also have this same symmetry. Of course, we should also consider interactions with states higher up in the conduction band, which would have the opposite effect. However, in a $\mathbf{k}\cdot\mathbf{p}$ framework, these generally have smaller matrix elements. Hence, one expects these states to be pushed up in wurtzite because of their lower symmetry.

Similarly, we can see that the zinc-blende states at the K_{wz} point in the valence band are considerably more spread out, the highest one of them lying only 2 eV below the valence-band maximum instead of 3 eV in wz. One can think of this as being a result of increasing interactions between these bands. This in turn affects the interactions with the conduction band, pushing up the conduction band minimum at K in zb versus that of the K_2 state in wz. In wz, the latter has purely p_x, p_y symmetry with x and y in the c-plane. In zb, this symmetry is broken and additional interactions push up the state. We note in passing, that the lowest conduction band state at K appears to be rather sensitive to nonspherical corrections to the potential. It is significantly lowered in FP versus ASA calculations. The reason for this is not fully understood, but may be related to the pure p-like and hence strongly asymetric character of this state.

There is a slightly different way of viewing the zb bandstructure which may further clarify these relations. Consider the cubic structure in a supercell containing three cubic unit cells in ABC stacking along [111]. Now, consider a slight distortion of the lattice along this axis (as for example, produced by a uniaxial pressure). This structure obviously still exhibits the 3-fold symmetry C_{3v} and belongs to the rhombohedral (or trigonal) Bravais lattice. We can hence call it the 3R structure, using a nomenclature of polytypes often used in the SiC literature. The Brillouin zone corresponding to this supercell has the hexagonal shape of the wurtzite BZ, but its height is only 2/3 of that of the wurtzite BZ. The primitive unit cell of the rhombohedral lattice is actually three times smaller and corresponds in this case to the conventional fcc unit cell with a slight distortion along [111]. Hence, its BZ (the conventional fcc BZ) is folded three times into the smaller BZ corresponding to the 3-layer supercell along the [111] stacking axis. The X-point of zinc-blende according to Table 1 corresponds to a point 2/3 of the ML axis in wz. This point would, in fact, be folded down onto the M point in the 3R supercell BZ.

IV. Trends in Band Structure

By inspection of the band structures of these and related wide bandgap materials, it soon becomes clear that the valence band maximum in all these materials is at Γ while for the conduction band, there are a few k-points "in competition" for the minimum: the Γ point, the X point of zinc-blende and the K-point of wurtzite. Figure 6 shows the variation of these eigenvalues with cation.

This figure allows us to explain the directness or indirectness of the gaps. In BN, the conduction band minimum is at K in wurtzite and at X in

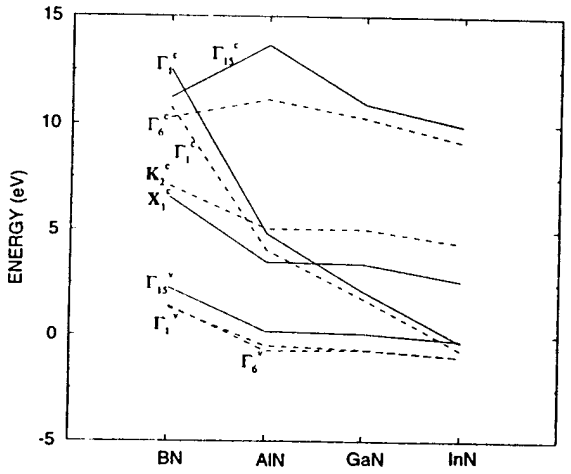

FIG. 6. Trend of band-edge eigenvalues of nitrides with cation. Solid line: zb eigenvalues; dashed line: wz.

zinc-blende. In AlN, the minimum is still at X in zinc-blende (but quite close to Γ), but switched to Γ in wurtzite. In GaN and InN, the minimum is at Γ in both cases. The reason for this trend is that the Γ_1^c states have a strong cation s-character. As one moves down in the periodic table, these states are lowered in energy with respect to corresponding p-like states. In other words, the s-p splitting is increasing. This is because s-states are nonzero at the nucleus and hence feel a stronger and stronger attractive potential as the atomic number Z increases. The states at X, on the other hand have mixed s-p character and also a strong component in the interstitial region. The relevant state at K has purely p-character. For second row elements such as C, B, and N, the p and s-states are particularly close in spatial and energetic extent. This is responsible for the k-point location of the minimum in BN. In fact, one can see in Fig. 6 that also the p-like conduction band states Γ_{15}^c in zb and Γ_6^c in wz are below the s-like Γ_1^c state in BN. The conduction-band minima locations in BN is the same as in SiC, and nearly the same as in diamond (because of the higher symmetry, in diamond, the conduction band moves slightly away from X leading to the well-known camel-back struc-

ture). The closeness between s and p-states in first row is also what leads to competition with π bonding and hence layered graphitic structures of carbon and BN.

The question discussed in the previous paragraph is not entirely straightforward. In fact, the problem is the choice of reference level. In a periodic crystal, there is no well-defined absolute reference level for the electrostatic potential (Kleinman, 1981). So, strictly speaking, the question of whether the gaps decrease from AlN to InN because the valence band goes up or the conduction band goes down cannot be answered meaningfully. One can only discuss such questions quantitatively when considering the two systems in contact, which leads to the band-offset problem at heterojunctions. That question has been discussed elsewhere (Albanesi and Lambrecht, 1994; Lambrecht *et al.*, 1996a). Here, we are only interested in a qualitative insight and some choice of reference level can be made. The choice adopted in Fig. 6 is the ASA reference level, which is the average electrostatic potential of the net charges per sphere and naturally suited for this purpose. One can think of this reference level as being closely related to the average potential in the interstitial region. On the other hand, Corkill, Rubio, and Cohen (1994) have argued that the gap reduction is related to the effect of the semicore d-electrons pushing up the valence band maximum. We have shown elsewhere (Lambrecht *et al.*, 1994) that this leads to only small direct effects near the valence band maximum once their effect on the bonding and hence lattice constant is properly taken into account. Also, under the superposition that the main effect comes from the d-states, it is difficult to understand where the difference between InN and GaN comes from.

It may be asked why in AlN, where the X minimum and Γ minimum are close in zb, the Γ point nevertheless wins out in wz. In fact, we have seen in the previous section that the Γ gap in wz is slightly larger than the zb gap (although by a very small amount). So, why does not the folded X state at $U = (2/3)ML$ end up below Γ in wz? Yeh, Wei, and Zunger (1994) have noted that in several compounds, the wz minimum at U appears to be the average of the folded X_C and L_C states. Since the folded L state is well above Γ and X, this then explains why the U state in wz is pushed up. However, there is no fundamental reason why this "average rule" should hold. We have argued above that the symmetry breaking is responsible for the X-folded state being pushed up in wz. We have also shown above that the symmetry breaking at Γ results only in a very small increase in gap because the states still are essentially of different angular momentum character.

The next question, one might ask is why this variation of gaps with cation is so much stronger in the nitrides series than for example in the As or P series. The reason is the high ionicity of the nitrides. As a result, the Γ_1^c

conduction band minimum has a more pure cation s-like character with less covalent admixing of the anion s-state. Hence, there is a greater sensitivity to the cation s-level trend with cation.

The ionic character of the nitrides deserves some further discussion. Several ionicity scales are in use, some of which are given in Table III for the nitrides and for comparison also for GaAs and ZnSe, a typical III–V and II–VI compound. In the popular Phillips scale of ionicity (noted below as f_i) (Phillips, 1973), the nitrides are less ionic than II–VI materials such as ZnSe, and slightly more ionic than other III–Vs such as arsenides or phosphides. The same is true in Harrison's sp^3 hybrid polarity scale (Harrison, 1989). In both of these scales, polarity* is determined by the ratio of the heteropolar part of the gap C to the total average bonding antibonding gap $\sqrt{E_h^2 + C^2}$, with E_h the homopolar part of the gap (corresponding to the group IV element of the appropriate row of the periodic table). The difference is that Phillips's scale is based on optical properties of semiconductors while Harrison's is based on atomic energies. In Harrison's definition, the heteropolar component of the gap is the difference in sp^3 hybrid energy levels of cation and anion and the covalent gap is based on the covalent interaction V between sp^3 orbitals pointing toward each other. Specifically,

$$\alpha_P = (E_c - E_a)/\sqrt{(E_c - E_a)^2 + 4V^2}. \tag{7}$$

One can obtain a similarly defined polarity scale based on ASA-LMTO calculations by making a transformation to a minimal basis set (Lambrecht and Segall, 1990). Unlike Harrison's polarity, this definition uses an internal reference level rather than the vacuum level for the orbital energies. More importantly, it is based on orbitals assigned to equal size atomic spheres rather than atomic orbitals. Garcia and Cohen (1993) introduced an ionicity scale based on the asymmetry in the charge distribution along the bonds, which is denoted as g in Table 3.

Both the ASA-LMTO polarity and Garcia and Cohen's ionicity scale assign a significantly more ionic character to the nitrides than to the II–VI compound ZnSe. In this view, the reason for the high ionicity of the nitrides is that the N2s and N2p levels are very deep compared to corresponding P3s and P3p valence states in phosphides and As4s and As4p states in arsenides. This in turn is due to the lack of a lower p-like core state. This reflects itself in the charge distribution when considering the latter in an unbiased way. That is the case in Garcia and Cohen's definition and in the ASA-LMTO based scale because the latter uses equal sphere sizes on anion

*Phillips ionicity is formally the square of what is here defined as polarity.

TABLE III

IONICITY AND RELATED PROPERTIES. ASA-LMTO BASED POLARITY α_P^{ASA}. GARCIA IONICITY g. HARRISON POLARITY α_P^H. SQUARE ROOT OF PHILLIPS IONICITY f_i. EFFECTIVE CHARGE PARAMETER S. WURTZITE STABILIZATION ENERGY $E_{wz} - E_{zb}$, TRANSITION PRESSURES TO ROCKSALT, AND BAND SPLITTINGS AT X

	α_P^{ASA}	g	α_P^H	$\sqrt{f_i}$	S^a	$E_{wz} - E_{zb}^b$ (mev/atom	P_t^c (GPa)	$X_3' - X_1'$ (eV)	$X_3' - X_1'^d$ (eV)
BN	0.475	0.484	0.41	0.506	0.86	20	850	5.6	4.9
AlN	0.807	0.794	0.59	0.670	1.55	−18.41	16.6	7.2	5.4
GaN	0.771	0.780	0.62	0.707	1.25	−9.88	51.8	6.4	3.5
InN	0.792	0.853	0.64	0.760	1.98	−11.44	21.6	7.0	3.3
GaAs	0.404	0.316	0.50	0.557	0.44	12.02		4.0	0.4
ZnSe	0.663	0.597	0.72	0.794	0.69	5.3		5.8	0.6

[a] From Kim, Lambrecht, and Segall (1996) for nitrides, and Martin (1970) for other.
[b] From Yeh *et al.* (1992) except for BN which is from Lam, Wentzcovitch, and Cohen (1990).
[c] From Christensen and Gorczyca (1994).
[d] From Lambrecht and Segall (1994).

and cation. This special character of second row elements of the periodic table is not captured well by the Phillips and Harrison scales.

Now, we discuss the relative ionicity among the nitrides. All scales agree that BN is the least ionic. From the bond-orbital point of view, this is because B also has quite deep levels being from the same row of the periodic table as N. The remaining nitrides have rather close ionicities with all models placing GaN in the middle. They differ however, in predicting either Al or In to be the most ionic. In any case, the difference in ionic character between these two appears to be quite small.

To judge ionicity scales, one needs to look at their predictive qualities for directly measurable quantities. One such quantity which is intuitively associated with ionicity is the dynamic effective charge Z^* and the associated parameter S, defined by Martin (1970),

$$S = Z^{*2}/\varepsilon = (\Omega/4\pi e^2)\mu(\omega_l^2 - \omega_t^2), \tag{8}$$

where Ω is the unit cell volume, μ the reduced mass, ε the electronic dielectric constant (i.e., at high frequency with respect to phonons but low frequency with respect to optical transitions), and ω_l and ω_t the longitudinal and transverse optic phonon frequencies at Γ. One can see in Table III, that S is significantly lower for GaAs and ZnSe than for the nitrides (in agreement with ASA-LMTO and Garcia scales) and follows exactly the same order as Garcia's scale for the nitrides.

High ionicity is also closely related to the preference for the hexagonal stacking of wurtzite. While this is a rather subtle problem requiring a delicate balance of band structure and electrostatic terms in the total energy, Cheng, Needs, and Heine (1987) showed that ionicity favors wurtzite from the point of view of the Madelung energy. A more elaborate relation to ionicity scales and atomic orbital radii was discussed by Yeh *et al.* (1992). Insofar as one considers the energy difference between wz and zb as a measure of ionicity, their calculations also predict the order of increasing ionicity to be B Ga In Al. Also, the considerably higher ionicity of the nitrides than ZnSe is consistent with that materials preference for zinc-blende.

It is well known that high ionicity favors the rocksalt structure. At high pressure bonds tend to become even more ionic. Thus, one expects that the transition pressures from tetrahedrally bonded to rocksalt structure would decrease with ionicity. Table III shows that the same non-monotonic order of ionicities with cation is followed by the transition pressures as by the ASA-LMTO scale.

The previously discussed quantities related to ionicities reflect in some sense average properties of the electronic structure. Returning now to the

band structure itself, there are some band splittings that can be viewed as direct measurements of the ionic character, because they are zero in the purely covalent semiconductors by symmetry, and therefore, are related to the asymmetric part of the potential. This is, for example, the case for the $X_3 - X_1$ splittings in zinc-blende. As Table 3 shows, the $X_3^c - X_1^c$ splitting, which is close to the ionicity gap between N2s and N2p like bands, follows exactly the same order as the ASA-LMTO polarity scale. The $X_3^c - X_1^c$ splitting on the other hand is smaller in GaN and InN than in BN. Of course, there is no reason why the band splittings of specific k-states should reflect exactly the same polarity as the average overall ionicity in the bonding that is embodied in the above ionicity scales. Nevertheless, the large values of the $X_3^c - X_1^c$ splittings compared to GaAs and ZnSe still reflect the high ionicity of the nitrides.

V. Experimental Probes

In this section, we discuss the experimental information on the band structures. Unlike in a naive single particle picture, we emphasize that there is no such thing as "the experimental band structure." While intuitively, it is clear that optical measurements probe differences between eigenstates of the system and hence should provide us with information on the band structure, such as the various gaps at different k-points, it is important to keep in mind, that we are in reality, probing a many-body system of interacting particles, which is only approximately described by the one-electron theory.

We have already outlined the general theoretical framework above. The experimental band structure could be defined as the spectrum of quasiparticle excitations from the ground state. In other words, it is the energy required to extract a particle or to add a particle to the system. In other words, they are differences of total energies of the N and $N-1$ or N and $N+1$ particle system. This spectrum is essentially obtained by photoemission and inverse photoemission spectroscopies respectively.

1. Photoemission

The many-body problem consists in the fact that when we extract an electron, the remaining electrons respond to this change. For example, if we extract an electron from a strongly localized state, such as a core-state, the remaining electrons will screen the hole left behind in a timeframe short with

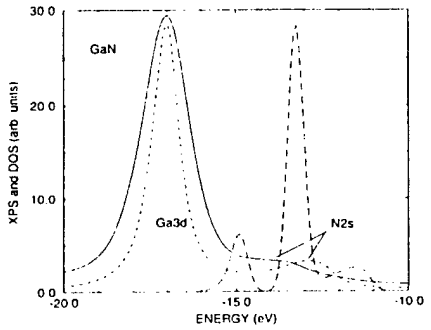

FIG. 7. XPS spectrum of w-GaN compared to calculated density of states. Solid line: experiment from Lambrecht *et al.* (1994); long-dashed line: LDA band theory with Ga3d band at −13 eV and forming bonding and antibonding states with N2s at −15 eV and −11.5 eV; short-dashed line: theory with shifted Ga3d band center by calculated self-energy shift of 4 eV. All energies are referenced to the valence band maximum.

respect to the time it takes the hole to delocalize over the solid. In other words, the translational symmetry of the solid is broken. Hence, one can think of this almost as of an impurity problem (the impurity being the atom which misses a core electron) and the binding energy of that core electron can thus be calculated as the energy of formation of such an impurity. This approach, which is called the ΔSCF approach, applies well, even to the semicore Ga3d and In4d electrons, and explains why these states appear about 4 eV lower than predicted by the straightforward LDA band theory. This is shown in Fig. 7. Further details can be found in Lambrecht *et al.* (1994).

For delocalized states, the above effects become in-principle negligibly small and even LDA theory should provide an adequate first approximation to the excitation spectrum, except for the gap correction. By comparing the density of states calculated from the Kohn-Sham LDA band structure with photoemission spectra, we can obtain information on the expectation value of the difference between the true self-energy operator and its LDA approximation. Figure 7 shows that the N2s peak from LDA (even after correcting for the Ga3d) still is shifted by about 1.2 ± 0.2 eV from its experimental value.

Figure 8 shows this comparison for AlN, where the situation is cleaner because there is no semicore d-band. One can see that when the valence

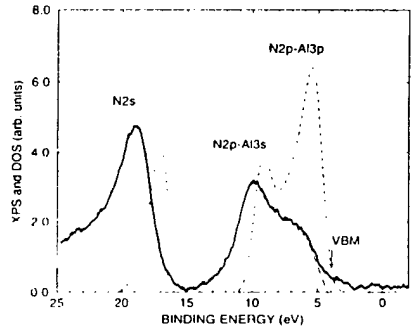

FIG. 8. X-ray photoemission spectrum and Density of States in AlN from King *et al.* (1996).

band maximum is aligned, the states near the bottom of the first band are shifted down in the experiment by about 0.5 eV and the N2s-like band is 1.9 eV underbinding in the LDA. Thus LDA underestimates bandwidths. These shifts are in quite satisfactory agreement with the GW calculations of Rubio, discussed in subsection 3. The N2s peak turns out to be near the X_1^v (in zb) or the deep M_1^v eigenvalues (in wz) for which they find GW corrections compared to LDA of 1.9 ± 0.1 eV in GaN and 2.0 ± 0.2 eV in AlN. Nevertheless, the GW calculations appear to slightly overestimate these shifts. This may be due to the fact that GW calculations are not entirely self-consistent but evaluated essentially by perturbation theory from LDA results.

We have here focused on recent XPS data that we could compare directly to the theory. Similar spectra have been obtained by UPS for GaN by Hunt *et al.* (1993), by XPS for GaN by Hedman and Martensson (1980), by XPS and UPS for AlN by Gautier, Duraud, and Le Gressus (1987), and for all three nitrides by Martin *et al.* (1996).

Very recently, a photoemission study of the band dispersion in zb GaN was carried out using synchrotron radiation by Ding *et al.* (1996). They used an angular resolved normal emission with varying photon energy in the range 30–80 eV. By assuming a parabolic final state band, one can then deduce the dispersion of the initial state band from the dispersion of the peaks with photon energy. They found the dispersion of the Δ_1 branch to coincide closely with LDA theory, placing the X_3^v band at −6.1 eV below

the valence-band maximum, in close agreement with the FP-LMTO calculations of Fiorentini, Methfessel, and Scheffler (1993), and our own group (Fig. 5). The GW calculations of Rubio *et al.* (1993) predict a 0.4 eV shift from the LDA values for this state and furthermore, their LDA value appears to be too low resulting in a value of -6.9 eV for this state. For the X_5^v state, the experiments find a higher value than the FP-LMTO calculations by about 0.8 eV. Again, GW calculations would further shift this band down by 0.2 eV. This discrepancy, however, as pointed out in Ding *et al.* (1996) may be due to experimental problems in resolving the peak position near the valence-band maximum. For the N2s–Ga3d region, they confirm the results of the earlier study presented above, that the Ga3d band lies well below the N2s band at respectively -17.7 eV and -14.2 eV. They find, however, a signficantly smaller dispersion of the N2s band than our theoretical predictions, only 0.65 eV compared to about 3 eV in the theory. We note, however, that the N2s band is only clearly resolved as a peak near the X_1^v state. Near the Γ_1^v state, the N2s peak only appears as a shoulder on the dominating Ga3d peak. This can also be seen from the errorbars on their measurements.

From the above, it appears that the occupied valence states and even semi-core states are quite well understood. Unfortunately, the situation is not as clear for conduction band states. At this time, there are to our knowledge, no inverse photoemission data available for the nitrides. Hence, we must obtain our information more indirectly from optical measurements. This has the added complication that one really measures two-particle excitations: in other words, the electron and hole interact with each other and produce excitonic effects. While these are clearly important near the band edges, where they lead to well defined bound states, they might be hoped to be somewhat less important within the continuum. We will see that even this is not quite the case in GaN!

2. UV Optics

Since the most reliable data are available on GaN, we focus first on GaN. UV reflectivity measurements for GaN for a range of 10–30 eV have been available since 1980 (Olson, Lynch, and Zehe, 1981). Recently, there has been renewed activity. In Lambrecht *et al.* (1995), a detailed analysis is presented of UV-reflectivity measurements in the range 0–35 eV using synchrotron radiation for wurtzite GaN. The experimental data were in good agreement with the older data, but had previously not been analyzed in similar detail. The analysis is based on calculated optical response functions using an ASA muffin-tin orbital basis set and using the LDA

except for a constant shift of the conduction band states. Spectroscopic ellipsometry measurements were presented for both zinc-blende and wurtzite GaN by Logothetidis *et al.* (1994), Petalas *et al.* (1995), and Janowitz *et al.* (1994). Petalas *et al.* (1995) includes comparisons to FP-LMTO calculations of the optical response function. Christensen and Gorczyca (1994) used essentially the same computational approach as Lambrecht *et al.* (1995) for optical response functions of the whole series of III-nitrides. As expected, the calculated response functions agree very well between these two sets of calculations. There are nevertheless, some differences in assignments of peaks to particular parts of the BZ, reflecting the fact that this interpretational part of the work is not an entirely automatic and straightforward task. From both our (Lambrecht *et al.*, 1995) work and the work of Christensen and Gorczyca (1994), it is clear that the peaks in optical response functions do not, generally speaking, correspond to well-defined transitions at high-symmetry k-points, but rather to extended regions of k-space. They are dominated by joint density of state effects, that is, extended regions of nearly parallel bands. The peaks in the measurements often correspond to superpositions of different contributions. Thus, the assignments to high-symmetry k-point transitions on the basis of energy coincidence and visual inspection of the bands as given in Logothetidis *et al.* (1994) is clearly a huge oversimplification.

At present, the various papers present somewhat conflicting interpretations. Both Petalas *et al.* (1995) and Janowitz *et al.* (1994) compare their measured results directly to LDA, calculated response functions, in the latter, to the calculated results of Christensen and Gorczyca (1994). In that case, in zinc-blende, the peaks around 7.0–7.5 eV (labeled E_{1C} and E_{2C}) agree well with theory, while higher peaks and the minimum gap are underestimated. In wurtzite, the experimental E_{1H}, E_{2H} peaks resolved in the spectroscopic ellipsometry are aligned with the peaks labeled D and E in Lambrecht *et al.* (1995), while if we shift up the theory by 1 eV, they align with C and D. These are reproduced in Fig. 9. The (rather weak in theory) peak C is also present in the FP-LMTO calculated spectra of Petalas *et al.* (1995), but is somehow ignored in this work, presumably under the assumption that it would be obscured by the broadening.

In our view, this interpretation is not very satisfactory. For wurtzite, we obtain consistent results for the minimum gap and for transitions up to 15 eV when including a 1 eV upward shift of the gap. Also, the Ga 3d transitions to the conduction band (in the range 20–30 eV) are clearly identified, and fall in the right place when including the 1 eV shift of the conduction band and the 4 eV downward shift of the corehole consistent with XPS. As mentioned earlier, a gap correction by 1 eV is required by GW calculations. Unlike the GW calculations discussed in Section 3, however,

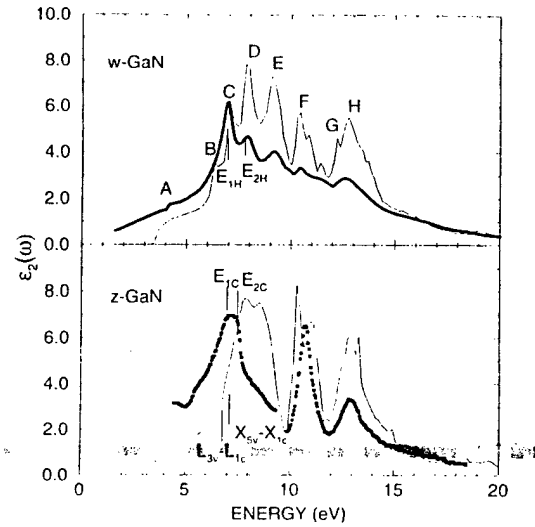

FIG. 9. UV optical response functions of wurtzite and zincblende GaN. Thick lines: experiment from Lambrecht *et al.* (1995) and Janowitz *et al.* (1994) for wz and zb respectively. For label explanation, see text.

one finds no clear trend for an increasing "correction" with increasing energy into the conduction band.

For zinc-blende GaN, there is, however a clear discrepancy in that the E_{1C}, E_{2C} transitions appear almost 1 eV below their prediction from the LDA + constant (1 eV) shift model. This can be seen in Fig. 9 in the lower panel. Clearly, this cannot be attributed to non-constant GW corrections because the GW calculations would predict it to shift even higher. Our proposed explanation is that this reflects the importance of two-particle response function effects. In other words, excitonic effects (electron-hole interaction) play a significant role even in the continuum. This is equivalent to the statement that our present calculation of linear response which is at the RPA level does not include exchange or electron-hole coupling effects. This is actually well known to affect the detailed shapes of the spectra in other semiconductors (del Castillo-Mussot and Sham, 1985; Hanke and Sham, 1980), but appears here to take more the appearance of a peak shift

rather than a peak amplitude change. This is related to the fact that the excitonically shifted peaks appear in a region of low spectral density. This in turn, is related to the shape of the bands near the Γ_1 minimum. The effective mass is rather low and the next minima occur at significantly higher energy (several eV). This leads to a rather low spectral density between the minimum gap and the next transitions, with strong spectral weight in the E_{1C}, E_{2C} region. Furthermore, the energetic proximity of E_{1C} and E_{2C} in this material, the fact that they both form part of an extended region in k-space of very nearly parallel bands, and the small screening in GaN (due to the high ionicity) all help to increase excitonic effects. Further detail is provided in Lambrecht *et al.* (1996a). We note that similar effects probably play a role in wurtzite. In that case, however, they rather appear as discrepancies in peak amplitude rather than shifts. They correspond to the significant increase in spectral strength of peak *C* in the experiment compared to the theory. This may appear as a less dramatic discrepancy than for zinc-blende, because intensities are always more difficult to describe and are also affected by surface roughness (Lambrecht *et al.*, 1995), but is really a manifestation of the same underlying physics of shifting of spectral weight by the excitonic effects. Including these properly will also require to include local-field corrections.

3. X-RAY ABSORPTION

There remains the question of whether the conduction band shifts are really constant up to about 10 eV in the conduction band or are increasing as predicted by GW, and then possibly recorrected by excitonic effects. To that end, it is useful to consider a more direct probe of conduction band states, namely X-ray absorption near edge fine structure, known as NEXAFS or XANES. The N K-edge spectrum in GaN was recently measured by several groups (Katsikini *et al.*, 1996; Lambrecht *et al.*, 1996b). This spectrum essentially probes the N-p partial density of states in the conduction band because it corresponds to excitation of a N2s state to the N p-like empty states.

Figure 10 shows the absorption spectrum extracted from glancing angle X-ray reflectivity compared to our theoretical prediction based on the band structures using our usual LDA + constant shift approach and a shift of the core-level extracted from XPS (Martin *et al.*, 1994). The two measurements are for s-polarization and p-polarization respectively, which as explained elsewhere correspond to $\mathbf{E} \perp \mathbf{c}$ and $\mathbf{E} \parallel \mathbf{c}$ respectively. The calculation is polarization averaged. Although, there are intensity discrepancies, which are mostly due to the polarization effects, one can clearly see that the

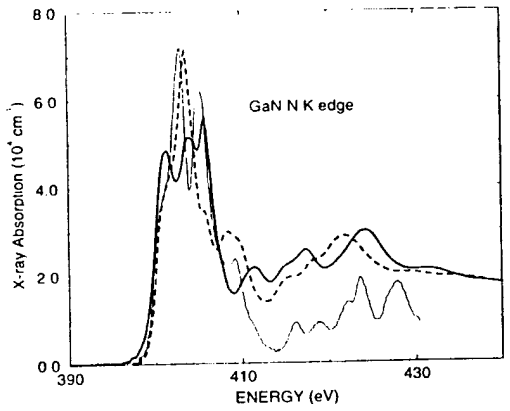

FIG. 10. Nitrogen K-edge. X-ray absorption spectrum of GaN, extracted from glancing angle reflectivity. Thick solid line, experiment for $\mathbf{E} \parallel \mathbf{c}$, dashed line, $\mathbf{E} \perp \mathbf{c}$, thin solid line polarization averaged theory.

peaks agree in position up to at least 10 eV above the conduction band minimum. This confirms the UV reflectivity results. If core-hole to conduction band excitonic effects play a role here, it is hard to see why they would equal the ones in UV and would similarly affect the higher peaks so much more than the states near the minimum gap. Hence, the most plausible explanation is that the actual quasiparticle energy shifts from the LDA Kohn Sham eigenvalues in the conduction band are indeed almost constant. The increasing trend found in the GW calculations thus is not bourne out by the measurements. This may be consistent with the fact that also the valence band state shifts appear to be a bit overestimated by current GW as was discussed above in connection with the photoemission results.

4. Other Nitrides

For the other nitrides, the experimental situation is much more incomplete. For AlN, there have been UV-reflectivity measurements by Loughin *et al.* (1993). They were analyzed in terms of an LCAO model. A comparison with our LMTO calculations is given in Lambrecht *et al.* (1996a) and

reveals significant discrepancies. This may be related to oxygen contamination of the samples. Our calculations agree well with those of Christensen and Gorczyca (1994). For InN, a comparison with experimental data by Guo *et al.* (1992) is presented in Christensen and Gorczyca (1994).

VI. Details Near the Band Edges

While in the remainder of the paper, we have discussed overall aspects of the band structure, such as bandwidths and transitions to states up to 10 eV or so, into the conduction band, the most important region of the band structure for practical applications in optoelectronics and transport is clearly the region in the immediate vicinity of the gap. For w-GaN, the reflectivity spectra of Dingle *et al.* (1971), Shan *et al.* (1995, 1996), Gil, Briot, and Aulombard (1995), photoluminescence excitation spectra by Monemar (1974), and photoluminescence spectra as well as calorimetric absorption and reflection spectroscopy by Eckey *et al.* (1996) show three well separated excitons labeled A, B, and C. Temperature dependent reflectivity data for zincblende GaN in the spectral region of the gap were presented by Ramírez-Flores *et al.* (1994), and reveal two excitons. To deal with these aspects of the band structure and the associated questions of effective masses, related to the curvature of the bands near the minima, we need meV precision. At this level, it is of crucial importance to include strain effects and spin-orbit coupling.

The appropriate theoretical framework for discussing the states near the band edges is the theory of invariants which provides the most general allowed form by group theory of the Hamiltonian up to terms of second order in $\mathbf{k}$. In addition, $\mathbf{k}\cdot\mathbf{p}$ theory provides perturbation theoretical expressions for the parameters in this Hamiltonian in terms of momentum matrix elements and energy band differences. The application of these theories to the zinc-blende and wurtzite have been described by Luttinger and Kohn (1955), Bir and Pikus (1974), Cho (1976), Sirenko *et al.* (1996). Following Sirenko *et al.* (1996), who traced the historic origins of this work in the Russian literature, we refer to the wurtzite Hamiltonian as the Rashba-Sheka-Pikus (RSP) Hamiltonian, while the zinc-blende Hamiltonian will be referred to as the Kohn-Luttinger Hamiltonian. Traditionally, the parameters in these models have been determined by experiment. For the nitrides, this information is still rather incomplete. Only the conduction band mass has been obtained by ODCR (Drechsler *et al.*, 1995). Attempts were made to extract crystal field splitting and spin-orbit coupling parameters from the exciton splittings. However, this has been hindered by the

incomplete knowledge of the strain state of the materials. A few groups have attempted to determine the parameters in these models by fitting these model band structures to first-principle calculations (Suzuki, Uenoyama, and Yanase, 1995; Kim, Lambrecht, and Segall, unpublished; Wei and Zunger, unpublished).

We first discuss the valence-band splittings at Γ. In the absence of spin-orbit coupling, the hexagonal crystal field splits the zincblende Γ_{15} state into a doublet Γ_6 and a singlet Γ_1 state (not counting spin degeneracy), whose splitting we shall denote by Δ_c. With the inclusion of the spin-orbit coupling, the Γ_6 states splits into a Γ_9 and Γ_7 state, while the Γ_1 becomes a Γ_7 state in the notation of the double group.

On the basis of symmetry, there are two spin-orbit coupling terms in the effective Hamiltonian for the valence-band manifold,

$$H_{SO} = \Delta_2 L_z \sigma_z + \sqrt{2}\Delta_3 (L_+ \sigma_- + L_- \sigma_+). \tag{9}$$

in which L_z, $L_\pm$ are the spherical tensor components of the $L = 1$ angular momentum operator and σ is the Pauli spin vector, also given in spherical tensor components. However, the spin-orbit coupling derives mainly from the inner part of the atom, and hence, is rather insensitive to the crystal structure and strain and one thus finds $\Delta_2 = \Delta_3 = \Delta_0/3$ with the Δ_0 the spin-orbit splitting in zinc-blende. For the same reasons, it can be confidently calculated within ASA-LMTO. Using this quasi-cubic approximation (Hopfield, 1960; Bir and Pikus, 1974), one finds for the $\Gamma_9 - \Gamma_7$ splittings, which correspond to the A-B, A-C exciton splittings,

$$E_{\Gamma_9} - E_{\Gamma_7} = \frac{\Delta_c + \Delta_0}{2} \pm \frac{1}{2}\sqrt{(\Delta_c + \Delta_0)^2 - \frac{8}{3}\Delta_0\Delta_c}. \tag{10}$$

The ASA-LMTO calculated spin-orbit parameters for the III-nitrides are given in Table IV. For GaN, the value is in good agreement with the data for zinc-blende by Ramírez-Flores *et al.* (1994). We also compare with the values obtained with LAPW calculations by Wei and Zunger (1996a). The very small value for InN is of interest. At first sight, it is counterintuitive that for the heavier element, spin-orbit coupling is smaller. The reason is that the effective spin-orbit splitting contains a negative contribution from the semicore d-states. The latter is the strongest in InN and almost completely cancels the otherwise dominant N2p contribution. This d-band effect was first noted by Cardona (1963) for Cu-halides and explained by Shindo, Morita, and Kamimura (1965). Further details are given in Lambrecht *et al.* (1996a).

TABLE IV

SPIN-ORBIT SPLITTING Δ_0 (IN MEV) IN ZINC-BLENDE NITRIDES

BN	22			
AlN	19			19
GaN	19	21	17 ± 1	15
InN	3	19		6

[a]Ramírez-Flores, *et al.* (1994).
[b]Wei, S. H. and Zunger, A. (1996a).

Unlike the spin-orbit coupling, the crystal field splitting Δ_c is very sensitive to strain. Gil, Briot, and Aulombard (1995) analyzed the data available on the exciton splittings and showed that they are correlated with the thickness of the films grown in sapphire. From the bandgap reduction (overall shift of the excitons) and knowing the bandgap deformation potential, one can then extract the hydrostatic component of the strain. Assuming that the crystals are biaxially strained, one obtains a further relation $\varepsilon_{zz} = -2C_{13}/C_{33}\varepsilon_{xx}$ between the two independent strain components (normal to the basal plane ε_{zz} and in-plane $\varepsilon_{xx} = \varepsilon_{yy}$). Here, C_{13} and C_{33} are elastic constants which can be found in Kim, Lambrecht, and Segall (1994). From the thickest films ($\sim 500\,\mu$m) (Eckey *et al.*, 1996) one can obtain the zero strain limit (Δ_1) and from the slope of the splitting with strain, one obtains a uniaxial deformation potential, known as D_3 in Bir and Pikus (1974) notation. Explicitly, one has

$$\Delta_c = E_{\Gamma_6} - E_{\Gamma_7} = \Delta_1 + (3/2)D_3\varepsilon_{zz}. \tag{11}$$

The analysis of Gil, Briot, and Aulombard (1995) gives $\Delta_1 = 10$ meV. Their value for D_3, 3.71 eV, is somewhat inaccurate due to the use of old and inaccurate data on the elastic constants. We have recently reanalyzed these data including also newer data on GaN on SiC substrates and found $D_3 = 5.7$ eV obtained directly from our first-principles calculations is in good agreement with the data. This can be seen in Fig. 11.

The calculated values for the zero-strain value of the crystal field splitting both by us (19 meV at $u = 0.379$ and 36 meV at the more accurate $u = 0.377$) and Wei and Zunger (1996a) (42 meV) appear too high. This happens even though both calculations include carefully the internal parameter u relaxation and use accurate experimental lattice constants a and c/a. Clearly, we are struggling with the accuracy limitations of current band structure methods at this point. If one uses the ideal value of $u = 3/8$ instead, one obtains a value that is even larger, about 73 meV as in Suzuki, Uenoyama, and Yanase (1995). The remaining discrepancy is related to the LDA.

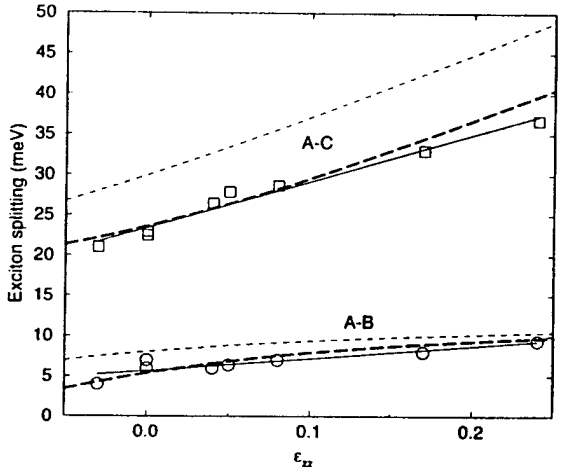

FIG. 11. Exciton splittings as function of uniaxial strain component ε_{zz}. The circles and squares indicate experimental values for AB and AC splitting respectively. Full lines are linear fits. The dashed lines are our calculated results using $A_6 = 19$ meV, $D_3 = -5.7$ meV and $A_7 = 19$ and 10 meV respectively, for the short-thin and long-thick dashes.

For AlN, both Wei and Zunger (1996a), Suzuki, Uenoyama, and Yanase (1995), and Kim, *et al.* (1997) find that the Γ_1 state lies above the Γ_6 by respectively 217 meV, 58 meV, and 215 meV. Again, the discrepancy in Suzuki, Uenoyama, and Yanase (1995) is related to the use of the ideal u value. No experimental data on these splittings are available to our knowledge. The strain dependence is again given in terms of the D_3 deformation potential for which we find a value of 9.6 eV (Kim, *et al.*, 1997). For InN, Wei and Zunger (1996a) give a value of 41 meV for Δ_1, close to that of GaN. In the case of InN, however, one should be strongly concerned about correction effects beyond LDA, because the LDA bandgap turns out to be negative or very close to zero, depending on slight details of the calculations.

We now turn to the inverse mass-like parameters of the effective Hamiltonians. In wurtzite, the independent parameters are essentially the effective masses of light, heavy, and split-off hole bands in the two inequivalent crystal directions: in-plane and perpendicular to the basal plane. The values

TABLE V

KOHN-LUTTINGER PARAMETERS (IN UNITS $\hbar^2/2m_0$) FOR ZINC-BLENDE AlN AND GaN

	AlN	GaN
A	−2.81	−5.05
B	−0.69	−1.17
C	−3.51	−5.85

given by Kim, *et al.* (1997) for GaN and AlN generally agree well with those by Suzuki, Uenoyama, and Yanase (1995). The largest discrepancies occur for the in-plane heavy hole mass, which is so large in AlN, that it is difficult to extract from parabolic fits to the bands. The results also agree closely with the predictions of the quasicubic model (Bir and Pikus, 1974). We can hence describe both wurtzite and zinc-blende valence bands fairly well, with the three usual Kohn-Luttinger parameters given in Table V. In terms of these, one can obtain the RSP parameters and the effective masses in WZ using the relations given in Table VI, where numerical values are also given. We give both the values fitted directly to wurtzite bands, and the ones obtained from the quasicubic model using fits to the zinc-blende bands. For InN, these data are still lacking because of the more substantial problems of LDA for this material.

TABLE VI

WURTZITE RASHBA-SHEKA-PIKUS PARAMETERS IN TERMS OF ZINC-BLENDE KOHN-LUTTINGER PARAMETERS AND WURTZITE EFFECTIVE MASSES AND THEIR VALUES IN AlN AND GaN OBTAINED FROM DIRECT CALCULATION AND IN QUASICUBIC APPROXIMATION (IN PARENTHESES)*

		AlN	GaN
A_1	$(A + 2B + 2C)/3$	−3.9 (−3.7)	−6.4 (−6.4)
A_2	$(A + 2B - C)/3$	−0.3 (−0.2)	−0.5 (−0.5)
A_3	$-C$	3.6 (3.5)	5.9 (5.9)
A_4	$C/2$	1.3 (1.7)	2.5 (2.9)
A_5	$(A - B + 2C)/6$	1.5 (1.5)	2.6 (2.6)
A_6	$-(2A - 2B + C)/3\sqrt{2}$	1.6 (1.8)	3.1 (3.2)
$m^{\perp}_{hh} = m^{\perp}_{lh}$	$-(A_1 + A_3)^{-1}$	3.5 (4.4)	2.0 (2.0)
$m^{\perp}_{split}$	$-A_1^{-1}$	0.3 (0.3)	0.2 (0.2)
$m^{\parallel}_{hh}$	$-(A_2 + A_4 + A_5)^{-1}$	11.1 (2.2)	2.0 (1.2)
$m^{\parallel}_{lh}$	$-(A_2 + A_4 - A_5)^{-1}$	0.4 (0.3)	0.2 (0.2)
$m^{\parallel}_{split}$	$-A_2^{-1}$	4.0 (4.5)	2.0 (2.0)

*Units are $\hbar^2/2m_0$ for A_i and m_0 for masses.

VII. Outlook for Future Work

From the previous sections, it becomes clear that the basic features of the band structures of the pure nitrides, their trends, and relations between zinc-blende and wurtzite are by now rather well understood. To be sure, there are some aspects that still require refinements, for example, inclusion of spin-orbit coupling effects on the higher conduction band states, determining the corrections beyond LDA with greater accuracy, understanding the relations between the fitted KL and RSP model Hamiltonian parameters and their expressions in terms of the critical point energy gaps and the matrix elements in $\mathbf{k}\cdot\mathbf{p}$ theory.

Mostly, however, at this point, there is a lack of experimental data to test the theoretical data base. Angular resolved photoemission and inverse photoemission spectroscopy are highly desirable to challenge the accuracy of the present band structure theories, in particular, to study the deviations from LDA and to test the accuracy of GW on the k-dependence and state dependence of the self-energy corrections as well as the lifetime effects on those states. In the area of UV optical spectra, many-body effects need to be included. It should be added, that even for much better understood semiconductors, this statement is equally valid. Also, at this moment, only for GaN, there have been extensive studies in the UV range for both zinc-blende and wurtzite. Even in GaN, the polarization dependence has not been studied experimentally. For AlN, InN, and BN, synchrotron radiation studies of UV reflectivity and or ellipsometry have not been performed, presumably for lack of adequate samples. Electroreflectivity of all these materials may further help to identify critical point transitions.

The present review was limited to the pure nitrides. The other area where one can expect much progress in the near future is the band structure of mixed materials. There has already been some body of work on alloys (Jenkins and Dow, 1989; Wright and Nelson, 1995b; Albanesi, Lambrecht, and Segall, 1993; Lambrecht, 1997; Kim, Limpijumnong, Lambrecht, and Segall; Wei and Zunger, 1996b; Neugebauer and Van de Walle, 1995), but it has been mostly limited to zinc-blende alloys. Virtual crystal theories will clearly be inadequate because of the large size mismatches between the cations (especially those containing In) and strong bandgap variation among the nitrides. The effects of short-range and long-range ordering in the wurtzite structure based alloys are not understood at all. Finally, the electronic structure of superlattices and other layered structures of reduced dimensionality will clearly attract great interest. These are particularly interesting because of the polar nature of the crystals. One may expect that just like (111) oriented superlattices in other III–Vs, the wurtzite (0001) superlattices will exhibit interesting spontaneous electric field and piezoelectric effects. While some studies of the band line-ups have already appeared

(Lambrecht *et al.*, 1996a; Albanesi and Lambrecht, 1994), the study of the optical properties and band structure of these systems is clearly still in its initial stages.

ACKNOWLEDGMENTS

It is a pleasure to thank my colleague Professor Segall, and the students (Kwiseon Kim, Sukit Limpijumnong) and research associates (Sergey Rashkeev, Eduardo Albanesi) of our research group who collaborated on various aspects of the study of nitrides over the past few years. I would also like to thank various people for sharing their experimental data with us, H. Morkoç and G. Martin, J. C. Rife and D. K. Wickenden, T. Suski and K. Jablonska, R. F. Davis and S. W. King, C. Janowitz, S. Loughlin. Finally, this work would not have been possible without the support of the National Science Foundation and the Office of Naval Research.

NOTE ADDED IN PROOF

After submission of this manuscript, other studies relevant to section V.1, and V.3 appeared: C. B. Stagarescu, L. C. Duda, K. E. Smith, J. H. Guo, J. Nordgren, R. Singh, and T. D. Moustakas, (1996) *Phys. Rev. B* **54**, R17335 and K. E. Smith, S. S. Dhesi, L. C. Duda, C. B. Stagarescu, J. H. Guo, J. Nordgren, R. Singh, and T. D. Moustakas, (1997) in *III-V Nitrides*, F. A. Ponce, T. D. Moustakas, I. Akasaki, and B. A. Monemar, Mater. Res. Soc. Symp. Proc. MRS Pittsburgh, **449**, 787–92.

REFERENCES

Albanesi, E. A., Lambrecht, W. R. L., and Segall, B. (1993). *Phys. Rev. B* **48**, 17841.
Albanesi, E. A., Lambrecht, W. R. L. (1994). In *Diamond, SiC and Nitride Wide Bandgap Semiconductors* (C. H. Carter, Jr., G. Gildenblat, S. Nakamura, and R. J. Nemanich, eds.). *Mater. Res. Soc. Symp. Proc.* MRS, Pittsburgh **339**, 607–612.
Andersen, O. K. (1975). *Phys. Rev. B* **12**, 3060.
Andersen, O. K., Postnikov, A. V., and Savrasov, Yu. S. (1992). In *Applications of Multiple Scattering Theory to Materials Science*, (W. H. Butler, P. H. Dederichs, A. Gonis, and R. L. Weaver, eds.), *Mater. Res. Soc. Symp. Proc. MRS, Pittsburgh*, **253**, 37.
Aryasetiawan, F., and Gunnarsson, O. (1994). *Phys. Rev. B* **49**, 7219; *Phys. Rev. B* **49**, 16214.
Bloom, S. (1971). *J. Phys. Chem. Sol.* **32**, 2027.
Bloom, S., Harbeke, G., Meier, E., and Ortenburger, I. B. (1974). *Phys. Stat. Sol. B* **66**, 161.
Bir, G. L., and Pikus, G. E. (1974). *Symmetry and Strain-Induced Effects in Semiconductors*, John Wiley & Sons, New York.
Blöchl, P. E. (1994). *Phys. Rev. B* **50**, 17953.
Boguslawski, P., Briggs, E. L., and Bernholc, J. (1995). *Phys. Rev. B* **51**, 17255.
Bourne, J., and Jacobs, R. L. (1972). *J. Phys. C: Solid State Physics* **5**, 3462.

Cardona, M. (1963). *Phys. Rev.* **129,** 69.
Cheng, C. Needs, R. J., and Heine, V. (1987). *Europhys. Lett.* **3,** 475.
Chen, J. Levine, Z. H., and Wilkins, J. W. (1995). *Appl. Phys. Lett.* **66,** 1129.
Ching, W. Y., and Harmon, B. N. (1986). *Phys. Rev. B* **34,** 5305.
Cho, K. (1976). *Phys. Rev. B* **14,** 4463.
Christensen, N. E., and Gorczyca, I. (1993). *Phys. Rev. B* **47,** 4307.
Christensen, N. E., and Gorczyca, I. (1994). *Phys. Rev. B* **50,** 4397.
Corkill, J. L., Rubio, A., and Cohen, M. L. (1994). *J. Phys. Condens. Mat.* **6,** 961.
del Castillo-Mussot, M., and Sham, L. J. (1985). *Phys. Rev. B* **31,** 2092.
Ding, S. A., Neuhold, G., Weaver, J. H., Häberle, P., Horn, K., Brandt, O., Yang, O., and Ploog, K. (1996). *J. Vac. Sci. Technol. A* **14,** 819.
Dingle, R., Sell, D. D., Stokowski, S. E., and Ilegems, M. (1971). *Phys. Rev. B* **4,** 1211.
Dreschsler, M., Meyer, B. K., Hoffmann, D. M., Detchprohm, D., Amano, H., and Akasaki, I. (1995). *Jpn. J. Appl. Phys.* **34,** L1178.
Eckey, L., Podlowskii, L., Göldner, A., Hoffman, A., Broser, I., Meyer, B. K., Volm, D., Streibl, T., Detchprohm, T., Amano, H., and Akasaki, I. (1996). In *Silicon Carbide and Related Materials 1995*, (S. Nakashima, H. Matsunami, S. Yoshida, and H. Harima, eds.), Institute of Physics Conference Series No. 142, IOP, London, p. 943.
Fiorentini, V., Methfessel, M., and Scheffler, M. (1993). *Phys. Rev. B* **47,** 13353.
Foley, C. P., and Tansley, T. L. (1986). *Phys. Rev. B* **33,** 1430.
Garcia, A., and Cohen, M. L. (1993). *Phys. Rev. B* **47,** 4215.
Gautier, M., Duraud, J. P., and Le Gressus, C. (1986). *Surf. Sci.* **178,** 201; (1987). *J. Appl. Phys.* **61,** 574.
Gil, B., Briot, O., and Aulombard, R.-L. (1995). *Phys. Rev. B* **52,** R17028.
Godby, R. W., Schlüter, M., and Sham, L. J. (1988). *Phys. Rev. B* **37,** 10159.
Gorczyca, I., Christensen, N. E., Perlin, P., Grzegory, I., Jun, J., and Bockowski, M. (1991). *Solid State Commun.* **79,** 1033; Gorczyca, I., and Christensen, N. E. (1991). *Solid State Commun.* **80,** 335; Gorczyca, I., and Christensen, N. E. (1993). *Phys. B* **185,** 410; Perlin, P., Gorczyca, I., Porowski, S., Suski, T., Christensen, N. E., and Polian, A. (1993). *Jpn. J. Appl. Phys.* **32,** Suppl. **32-1,** 334; Perlin, P., Gorczyca, I., Christensen, N. E., Grzegory, I., Teisseyre, H., and Suski, T. (1992). *Phys. Rev. B* **45,** 13307.
Gorczyca, I., Christensen, N. E., Pelzer y Blanca, E. L., and Rodriguez, C. O. (1995). *Phys. Rev. B* **51,** 11936.
Grinajew, S. H., Malachow, W. J., and Czaldyszew, W. A. (1986). *Izv. Viz. Fiz. (USSR)* **29,** 69.
Guo, Q., Kato, O., Fujisawa, M., and Yoshida, A. (1992). *Solid State Commun.* **83,** 721.
Hamann, D. R., Schlüter, M., and Chiang, C. (1979). *Phys. Rev. Lett.* **43,** 1494.
Hanke, W., and Sham, L. J. (1975). *Phys. Rev. B* **12,** 4501; (1980). *Phys. Rev. B* **21,** 4656.
Harrison, W. A. (1989). *Electronic Structure and Properties of Solids*, Dover, New York.
Hedin, L., and Lundqvist, S. (1969). In *Solid State Physics* **23,** 1.
Hedman, J., and Martensson, N. (1980). *Physica Scripta* **22,** 176.
Hejda, B., and Hauptmanová, K. (1969). *Phys. Status Solidi* **36,** K95.
Hohenberg, P., and Kohn, W. (1964). *Phys. Rev.* **136,** B864; Kohn, W., and Sham, L. J. (1965). *ibid.* **140,** A1133.
Hopfield, J. J. (1960). *J. Phys. Chem. Solids* **15,** 97.
Huang, M. Z., and Ching, W. Y. (1985). *J. Chem. Phys. Sol.* **46,** 977.
Hunt, R. W., Vanzetti, L., Castro, T., Chen, K. M., Sorba, L., Cohen, P. I., Gladfelder, W., Van Hove, J. M., Kuznia, J. N., Asif Khan, M., and Franciosi, A. (1993). *Physica B* **185,** 415.
Hybertsen, M., and Louie, S. G. (1986). *Phys. Rev. B* **34,** 5390.
Janowitz, C., Cardona, M., Johnson, R. L., Cheng, T., Foxon, T., Günther, O., and Jungk, G. (1994). *BESSY Jahresbericht*, p. 230.
Jenkins, D. W., and Dow, J. D. (1989). *Phys. Rev. B* **39,** 3317.
Jones, D., and Lettington, A. H. (1969). *Solid State Commun.* **11,** 701; (1969). *ibid.* **7,** 1319.

Karch, K., Portish, G., Bechstedt, F., Pavone, P., and Strauch, D. (1996). In *Silicon Carbide and Related Materials 1995* (S. Nakashima, H. Matsunami, S. Yoshida, and H. Harima, eds.), Institute of Physics Conference Series No. 142, IOP, London, p. 967.
Katsikini, M., Paloura, E. C., Kalomiros, J., Bressler, P., and Moustakas, T. (1996). In *Proceedings of the 23rd International Conference on the Physics of Semiconductors* (M. Scheffler and R. Zimmermann, eds.), World Scientific, Singapore, p. 573.
Kerker, G. (1980). *J. Phys. C: Solid State Physics* **13,** L189.
Kim, K., Lambrecht, W. R. L., Segall, B., and van Schilfgarde, M. (1997). *Phys. Rev. B* **56,** (Sept 15) in press.
Kim, K., Lambrecht, W. R. L., and Segall, B. (1994). *Phys. Rev. B* **50,** 1502.
Kim, K., Lambrecht, W. R. L., and Segall, B. (1996). *Phys. Rev. B* **53,** 16310.
Kim, K., Limpijumnong, S., Lambrecht, W. R. L., and Segall, B. (1997). In *III–V Nitrides* (F. A. Ponce, T. D. Moustakas, I. Akasaki, B. A. Monemar) Mater. Res. Soc. Symp. Proc. MRS Pittsburgh, **449,** 929–934.
King, S. W., Benjamin, M. C., Nemanich, R. J., Davis, R. F., and Lambrecht, W. R. L. (1996). In *Gallium Nitride and Related Materials* (F. Ponce, R. D. Dupuis, S. Nakamura, and J. A. Edmond, eds.), *Mater. Res. Soc. Symp. Proc. MRS, Pittsburgh*, **395,** 375.
Klienman, L. (1981). *Phys. Rev. B* **24,** 7412.
Kobayashi, A., Sankey, O. F., Volz, S. M., and Dow, J. D. (1983). *Phys. Rev. B* **28,** 935.
Lambrecht, W. R. L., and Segall, B. (1990). *Phys. Rev. B* **41,** 2832.
Lambrecht, W. R. L., and Segall, B. (1992). In *Wide Band Gap Semiconductors* (T. D. Moustakas, J. I. Pankove, and Y. Hamakawa, eds.), *Mater. Res. Soc. Symp. Proc.* **242,** 367.
Lambrecht, W. R. L., and Segall, B. (1994). In *Properties of Group III Nitrides* (J. H. Edgar, ed.), Electronic Materials Information Service (EMIS) Datareviews Series (Institution of Electrical Engineers, London, Chapter 5.
Lambrecht, W. R. L. (1994). In *Diamond, Silicon Carbide and Nitride Wide Bandgap Semiconductors* (C. H. Carter, Jr., G. Gildenblat, S. Nakamura, and R. J. Nemanich, eds.), *Mater. Res. Soc. Symp. Proc.* **339,** 565–582.
Lambrecht, W. R. L. (1997). *Solid State Electronics*, **41,** 195–199.
Lambrecht, W. R. L., Segall, B., Strite, S., Martin, G., Agarwal, A., Morkoç, H., and Rockett, A. (1994). *Phys. Rev. B* **50,** 14155.
Lambrecht, W. R. L., Segall, B., Rife, J., Hunter, W. R., and Wickenden, D. K. (1995). *Phys. Rev. B* **51,** 13516.
Lambrecht, W. R. L., Kim, K., Rashkeev, S. N., and Segall, B. (1996a). In *Gallium Nitride and Related Materials* (F. Ponce, R. D. Dupuis, S. Nakamura, and J. A. Edmond, eds.), *Mater. Res. Soc. Symp. Proc. MRS, Pittsburgh* **395,** 455.
Lambrecht, W. R. L., Rashkeev, S. N., Segall, B., Lawniczak-Jablonska, K., Suski, T., Gullikson, E. M., Underwood, J. H., Perera, R. C. C., Rife, J. C., Grzegory, I., Porowski, S., and Wickenden, D. K. (1997). *Phys. Rev. B*, **55,** 2612.
Lam, P. K., Wentzcovitch, R. M., and Cohen, M. L. (1990). In *Materials Science Forum*, Trans Tech Publications, Switzerland, **54/55,** 165–192.
Landolt-Börnstein: *Numerical Data and Functional Relationships in Science and Technology* (O. Madelung, ed.), Group III, Vol. 22a, Springer, Berlin.
Logothetidis, S., Petalas, J., Cardona, M., and Moustakas, T. D. (1994). *Phys. Rev. B* **50,** 18017.
Loughlin, S., French, R. H., Ching, W. Y., Xu, Y. N., and Slack, G. A. (1993). *Appl. Phys. Lett.* **63,** 1182.
Luttinger, J. M. (1956). *Phys. Rev.* **102,** 1030; Luttinger, J. M., and Kohn, W. (1955). *Phys. Rev.* **97,** 869.
Martin, G., Strite, S., Botchkarev, A. Agarwal, A., Rockett, A., Morkoç, H., Lambrecht, W. R. L., and Segall, B. (1994). *Appl. Phys. Lett.* **65,** 610.
Martin, G., Botchkarev, A., Rockett, A., and Morkoç, H. (1996). *Appl. Phys. Lett.* **68,** 2541.
Martin, R. (1970). In *Phys. Rev. B* **1,** 4005.

Methfessel, M. (1988). *Phys. Rev. B* **38,** 1537.
Min, B. J., Chan, C. T., and Ho, K. M. (1992). *Phys. Rev. B* **45,** 1159.
Miwa, K., and Fukumoto, A. (1993). *Phys. Rev. B* **48,** 7897.
Monemar, B. A. (1974). *Phys. Rev. B* **10,** 676.
Muñoz, A., and Kunc, K. (1993). *Physica B* **185,** 422; (1991). *Phys. Rev. B* **44,** 10372.
Muñoz, A., and Kunc, K. (1993). *J. Phys. Condens. Matter* **5,** 6015.
Neugebauer, J., and Van de Walle, C. G. (1994). *Phys. Rev. B* **50,** 8067; Northrup, J. E., and Neugebauer, J. (1996). *Phys. Rev. B* **53,** R10477.
Neugebauer, J., and Van de Walle, C. G. (1995). *Phys. Rev. B* **51,** 10568.
Okumura, H., Ohta, K., Ando, K., Rühle, W. W., Nagamoto, T., and Yoshida, S. (1996). In *Silicon Carbide and Related Materials 1995* (S. Nakashima, H. Matsunami, S. Yoshida, and H. Harima, eds.), Institute of Physics Conference Series No. 142, IOP, London, p. 939.
Olson, C. G., Lynch, D. W., and Zehe, A. (1981). *Phys. Rev. B* **24,** 4629.
Palummo, M., Bertoni, C. M., Reining, L., and Finocchi, F. (1993). *Physica B* **185,** 404.
Palummo, M., Reining, L., Godby, R. W., Bertoni, C. M., and Börnsen, N. (1994). *Europhysics Lett.* **26,** 607.
Palummo, M., Del Sole, R., Reining, L., Bechstedt, F., and Cappellini, G. (1995). *Solid State Commun.* **95,** 393.
Pandey, R., Jaffe, J. E., and Harrison, N. M. (1993). *J. Mater. Res.* **8,** 1922.
Perdew, J. P., and Levy, M. (1983). *Phys. Rev. Lett.* **51,** 1884.
Petalas, J., Logothetidis, S., Boutadakis, S., Alouani, M., and Wills, J. M. (1995). *Phys. Rev. B* **52,** 8082.
Phillips, J. C. (1973). *Bonds and Bands in Semiconductors*, Academic, New York.
Ramírez-Flores, G., Navarro-Contreras, H., Lastras-Martínez, A., Powell, R. C., and Greene, J. E. (1994). *Phys. Rev. B* **50,** 8433.
Rubio, A., Corkill, J. L., Cohen, M. L., Shirley, E. L., and Louie, S. G. (1993). *Phys. Rev. B* **48,** 11810.
Ruiz, E., Alvarez, S., and Alemany, P. (1994). *Phys. Rev. B* **49,** 7115.
Sham, L. J., and Kohn, W. (1966). *Phys. Rev.* **145,** A561.
Sham, L. J., and Schlüter, M. (1983). *Phys. Rev. Lett.* **51,** 1888.
Shan, W., Schmidt, T. J., Yang, X. H., Hwang, S. J., Song, J. J., and Goldenberg, B. (1995). *Appl. Phys. Lett.* **66,** 985.
Shan, W., Fisher, A. J., Song, J. J., Bulman, G. E., Kong, H. S., Leonard, M. T., Perry, W. G., Bremser, M. D., and Davis, R. F. (1996). *Appl. Phys. Lett.*, **69,** 740.
Shindo, K., Morita, A., and Kamimura, H. (1965). *J. Phys. Soc. Jpn.* **20,** 2054.
Sirenko, Yu. M., Jeon, J.-B., Kim, K. W., Littlejohn, M. A., and Stroscio, M. A. (1996). *Phys. Rev. B* **53,** 1997.
Suzuki, M., Uenoyama, T., and Yanase, A. (1995). *Phys. Rev. B* **52,** 8132.
Tyagai, V. A., Evtigneev, A. M., Krasiko, A. N., Andreeva, A. F., and Malakov, V. Ya. (1977). *Fiz. Tekh. Poluprovodn.* **11,** 2142, English translation in (1977). *Sov. Phys. Semicond.* **11,** 1257.
Van Camp, P. E., Van Doren, V. E., and Devreese, J. T. (1989). *Solid State Commun.* **71,** 1055; (1992). *ibid.* **81,** 23; (1991). *Phys. Rev. B* **44,** 9056.
Vanderbilt, D. (1990). *Phys. Rev. B* **41,** 7892.
Wei, S. H., and Zunger, A. (1996c). *Appl. Phys. Lett.* **69,** 2719.
Wei, S. H., and Zunger, A. (1996b). *Phys. Rev. Lett.* **76,** 664.
Wright, A. F., and Nelson, J. S. (1994). *Phys. Rev. B* **50,** 2159; (1995a). *ibid.* **51,** 7866.
Wright, A. F., and Nelson, J. S. (1995). *Appl. Phys. Lett.* **66,** 3051; (1995a). *ibid.* **66,** 3465.
Xu, Y.-N., and Ching, W. Y. (1993). *Phys. Rev. B* **48,** 4335.
Yeh, C.-Y., Lu, Z. W., Froyen, S., and Zunger, A. (1992). *Phys. Rev. B* **46,** 10086.
Yeh, C.-Y., Wei, S.-H., and Zunger, A. (1994). *Phys. Rev. B* **50,** 2715.

SEMICONDUCTORS AND SEMIMETALS, VOL. 50

CHAPTER 13

Phonons and Phase Transitions in GaN

N. E. Christensen

INSTITUTE OF PHYSICS AND ASTRONOMY
UNIVERSITY OF AARHUS
DK-8000 AARHUS
DENMARK

P. Perlin

HIGH PRESSURE RESEARCH CENTER
POLISH ACADEMY OF SCIENCES
SOKOŁOWSKA 29/37
PL-01-142 WARSAW
POLAND

I. Introduction

Among the III–V nitrides GaN is technologically the most interesting compound, in particular because of its optical properties making it a promising material (Mohammad, and Morkoç, 1996) for optoelectronic devices operating in the blue regime. The understanding of the electronic,

ISBN 0-12-752158-5
0080-8784/98

XPS MEASUREMENT OF THE SiC/AlN BAND-OFFSET AT THE (0001) INTERFACE

Sean W. King,* Mark C. Benjamin,** Robert J. Nemanich**, Robert F. Davis * and Walter R. L. Lambrecht †
*Department of Materials Science and Engineering, North Carolina State University, Raleygh, NC 27695
**Department of Physics, North Carolina State University, Raleigh, NC 27695
†Department of Physics, Case Western Reserve University, Cleveland, OH 44106

ABSTRACT

X-ray photoelectron spectroscopy is used to determine the band-offset at the SiC/AlN (0001) interface. First, the valence band spectra are determined for bulk materials and analyzed with the help of calculated densities of states. Core levels are then measured across the interface for a thin film of 2H-AlN on 6H-SiC and allow us to extract a band offset of 1.4 ±0.3 eV. The analysis of the discrepancies between measured peak positions and densities of states obtained within the local density approximation provides information on self-energy corrections in good agreement with independent calculations of the latter.

INTRODUCTION

Silicon carbide wafers are being used increasingly as substrates for the growth of III-V nitride thin films. In particular, SiC is rater closely lattice matched to AlN (0.9 %) which is often used as a buffer layer for GaN growth. The availability of bulk 6H-SiC substrate wafers of high quality is intrumental for this purpose. Since SiC can also be grown on AlN layers on SiC [1], one may also consider the use of SiC as an active quantum well layer in a AlN/SiC/AlN heterostructure device. From both points of view, the band-offset at the SiC/AlN interface is of obvious interest. To date, only two previous values are available: a theoretical value by Lambrecht and Segall [2] which was for the (110) interface between zincblende SiC and AlN; and an experimental value obtained indirectly from measurements of the Fermi level of 2H-AlN grown on 6H-SiC (0001) by Benjamin et al. [3]. The investigations described here provide a more direct experimental determination of the band offset at the basal plane interface between 6H-SiC and wurtzite AlN. The procedure consists of measuring the core levels at the interface between a thin film of AlN (0001) grown on a 6H-SiC(0001) substrate and separately determining the energy of the valence band edges with respect to the core levels for thick films. The calculated densities of states are used to aid in the determination of the valence band edge and allow us to obtain some additional information on the electronic structure of the materials. In particular, we obtain results for the difference in quasi-particle self-energy shifts of the N2s and C2s bands with respect to those of the upper N2p and C2p like valence bands.

EXPERIMENT

A unique and integrated ultra high vacuum (UHV) system consisting of a 36 ft. long UHV transfer line to which several thin film deposition and surface analysis units are connected was employed in this research. The details of this integrated system have been previously described [4]. The as-received, n-type ($N_d \approx 10^{17-18}/cm^3$), vicinal 6H-SiC(0001)$_{Si}$ substrate wafers containing a one micron thick, n-type ($N_d \approx 10^{16-17}/cm^3$) 6H-SiC(0001)$_{Si}$ epitaxial layer were sequentially dipped in 10% HF for 5–10 min. to remove the thermally grown 750 Å silicon oxide surface layer, rinsed in 18.4 MΩ de-ionized water, blown dry with N_2, mounted to a molybdenum sample holder, loaded into ultra high vacuum (UHV) and degassed at 250, 500, 700, and 900°C for 30 min. each and annealed in a $10-7-10^{-6}$

Mat. Res. Soc. Symp. Proc. Vol. 395 © 1996 Materials Research Society

,er than that of the valence band maximum while the latter finds this correction
1.6 eV. The present measurement indicates that the former two are in better
with experiment. In summary then, we find that the valence-band maximum
rgy scale of Fig. 1 lies at 2.2 ±0.2 eV. We also see that this agrees well with a
ıight line extrapolation from the half height point of the experimental valence

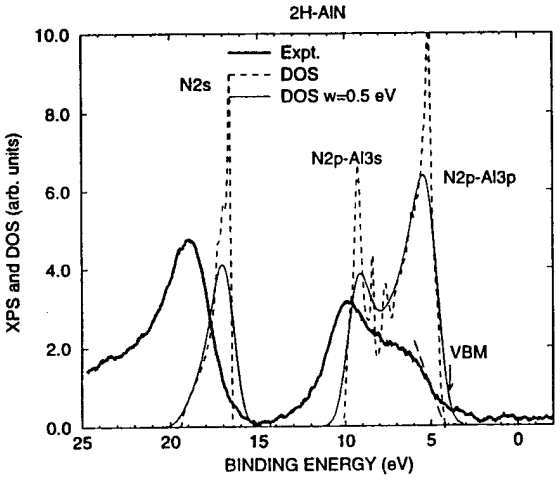

XPS spectra (arbitrary units) and densities of states (in states per unit cell per
AlN.

shows a similar analysis for the valence-band spectrum of AlN. In this case, we
he upper valence band width is only 6 eV wide (in the theoretical DOS). Rubio et
W calculations predict a 2.0 eV shift for the N2s peak and a 0.6 eV shift for the
like peak. We see that if we align one of these including the above correction,
for the other is well reproduced. Due to the insulating nature of AlN, some
g and shifting of the AlN core levels and valence band spectra may be expected
ırging. No direct evidence of these effects was found. We thus conclude that the
leposited sufficiently thin (200 Å) that the underlying conducting SiC substrate
charging. With respect to the same Au $4f_{7/2}$ based reference level, we then find
e-band maximum of AlN lies at 4.1 eV and is again in good agreement with a
ıight line extrapolation of the edge. The core levels for the bulk and interface
own in Table I have also been measured on the same energy scale as employed
ıdies described above.
data are then substituted in the expression

$$-\Delta E_v = (E_v^{SiC} - E_c^{SiC})_b - (E_v^{AlN} - E_c^{AlN})_b + (E_c^{SiC} - E_c^{AlN})_i, \qquad (1)$$

subscripts b and i indicate bulk and interface respectively. While in the above
$_c$ are all positive electron binding energies, it is customary to give ΔE_v in terms
rgy levels which are the negative of the binding energies. Hence the minus sign
t of Eq. 1. Using different core levels and remembering the uncertainties in the
of each valence-band spectrum we finally arrive at a value of $\Delta E_v = 1.4 \pm 0.3$

Table I: Valence-band maxima and core levels measured on the same Au $4f_{7/2}$ based reference scale

bulk SiC	
Si 2p	101.3
C 1s	283.5
VBM	2.2
bulk AlN	
Al 2p	75.3
N 1s	398.5
VBM	4.1
AlN/SiC heterojunction	
Si 2p	101.5
C 1s	283.6
Al 2p	74.9
N1s	398.2

DISCUSSION

The value obtained for the band-offset is in quite good agreement with the previously calculated offset of 1.5 eV for the (110) zincblende interface [2]. This is perhaps somewhat surprising since the latter is a non-polar interface while here we deal with a polar heterovalent interface. In fact, from simple electron counting rules, one expects that a purely N terminated surface would have an excess of 1/4 electron and thus must reconstruct its surface for example by having one N vacancy every 4 N atoms in order to maintain charge neutrality. In reality one may have a missing dimer every 4 instead of a simple vacancy or any other arrangement which is equivalent in net charge. At present, it is not known on an atomic scale what the interface structure is like, but we may note that if 1/4 of the N are missing at the interface, this is for electron counting purposes equivalent to mixing the nitrogen layer with C (group IV) anions. One expects that this would lower the dipole from that of a non-polar interface [16] by a few 0.1 eV. However, a slightly larger degree of intermixing may completely wipe out this interface dependence. This may indicate indirectly that there are an equal number of Al-C and N-Si bonds at the interface. In the absence of further information on the interface structure, we caution that this interpretation is at present only speculative and will require further study. We also note that while interface specific effects on band-offsets have in the past been predicted theoretically for several semiconductor heterostructures, especially heterovalent ones, these have generally not been observed. This indicates that realistic interfaces have some degree of disorder not accounted for by these theoretical predictions.

The value of 1.4 eV obtained for the SiC/AlN bandoffset is larger than the previously reported experimental value of 0.8 eV [3]. The discrepancies between these two values may be related to the experimental techniques or to the preparation of the SiC/AlN interface. The experiments described in this report employed recently developed surface preparation processes that result in atomically clean and ordered SiC prior to AlN deposition. In contrast, the SiC surface preparation of the prior study would typically exhibit a small amount of oxygen at the interface, ~25–50% ML. In addition the gas source MBE employed in present study results in a higher quality interface as opposed to the ECR technique employed previously. The ECR technique has been shown to result in more damage and an excess of Si-N bonding at the interface [17]. In the study presented in this paper, no oxygen was detected at the SiC/AlN interface. Furthermore, the use of an initial Al flux prior to ammonia exposure avoids the formation of a large amount of Si-N bonding.

1.0 eV larger than that of the valence band maximum while the latter finds this correction to be 1.4–1.6 eV. The present measurement indicates that the former two are in better agreement with experiment. In summary then, we find that the valence-band maximum on the energy scale of Fig. 1 lies at 2.2 ±0.2 eV. We also see that this agrees well with a simple straight line extrapolation from the half height point of the experimental valence band edge.

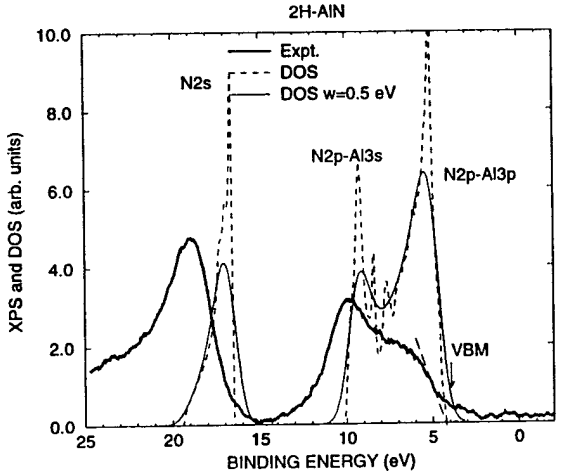

Figure 2: XPS spectra (arbitrary units) and densities of states (in states per unit cell per eV) of 2H-AlN.

Fig. 2 shows a similar analysis for the valence-band spectrum of AlN. In this case, we find that the upper valence band width is only 6 eV wide (in the theoretical DOS). Rubio et al.'s [14] *GW* calculations predict a 2.0 eV shift for the N2s peak and a 0.6 eV shift for the N2p-Al3s like peak. We see that if we align one of these including the above correction, the shift for the other is well reproduced. Due to the insulating nature of AlN, some broadening and shifting of the AlN core levels and valence band spectra may be expected due to charging. No direct evidence of these effects was found. We thus conclude that the AlN was deposited sufficiently thin (200 Å) that the underlying conducting SiC substrate prevented charging. With respect to the same Au $4f_{7/2}$ based reference level, we then find the valence-band maximum of AlN lies at 4.1 eV and is again in good agreement with a direct straight line extrapolation of the edge. The core levels for the bulk and interface system shown in Table I have also been measured on the same energy scale as employed for the studies described above.

These data are then substituted in the expression

$$-\Delta E_v = (E_v^{SiC} - E_c^{SiC})_b - (E_v^{AlN} - E_c^{AlN})_b + (E_c^{SiC} - E_c^{AlN})_i, \qquad (1)$$

where the subscripts b and i indicate bulk and interface respectively. While in the above E_v and E_c are all positive electron binding energies, it is customary to give ΔE_v in terms of the energy levels which are the negative of the binding energies. Hence the minus sign on the left of Eq. 1. Using different core levels and remembering the uncertainties in the alignment of each valence-band spectrum we finally arrive at a value of $\Delta E_v = 1.4 \pm 0.3$ eV.

Table I: Valence-band maxima and core levels measured on the same Au $4f_{7/2}$ based reference scale

bulk SiC	
Si 2p	101.3
C 1s	283.5
VBM	2.2
bulk AlN	
Al 2p	75.3
N 1s	398.5
VBM	4.1
AlN/SiC heterojunction	
Si 2p	101.5
C 1s	283.6
Al 2p	74.9
N1s	398.2

DISCUSSION

The value obtained for the band-offset is in quite good agreement with the previously calculated offset of 1.5 eV for the (110) zincblende interface [2]. This is perhaps somewhat surprising since the latter is a non-polar interface while here we deal with a polar heterovalent interface. In fact, from simple electron counting rules, one expects that a purely N terminated surface would have an excess of 1/4 electron and thus must reconstruct its surface for example by having one N vacancy every 4 N atoms in order to maintain charge neutrality. In reality one may have a missing dimer every 4 instead of a simple vacancy or any other arrangement which is equivalent in net charge. At present, it is not known on an atomic scale what the interface structure is like, but we may note that if 1/4 of the N are missing at the interface, this is for electron counting purposes equivalent to mixing the nitrogen layer with C (group IV) anions. One expects that this would lower the dipole from that of a non-polar interface [16] by a few 0.1 eV. However, a slightly larger degree of intermixing may completely wipe out this interface dependence. This may indicate indirectly that there are an equal number of Al-C and N-Si bonds at the interface. In the absence of further information on the interface structure, we caution that this interpretation is at present only speculative and will require further study. We also note that while interface specific effects on band-offsets have in the past been predicted theoretically for several semiconductor heterostructures, especially heterovalent ones, these have generally not been observed. This indicates that realistic interfaces have some degree of disorder not accounted for by these theoretical predictions.

The value of 1.4 eV obtained for the SiC/AlN bandoffset is larger than the previously reported experimental value of 0.8 eV [3]. The discrepancies between these two values may be related to the experimental techniques or to the preparation of the SiC/AlN interface. The experiments described in this report employed recently developed surface preparation processes that result in atomically clean and ordered SiC prior to AlN deposition. In contrast, the SiC surface preparation of the prior study would typically exhibit a small amount of oxygen at the interface, ~25–50% ML. In addition the gas source MBE employed in present study results in a higher quality interface as opposed to the ECR technique employed previously. The ECR technique has been shown to result in more damage and an excess of Si-N bonding at the interface [17]. In the study presented in this paper, no oxygen was detected at the SiC/AlN interface. Furthermore, the use of an initial Al flux prior to ammonia exposure avoids the formation of a large amount of Si-N bonding.

These factors can strongly influence the band alignment between two semiconductors. In addition, the initial study also assumed flat bands in the SiC near the interface while upward band bending was noted as a distinct possibility. Since that band-offset value was based on the assumption of alignment of the measured Fermi level of AlN and the bulk n-type doped SiC, it indeed probes the macroscopic band alignement (affected by band bending) rather than the offset in the immediate vicinity of the interface. This differs from the present XPS investigation because of the limited escape depth of the photoelectrons.

CONCLUSION

By combining XPS studies of the valence band spectra with calculated DOS and a careful analysis of the alignment between the two taking into account known self-energy corrections to the LDA band structures, the positions of the valence band maxima of 6H-SiC and 2H-AlN with respect to their core levels has been determined. A subsequent measurement of core levels at the heterojunction between a thin film of 2H-AlN grown on top of 6H-SiC then allowed us to extract a band offset of 1.4 ± 0.3 eV. The latter is in good agreement with the calculated value of the (110) zincblende SiC/AlN which indicates that the expected polar interface specific effects were compensated by some degree of disorder.

The work at CWRU was supported by NSF (DMR-92-22387); the research at NCSU was supported by ONR (N00014-92-J-1477). Appreciation is expressed to Cree Research Inc. for the 6H-SiC wafers used in this study.

REFERENCES

1. L.B. Rowland, R.S. Kern, S. Tanaka, and R.F. Davis, *Appl. Phys. Lett.* **62**, 3333 (1993).
2. W. R. L. Lambrecht ant B. Segall, *Phys. Rev. B* **43**, 7070 (1991).
3. M. C. Benjamin, C. Wang, R. F. Davis, and R. J. Nemanich, *Appl. Phys. Lett.* **64**, 3288 (1994).
4. Jacob van der Weide. Ph.D. dissertation, North Carolina State University, 1993.
5. S. W. King, R. J. Nemanich, and R. F. Davis, unpublished.
6. O. K. Andersen, O. Jepsen, M. Šob, in *Electronic Band Structure and its Applications*, ed. M. Yussouf (Springer, Heidelberg 1987), p. 1
7. W. Kohn and L. J. Sham *Phys. Rev.* **140**, A1133 (1965)
8. L. J. Sham and W. Kohn, *Phys. Rev.* **145**, A561 (1966).
9. W. R. L. Lambrecht, B. Segall, M. Yoganathan, W. Suttrop, R. P. Devaty, W. J. Choyke, J. A. Edmond, J. A. Powell, and M. Alouani, *Phys. Rev. B* **50** 10722 (1994).
10. L. Hedin, *Phys. Rev.* **139**, A796 (1965).
11. M. Rohlfing, P. Krüger, J. Pollmann *Phys. Rev. B* **48**, 1791 (1993).
12. W. H. Backes, P. A. Bobbert, W. van Haeringen *Phys. Rev. B* **51** 4950 (1995)
13. B. Wenzien, P. Käckell, F. Bechstedt *Phys. Rev. B* **52**, 10897 (1995)
14. A. Rubio, J. L. Corkill, M. L. Cohen, E. L. Shirley,a nd S. G. Louie, *Phys. Rev. B* **48**, 11810 (1993).
15. M. C. Benjamin, S. W. King, R. F. Davis, and R. J. Nemanich, unpublished.
16. W. R. L. Lambrecht and B. Segall, *Phys. Rev. B* **41**, 2832 (1990).
17. Z. Sitar, L. L. Smith, and R. F. Davis, *J. Cryst. Growth* **141**, 11 (1994).